POLYPUBLIE
Polytechnique Montréal

POLYTECHNIQUE MONTRÉAL
UNIVERSITÉ D'INGÉNIERIE

Titre: Millimeter-wave direct digital receiver
Title:

Auteur: Ji Li
Author:

Date: 1996

Type: Mémoire ou thèse / Dissertation or Thesis

Référence: Li, J. (1996). Millimeter-wave direct digital receiver [Thèse de doctorat, École Polytechnique de Montréal]. PolyPublie. https://publications.polymtl.ca/31092/
Citation:

Document en libre accès dans PolyPublie
Open Access document in PolyPublie

URL de PolyPublie: https://publications.polymtl.ca/31092/
PolyPublie URL:

Directeurs de recherche: Rénato Bosisio, & Ke Wu
Advisors:

Programme: Non spécifié
Program:

Ce fichier a été téléchargé à partir de PolyPublie, le dépôt institutionnel de Polytechnique Montréal
This file has been downloaded from PolyPublie, the institutional repository of Polytechnique Montréal

https://publications.polymtl.ca

UNIVERSITÉ DE MONTRÉAL

MILLIMETER-WAVE DIRECT DIGITAL RECEIVER

JI LI

DÉPARTEMET DE GÉNIE ÉLECTRIQUE ET DE GÉNIE INFORMATIQUE

ÉCOLE POLYTECHNIQUE DE MONTRÉAL

THÈSE PRÉSENTÉE EN VUE DE L'OBTENTION DU DIPLÔME DE

PHILOSOPHIAE DOCTOR (Ph.D.)

(GÉNIE ÉLECTRIQUE)

MAI 1996

© Ji Li, 1996.

National Library of Canada
Bibliothèque nationale du Canada

Acquisitions and Bibliographic Services Branch
Direction des acquisitions et des services bibliographiques

395 Wellington Street
Ottawa, Ontario
K1A 0N4

395, rue Wellington
Ottawa (Ontario)
K1A 0N4

Your file *Votre référence*

Our file *Notre référence*

The author has granted an irrevocable non-exclusive licence allowing the National Library of Canada to reproduce, loan, distribute or sell copies of his/her thesis by any means and in any form or format, making this thesis available to interested persons.

L'auteur a accordé une licence irrévocable et non exclusive permettant à la Bibliothèque nationale du Canada de reproduire, prêter, distribuer ou vendre des copies de sa thèse de quelque manière et sous quelque forme que ce soit pour mettre des exemplaires de cette thèse à la disposition des personnes intéressées.

The author retains ownership of the copyright in his/her thesis. Neither the thesis nor substantial extracts from it may be printed or otherwise reproduced without his/her permission.

L'auteur conserve la propriété du droit d'auteur qui protège sa thèse. Ni la thèse ni des extraits substantiels de celle-ci ne doivent être imprimés ou autrement reproduits sans son autorisation.

ISBN 0-612-17810-2

Canada

Name Ji Li

Dissertation Abstracts International is arranged by broad, general subject categories. Please select the one subject which most nearly describes the content of your dissertation. Enter the corresponding four-digit code in the spaces provided.

Applied Sciences: Electronics and Electrical Engineering — SUBJECT TERM

0544 — SUBJECT CODE

U·M·I

Subject Categories

THE HUMANITIES AND SOCIAL SCIENCES

COMMUNICATIONS AND THE ARTS
Architecture 0729
Art History 0377
Cinema 0900
Dance 0378
Fine Arts 0357
Information Science 0723
Journalism 0391
Library Science 0399
Mass Communications 0708
Music 0413
Speech Communication 0459
Theater 0465

EDUCATION
General 0515
Administration 0514
Adult and Continuing 0516
Agricultural 0517
Art 0273
Bilingual and Multicultural 0282
Business 0688
Community College 0275
Curriculum and Instruction 0727
Early Childhood 0518
Elementary 0524
Finance 0277
Guidance and Counseling 0519
Health 0680
Higher 0745
History of 0520
Home Economics 0278
Industrial 0521
Language and Literature 0279
Mathematics 0280
Music 0522
Philosophy of 0998
Physical 0523
Psychology 0525
Reading 0535
Religious 0527
Sciences 0714
Secondary 0533
Social Sciences 0534
Sociology of 0340
Special 0529
Teacher Training 0530
Technology 0710
Tests and Measurements 0288
Vocational 0747

LANGUAGE, LITERATURE AND LINGUISTICS
Language
- General 0679
- Ancient 0289
- Linguistics 0290
- Modern 0291

Literature
- General 0401
- Classical 0294
- Comparative 0295
- Medieval 0297
- Modern 0298
- African 0316
- American 0591
- Asian 0305
- Canadian (English) 0352
- Canadian (French) 0355
- English 0593
- Germanic 0311
- Latin American 0312
- Middle Eastern 0315
- Romance 0313
- Slavic and East European 0314

PHILOSOPHY, RELIGION AND THEOLOGY
Philosophy 0422
Religion
- General 0318
- Biblical Studies 0321
- Clergy 0319
- History of 0320
- Philosophy of 0322

Theology 0469

SOCIAL SCIENCES
American Studies 0323
Anthropology
- Archaeology 0324
- Cultural 0326
- Physical 0327

Business Administration
- General 0310
- Accounting 0272
- Banking 0770
- Management 0454
- Marketing 0338

Canadian Studies 0385
Economics
- General 0501
- Agricultural 0503
- Commerce-Business 0505
- Finance 0508
- History 0509
- Labor 0510
- Theory 0511

Folklore 0358
Geography 0366
Gerontology 0351
History
- General 0578
- Ancient 0579
- Medieval 0581
- Modern 0582
- Black 0328
- African 0331
- Asia, Australia and Oceania 0332
- Canadian 0334
- European 0335
- Latin American 0336
- Middle Eastern 0333
- United States 0337

History of Science 0585
Law 0398
Political Science
- General 0615
- International Law and Relations 0616
- Public Administration 0617

Recreation 0814
Social Work 0452
Sociology
- General 0626
- Criminology and Penology 0627
- Demography 0938
- Ethnic and Racial Studies 0631
- Individual and Family Studies 0628
- Industrial and Labor Relations 0629
- Public and Social Welfare 0630
- Social Structure and Development 0700
- Theory and Methods 0344

Transportation 0709
Urban and Regional Planning 0999
Women's Studies 0453

THE SCIENCES AND ENGINEERING

BIOLOGICAL SCIENCES
Agriculture
- General 0473
- Agronomy 0285
- Animal Culture and Nutrition 0475
- Animal Pathology 0476
- Food Science and Technology 0359
- Forestry and Wildlife 0478
- Plant Culture 0479
- Plant Pathology 0480
- Plant Physiology 0817
- Range Management 0777
- Wood Technology 0746

Biology
- General 0306
- Anatomy 0287
- Biostatistics 0308
- Botany 0309
- Cell 0379
- Ecology 0329
- Entomology 0353
- Genetics 0369
- Limnology 0793
- Microbiology 0410
- Molecular 0307
- Neuroscience 0317
- Oceanography 0416
- Physiology 0433
- Radiation 0821
- Veterinary Science 0778
- Zoology 0472

Biophysics
- General 0786
- Medical 0760

EARTH SCIENCES
Biogeochemistry 0425
Geochemistry 0996
Geodesy 0370
Geology 0372
Geophysics 0373
Hydrology 0388
Mineralogy 0411
Paleobotany 0345
Paleoecology 0426
Paleontology 0418
Paleozoology 0985
Palynology 0427
Physical Geography 0368
Physical Oceanography 0415

HEALTH AND ENVIRONMENTAL SCIENCES
Environmental Sciences 0768
Health Sciences
- General 0566
- Audiology 0300
- Chemotherapy 0992
- Dentistry 0567
- Education 0350
- Hospital Management 0769
- Human Development 0758
- Immunology 0982
- Medicine and Surgery 0564
- Mental Health 0347
- Nursing 0569
- Nutrition 0570
- Obstetrics and Gynecology 0380
- Occupational Health and Therapy 0354
- Ophthalmology 0381
- Pathology 0571
- Pharmacology 0419
- Pharmacy 0572
- Physical Therapy 0382
- Public Health 0573
- Radiology 0574
- Recreation 0575
- Speech Pathology 0460
- Toxicology 0383

Home Economics 0386

PHYSICAL SCIENCES

Pure Sciences
Chemistry
- General 0485
- Agricultural 0749
- Analytical 0486
- Biochemistry 0487
- Inorganic 0488
- Nuclear 0738
- Organic 0490
- Pharmaceutical 0491
- Physical 0494
- Polymer 0495
- Radiation 0754

Mathematics 0405
Physics
- General 0605
- Acoustics 0986
- Astronomy and Astrophysics 0606
- Atmospheric Science 0608
- Atomic 0748
- Electronics and Electricity 0607
- Elementary Particles and High Energy 0798
- Fluid and Plasma 0759
- Molecular 0609
- Nuclear 0610
- Optics 0752
- Radiation 0756
- Solid State 0611

Statistics 0463

Applied Sciences
Applied Mechanics 0346
Computer Science 0984
Engineering
- General 0537
- Aerospace 0538
- Agricultural 0539
- Automotive 0540
- Biomedical 0541
- Chemical 0542
- Civil 0543
- Electronics and Electrical 0544
- Heat and Thermodynamics 0348
- Hydraulic 0545
- Industrial 0546
- Marine 0547
- Materials Science 0794
- Mechanical 0548
- Metallurgy 0743
- Mining 0551
- Nuclear 0552
- Packaging 0549
- Petroleum 0765
- Sanitary and Municipal 0554
- System Science 0790

Geotechnology 0428
Operations Research 0796
Plastics Technology 0795
Textile Technology 0994

PSYCHOLOGY
General 0621
Behavioral 0384
Clinical 0622
Developmental 0620
Experimental 0623
Industrial 0624
Personality 0625
Physiological 0989
Psychobiology 0349
Psychometrics 0632
Social 0451

Nom Ji Li

Dissertation Abstracts International est organisé en catégories de sujets. Veuillez s.v.p. choisir le sujet qui décrit le mieux votre thèse et inscrivez le code numérique approprié dans l'espace réservé ci-dessous.

Génie électronique et électrique — SUJET

0544 — CODE DE SUJET

U·M·I

Catégories par sujets

HUMANITÉS ET SCIENCES SOCIALES

COMMUNICATIONS ET LES ARTS
Architecture 0729
Beaux-arts 0357
Bibliothéconomie 0399
Cinéma 0900
Communication verbale 0459
Communications 0708
Danse 0378
Histoire de l'art 0377
Journalisme 0391
Musique 0413
Sciences de l'information 0723
Théâtre 0465

ÉDUCATION
Généralités 515
Administration 0514
Art 0273
Collèges communautaires 0275
Commerce 0688
Économie domestique 0278
Éducation permanente 0516
Éducation préscolaire 0518
Éducation sanitaire 0680
Enseignement agricole 0517
Enseignement bilingue et multiculturel 0282
Enseignement industriel 0521
Enseignement primaire. 0524
Enseignement professionnel 0747
Enseignement religieux 0527
Enseignement secondaire 0533
Enseignement spécial 0529
Enseignement supérieur 0745
Évaluation 0288
Finances 0277
Formation des enseignants 0530
Histoire de l'éducation 0520
Langues et littérature 0279
Lecture 0535
Mathématiques 0280
Musique 0522
Orientation et consultation 0519
Philosophie de l'éducation 0998
Physique 0523
Programmes d'études et enseignement 0727
Psychologie 0525
Sciences 0714
Sciences sociales 0534
Sociologie de l'éducation 0340
Technologie 0710

LANGUE, LITTÉRATURE ET LINGUISTIQUE
Langues
- Généralités 0679
- Anciennes 0289
- Linguistique 0290
- Modernes 0291

Littérature
- Généralités 0401
- Anciennes 0294
- Comparée 0295
- Mediévale 0297
- Moderne 0298
- Africaine 0316
- Américaine 0591
- Anglaise 0593
- Asiatique 0305
- Canadienne (Anglaise) 0352
- Canadienne (Française) 0355
- Germanique 0311
- Latino-américaine 0312
- Moyen-orientale 0315
- Romane 0313
- Slave et est-européenne 0314

PHILOSOPHIE, RELIGION ET THÉOLOGIE
Philosophie 0422
Religion
- Généralités 0318
- Clergé 0319
- Études bibliques 0321
- Histoire des religions 0320
- Philosophie de la religion 0322

Théologie 0469

SCIENCES SOCIALES
Anthropologie
- Archéologie 0324
- Culturelle 0326
- Physique 0327

Droit 0398
Économie
- Généralités 0501
- Commerce-Affaires 0505
- Économie agricole 0503
- Économie du travail 0510
- Finances 0508
- Histoire 0509
- Théorie 0511

Études américaines 0323
Études canadiennes 0385
Études féministes 0453
Folklore 0358
Géographie 0366
Gérontologie 0351
Gestion des affaires
- Généralités 0310
- Administration 0454
- Banques 0770
- Comptabilité 0272
- Marketing 0338

Histoire
- Histoire générale 0578
- Ancienne 0579
- Médiévale 0581
- Moderne 0582
- Histoire des noirs 0328
- Africaine 0331
- Canadienne 0334
- États-Unis 0337
- Européenne 0335
- Moyen-orientale 0333
- Latino-américaine 0336
- Asie, Australie et Océanie 0332

Histoire des sciences 0585
Loisirs 0814
Planification urbaine et régionale 0999
Science politique
- Généralités 0615
- Administration publique 0617
- Droit et relations internationales 0616

Sociologie
- Généralités 0626
- Aide et bien-âtre social 0630
- Criminologie et établissements pénitentiaires 0627
- Démographie 0938
- Études de l' individu et de la famille 0628
- Études des relations interethniques et des relations raciales 0631
- Structure et développement social 0700
- Théorie et méthodes. 0344
- Travail et relations industrielles 0629

Transports 0709
Travail social 0452

SCIENCES ET INGÉNIERIE

SCIENCES BIOLOGIQUES
Agriculture
- Généralités 0473
- Agronomie. 0285
- Alimentation et technologie alimentaire 0359
- Culture 0479
- Élevage et alimentation 0475
- Exploitation des pâturages 0777
- Pathologie animale 0476
- Pathologie végétale 0480
- Physiologie végétale 0817
- Sylviculture et faune 0478
- Technologie du bois 0746

Biologie
- Généralités 0306
- Anatomie 0287
- Biologie (Statistiques) 0308
- Biologie moléculaire 0307
- Botanique 0309
- Cellule 0379
- Écologie 0329
- Entomologie 0353
- Génétique 0369
- Limnologie 0793
- Microbiologie 0410
- Neurologie 0317
- Océanographie 0416
- Physiologie 0433
- Radiation 0821
- Science vétérinaire 0778
- Zoologie 0472

Biophysique
- Généralités 0786
- Medicale 0760

SCIENCES DE LA TERRE
Biogéochimie 0425
Géochimie 0996
Géodésie 0370
Géographie physique 0368
Géologie 0372
Géophysique 0373
Hydrologie 0388
Minéralogie 0411
Océanographie physique 0415
Paléobotanique 0345
Paléoécologie 0426
Paléontologie 0418
Paléozoologie 0985
Palynologie 0427

SCIENCES DE LA SANTÉ ET DE L'ENVIRONNEMENT
Économie domestique 0386
Sciences de l'environnement 0768
Sciences de la santé
- Généralités 0566
- Administration des hipitaux 0769
- Alimentation et nutrition 0570
- Audiologie 0300
- Chimiothérapie 0992
- Dentisterie 0567
- Développement humain 0758
- Enseignement 0350
- Immunologie 0982
- Loisirs 0575
- Médecine du travail et thérapie 0354
- Médecine et chirurgie 0564
- Obstétrique et gynécologie 0380
- Ophtalmologie 0381
- Orthophonie 0460
- Pathologie 0571
- Pharmacie 0572
- Pharmacologie 0419
- Physiothérapie 0382
- Radiologie 0574
- Santé mentale 0347
- Santé publique 0573
- Soins infirmiers 0569
- Toxicologie 0383

SCIENCES PHYSIQUES
Sciences Pures

Chimie
- Généralités 0485
- Biochimie 487
- Chimie agricole 0749
- Chimie analytique 0486
- Chimie minérale 0488
- Chimie nucléaire 0738
- Chimie organique 0490
- Chimie pharmaceutique 0491
- Physique 0494
- PolymÇres 0495
- Radiation 0754

Mathématiques 0405
Physique
- Généralités 0605
- Acoustique 0986
- Astronomie et astrophysique 0606
- Électronique et électricité 0607
- Fluides et plasma 0759
- Météorologie 0608
- Optique 0752
- Particules (Physique nucléaire) 0798
- Physique atomique 0748
- Physique de l'état solide 0611
- Physique moléculaire 0609
- Physique nucléaire 0610
- Radiation 0756

Statistiques 0463

Sciences Appliqués Et Technologie

Informatique 0984
Ingénierie
- Généralités 0537
- Agricole 0539
- Automobile 0540
- Biomédicale 0541
- Chaleur et ther modynamique 0348
- Conditionnement (Emballage) 0549
- Génie aérospatial 0538
- Génie chimique 0542
- Génie civil 0543
- Génie électronique et électrique 0544
- Génie industriel 0546
- Génie mécanique 0548
- Génie nucléaire 0552
- Ingénierie des systèmes 0790
- Mécanique navale 0547
- Métallurgie 0743
- Science des matériaux 0794
- Technique du pétrole 0765
- Technique minière 0551
- Techniques sanitaires et municipales 0554
- Technologie hydraulique 0545

Mécanique appliquée 0346
Géotechnologie 0428
Matières plastiques (Technologie) 0795
Recherche opérationnelle 0796
Textiles et tissus (Technologie) 0794

PSYCHOLOGIE
Généralités 0621
Personnalité 0625
Psychobiologie 0349
Psychologie clinique 0622
Psychologie du comportement 0384
Psychologie du développement 0620
Psychologie expérimentale 0623
Psychologie industrielle 0624
Psychologie physiologique 0989
Psychologie sociale 0451
Psychométrie 0632

UNIVERSITÉ DE MONTRÉAL

ÉCOLE POLYTECHNIQUE DE MONTRÉAL

Cette thèse intitulée:

MILLIMETER-WAVE DIRECT DIGITAL RECEIVER

présentée par: LI Ji

en vue de l'obtention du diplôme de: Philosophiae Doctor

a été dûment acceptée par le jury d'examen constitué de:

M. GIROUX Marcel, M.Sc.A, président

M. BOSISIO Renato G, M.Sc.A, membre et directeur de recherche

M. WU Ke, Ph.D., membre et co-directeur de recherche

M. HOULE Jean-Louis, Ph.D., membre

M. DELISLE Gilles Y, Ph.D., membre

To my parents, Bing, and Daiwei

Acknowledgment

I would like to thank professor Renato G. Bosisio, my research director, for his constant encouragement and support. Kind help from professor Ke Wu was very much appreciated. I also benefited from the discussions with professor Jean-Louis Houle and professor Mohamad Sawan.

My acknowledgment also goes to: David Maurin and Y. Xu for their help in the six-port MMIC/MHMIC circuit design; J. Gauthier for the fabrication and packaging of the circuits; and René Archambault for the HP workstation management and other kind help. The collaboration with Fabrice Lebegue on clock recovery algorithms was also an enjoyable experience.

Finally, I would like to acknowledge the chairman of my jury, professor Marcel Giroux, professor Iraj Najafi and the external jury member, professor Gilles Y. Delisle for their precious comments and time.

RÉSUMÉ

Dans les vingt dernières années, la technologie du 'six-port' a été développée en tant que nouveau moyen d'effectuer des mesures micro-ondes vectorielles mono ou multi-port. Au lieu de convertir les fréquences comme dans un analyseur de réseau conventionnel, un analyseur de réseau à jonction six-port mesure le rapport vectoriel des ondes réfléchies/sortantes en mesurant une série de niveaux de puissances micro-ondes à quatre de ses six ports. Une procédure adéquate de calibration préléminaire assure une précision du même ordre, voire meilleure, que les analyseurs de réseaux micro-ondes automatiques courant comme le Hewlett-Packard 8510 et le Wiltron 360.

Une bande d'ondes millimétriques, telle que la bande de 38 GHz, est devenue intéressante pour les services des communications personnelles (PCS) dans les dernières années du fait de la disponibilité d'un large spectre et d'une excellente possibilité de réutilisation des fréquences en différents endroits. Malheureusement, le coût des récepteurs pour les ondes millimétriques est généralement beaucoup plus élevé que celui des récepteurs pour les plus basses fréquences micro-ondes. C'est pour cela que la réduction du coût devient un facteur clé dans le succès du développement des PCS aux ondes millimétriques.

Cette thèse décrit le travail de génèse et la validation d'un nouveau type de récepteur numérique. Un résumé de la contribution originale faite par l'auteur en collaboration étroite avec son directeur de recherche, le professor Renato G. Bosisio:

1. Génèse d'un nouveau récepteur digital millimétrique utilisant le concept du discriminant en amplitude/phase/fréquence six-port permettant la détection non-cohérente par l'utilisation des jonctions six-port et proposition du nouveau type de récepteur numérique six-port basé sur le discriminant six-port.

2. La simulation par ordinateur des performances du récepteur numérique direct six-port, comparée à celles d'un récepteur I-Q (Inphase-Quadrature) conventionnel, a prouvé que le nouveau recepteur six-port atteint des performances comparables à celles d'un récepteur digital super-hétérodyne; elles sont de loin supérieures à celles d'un récepteur numérique direct IQ. On a obtenu une bonne corrélation entre la simulation par ordinateur et les résultats des mesures.

3. La validation par les mesures du récepteur six-port a prouvé la faisabilité de ce nouveau type de récepteur. Un montage de démonstration a été réalisé pour l'affichage des constallations et pour les mesures en temps réel du taux d'erreur.

4. Une nouvelle procédure de calibration a été établie: la calibration bi-fréquentielle pour récepteurs six-port. Cette procédure de calibration utilise le signal reçu comme source de calibration. Aucun standard externe ni équipement spécifique n'est requis;

La calibration du recépteur peut se réaliser lors de son opération ainsi on atteint la même précision de calibration qu'avec une méthode utilisant des standards externes.

5. Une méthode utilisant une référence de phase informatisée (référence par calcul) pour la détection PSK (Phase Shift Keying) cohérente a été développée. Cette méthode élimine la nécessité d'une synchronisation instantannée en phase de l'oscillateur local, ce qui est très difficile aux fréquences millimétriques.

6. Une nouvelle méthode de linéarisation du détecteur de puissance à diode a été développée: la calibration bifréquentielle du détecteur.

En plus du travail mentionné ci-haut, d'important efforts ont été consacrés pour:

1. le développement de tous les algorithmes de traitement reliés au récepteur numérique à l'aide du langage C;

2. la réalisation et le déverminage des logiciels et du montage du système et de mesure en temps réel;

3. La conception, la réalisation et la caractérisation des circuits six-port en technologies MHMIC/MMIC.

A la suite du travail décrit ci-dessus, il est possible de conclure que le récepteur numérique à six-port offre une alternative économique intéressante par rapport aux récepteurs super-hétérodynes conventionnels pour différents systèmes de communication de petite et de moyenne capacité. Cependant, le nouveau récepteur six-port doit être étudié avec plus de précision comporte des limites par rapport aux systèmes super-hétérodynes notamment pour des applications où la contre-interférence et la plage dynamique sont des préoccupations de premier plan.

ABSTRACT

Six-port technology has been under development in the past twenty years as a new way to perform vector single/multi-port microwave network measurements. Instead of performing frequency conversion as in a conventional vector microwave network analyzer, the six-port network analyzer acquires the vector ratio of reflected/outgoing waves by reading a set of microwave power levels at four of its six ports. A convenient calibration procedure ensures the same order or even better accuracy than conventional automatic vector microwave network analyzers such as the HP8510 and Wiltron 360.

In recent years, the millimeter wave band such as 38GHz band has become an attractive choice to personal communication services (PCS) backhaul in recent years due to vast spectrum availability and excellent frequency reusability. Unfortunately the cost of mm-wave receivers are in general much higher than its low-end microwave counterparts. Therefore cost reduction becomes a key factor in its competitiveness.

This thesis describes work on the proof-of-concept of a new digital receiver using six-port technology. Following is a summary of the original contributions made by the author in close collaboration with his research director, professor Renato G. Bosisio:

1. Innovation of the concept of Six-Port amplitude/phase/frequency discriminator (SPD), which enables non-coherent detection and the proposal of the new six-port direct digital millimeter-wave receiver (DMR) scheme based on the SPD concept.

2. Computer simulation of the performance of the proposed DMR in comparison with conventional I-Q receiver. The new DMR achieves comparable performance as super-heterodyne digital receiver, and is much superior to I-Q direct conversion digital receiver. A good agreement between computer simulation and measurement results has been achieved.

3. Measurements of the six-port receiver to validate the feasibility of the new scheme. Set-up of a demonstration system for real time bit error rate measurement and constellation display. This system is capable of dealing with both coherent and differential PSK modulations up to 16QAM.

4. Development of a new calibration procedure: Dual-tone calibration specially for DMR. The new calibration procedure uses the received signal as the source of calibration and requires no external standard or special hardware. Same order of accuracy as standard six-port calibration methods is achieved.

5. Development of a 'soft phase reference' method of coherent PSK detection.

6. Development of a new method for linearization of the diode power detector: Dual-tone diode detector calibration.

In addition to the work mentioned above, great efforts have also been made to:

1. Implement the digital processing algorithms for DMR in the C language.

2. Setup and debug (both hardware and software) the real-time demonstration/ measurement system.

3. Design and measure the six-port circuits of the DMR using MHMIC technology and initiate similar work for MMICs.

It is concluded that the new six-port DMR promises to be a cost-effective alternative to the conventional super-heterodyne digital receiver in various small or medium capacity communication systems. However, when a very large dynamic range (e.g. >100dB) is desired, the resolution of the analog to digital converters (ADCs) becomes a major limiting factor.

摘　要

在过去二十年里六端口技术作为一种单／多端口微波网络测量分析的新技术得到了充分的发展。六端口网络分析仪通过直接读取一组四个功率电平获取反射波／入射波矢量关系，而不必象传统矢量微波网络分析仪那样将信号转换到中频再处理。通过简单的校准之后六端口网络分析仪可获得与标准自动网络分析仪（例如HP8510 和 Wiltron360）同等甚至于更高的测量精度。

近年来毫米波段（例如38GHz）以其宽广的频谱资源和极好的频率再利用率成为未来个人通信系统的理想频段。遗憾的是目前毫米波接收机的成本远较低频段微接收机为高，因此毫米波个人通信系统成败的关键在于降低成本。

本论文讨论一种新形数字接收机方案：低成本六端口毫米波直接接收机的提出和验证。以下列出作者与其指导教授 Renato G. Bosisio 密切合作做出的开创性贡献：

1. 提出了六端口幅度/相位/频率鉴别器概念，将六端口应用推广至非相干检测，并在此基础上提出了六端口毫米波直接接收机方案。
2. 通过计算机模拟对六端口接收机和传统正交式接收机进行了性能比较，证明六端口接收机可获得与超外差接收机相当和远优于直接正交式接收机的性能。计算机模拟和实际测试的结果相吻合。
3. 通过实际测试验证了新方案的可行性。建立了可实时进行误码率测量和星座图显示的演示系统，此系统可进行高达8PSK的相干或非相干解调。

4. 提出了一种新校准方法：双载波校准。此方法利用接收到的载波做为校准源而不需任何外接标准和专用硬件。并利用此方法取得了与标准方法相同的精度。
5. 提出一种相干解调的"软参考相位"方法．此方法不需对本振源进行实时相位同步。
6. 提出二极管功率检波器线性化新方法：双载波法。

除了以上之外，作者亦致力于如下工作：

1. 用C语言实现了所有接收机的DSP算法。
2. 建立和调试实时测量／演示系统（硬件和软件）。
3. 薄膜集成和单片集成六端口电路的设计和测试。

通过以上工作证明六端口直接数字接收机为现有各种通信系统中使用的中小容量超外差数字接收机提供了一种廉价替代方案。另一方面，在一些对抗干扰和动态范围性能要求特别高的应用中，此种方案显示出其不足之处。

Récepteur Numérique Direct En Bande Millimétrique
(Condensé en français)

1. Introduction

Un nouveau récepteur numérique a été conçu de manière à réduire la complexité et le coût d'un récepteur numérique millimétrique. Il est bien connu que l'augmentation de la fréquence d'un signal cause une diminution proportionnelle de la longueur d'onde, et ceci rend très difficile la réalisation d'un coupleur hybride présentant une précision acceptable en amplitude et en phase. Bien que des circuits additionnels puissent être utilisés pour compenser les débalancements en phase et en amplitude des hybrides I-Q, cette méthode est évidemment complexe et la stabilité à long terme de tels circuits peut être mise en question.

La technologie des six-port a d'abord été développée comme une nouvelle méthode de measure automatisées de circuits micro-ondes. Le rapport vectoriel des ondes incidentes aux deux ports d'entrée peut être obtenu à partir des mesures de puissance aux quatre autres ports. Il n'est donc pas nécessaire de convertir le signal à une fréquence intermédiaire (IF) pour réaliser une comparaison en phase. Une propriété très intéressante des six-port est la possibilité d'éliminer les erreurs de mesure par une procédure de calibration appropriée.

2. Concept du nouveau récepteur numérique

2.1) Le discriminant en amplitude/phase/fréquence six-port:

La jonction six-port est un circuit fonctionnant aux fréquences micro-ondes et millimétriques, composé de dispositifs passifs comme des diviseurs de puissance et des coupleurs, et comportant deux ports d'entrée. La relation vectorielle entre les signaux d'entrées a_1 et a_2 peut être calculée par les puissances P_i's avec:

$$\frac{a_1}{a_2} = A = |A| \cdot e^{j\varphi} = \frac{\sum_{i=1}^{4} (R_i + jI_i) \cdot P_i}{\sum_{i=1}^{4} D_i \cdot P_i} \qquad (0.1)$$

où R_i, I_i et D_i sont des constantes complexes obtenues lors de la calibration.

La différence de fréquence Δf entre les sigaux d;entrées peut être obtenue en mesurant la vitesse de rotation de A:

$$\Delta f = \frac{d\varphi}{dt} \qquad (0.2)$$

En conséquence, une jonction six-port peut être utilisée comme un discriminant en amplitude, en phase et en fréquence. L'avantage d'un discriminant six-port par rapport aux circuits I-Q conventionnels est que les imperfections des composants en phase et en amplitude peuvent être éliminées. Ainsi, est-il possible d'effectuer une détection directe aux fréquences micro-ondes.

2.2) Récepteur numérique direct utilisant le six-port:

Le schéma bloc du nouveau type de récepteur est montré à la figure 0.1. Un filtre passe-bande et un amplificateur à faible bruit éliminent le bruit hors bande et augmentent ainsi la sensibilité. La démodulation est réalisée directement aux fréquences millimétriques ou micro-ondes par le discriminant six-port plutôt que par un démodulateur I-Q comme dans les récepteurs digitaux conventionnels. Ce six-port est utilisé pour détecter l'amplitude relative, la phase relative et la fréquence relative du signal par rapport à l'oscillateur local. Des diodes Schottky sont utilisées comme détecteurs de puissance. Le filtre passe-bas situé après les diodes permet d'éliminer l' "anti-aliasing" et de mettre en forme les impulsions. Une unité de traitement numérique du signal exécute les calculs nécessaires à la réalisation de la démodulation en plus de la restitution de la porteuse et de l'horloge.

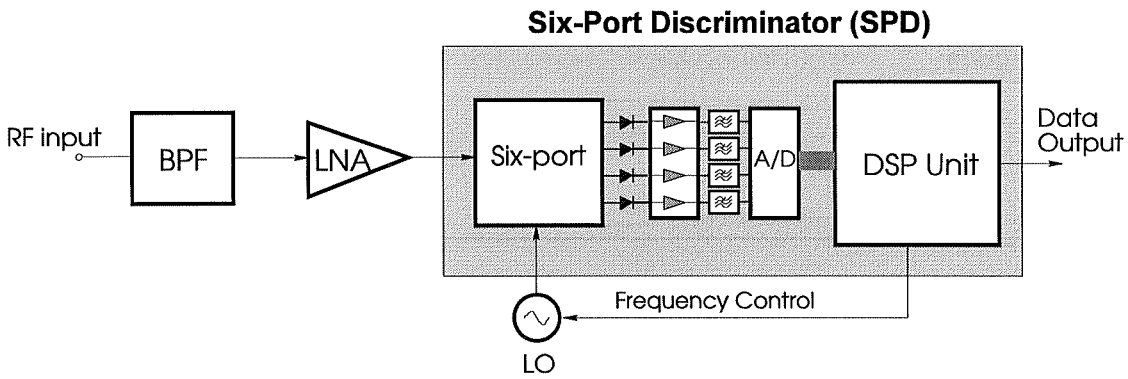

Figure 0.1 Diagramme bloc du récepteur numérique millimétrique avec son unité six-port.

Le recépteur six-port proposé excelle dans les aspects suivants:

Premièrement, les contraintes de fabrication sont grandement réduites. Un algorithme de calibration auxilliaire (voir le chapître 3) accomplit la calibration nécessaire du six-port à partir du signal reçu lui-même; il surveille en temps réel les opérations et met à jour les coefficients de calibration.

Deuxièmement, la présence d'une unité de traitement numérique du signal offre une grande flexibilité de fonctionnement au récepteur. Les détections différentielles et cohérentes sont toutes deux possibles (voir Chaptre 5). De plus, les fonctions de démodulation et de décodage peuvent être combinées pour augmenter plus avant l'intégration du système.

Troisièmement, le récepteur six-port proposé possède des propriétés uniques comme:

a) l'immunité à l'interférence des canaux voisins;

b) une variation dans le niveau du signal d'entrée: la plage dynamique du récepteur étant principalement fonction de la résolution du convertiseur analogique-numérique;

c) un fonctionnement large-bande possible avec un six-port de conception large-bande: la vitesse maximale de transmission des données n'étant limitée que par le convertisseur A/D et par l'unité de DSP.

3. Simulation informatique des performances du recépteur six-port

Des simulations informatiques du recépteur six-port ont été réalisées une première fois en utilisant des programmes "maison" puis en utilisant le SPW (Signal Processing Worksystem) du groupe Alta. Le logiciel MDS de HP a été utilisé pour la conception et l'analyse des composants micro-ondes du recépteur comme la jonction six-port, les diodes détectrices de puissance, les amplificateurs faible bruit et les filtres passe-bas.

3.1) Le six-port du recépteur:

La figure 0.2 illustre un modèle de base pour le discriminant six-port correspondant au diagramme-bloc de la figure 0.1.

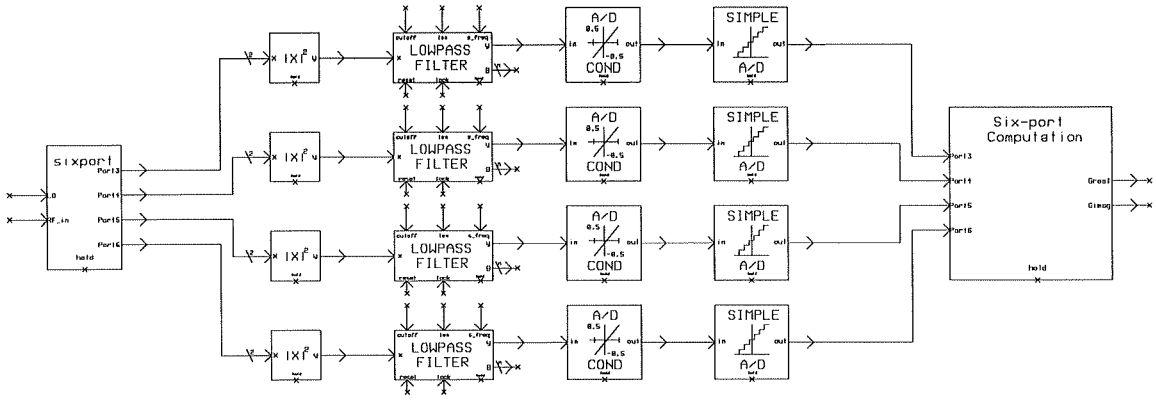

Figure 0.2. Le modéle de six-port du récepteur (excluant les filtres RF et l'amplificateur faible bruit) utilisé avec SPW.

3.2) Quelques résultats de simulation informatique

3.2.1) La dégradation des performances du récepteur dû aux imperfections des composants:

En utilisant le taux d'erreur par bit "bit error rate" (BER) comme une mesure directe des performances du récepteur et en considérant un récepteur parfait, la seule quantité restant à considérer est le bruit. La figure 0.3 montre le BER en fonction de E_b/N_0 en présence de différents ordres d'imperfection en phase et en amplitude.

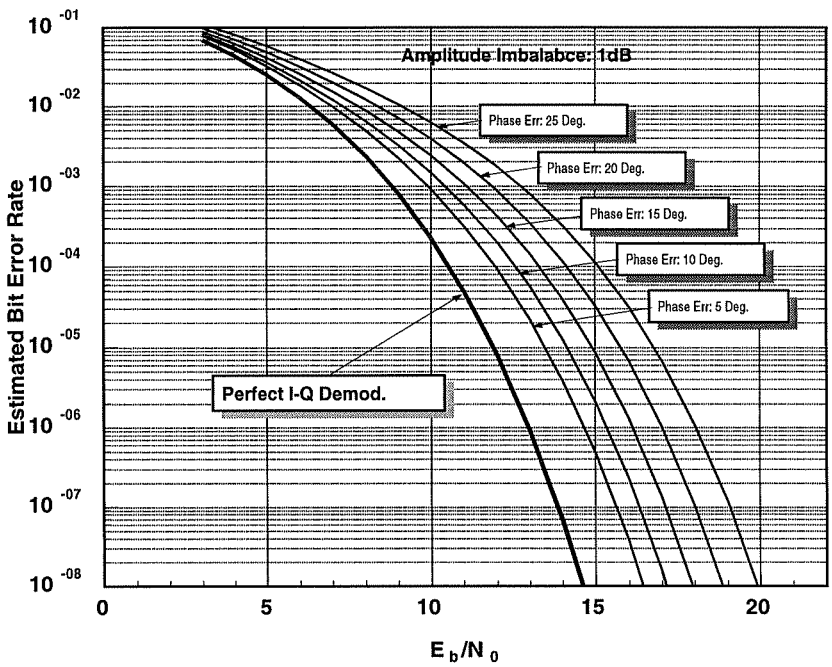

Figure 0.3 Dégradation du BER d'un récepteur 4PSK typique en présence d'une erreur de phase et d'amplitude dans un circuit démodulation.

3.2.2) Plage d'opération dynamique

Une particularité du récepteur six-port est sa tolérance aux variations dans le niveau du signal d'entrée. Le niveau minimum de signal permettant la détection dépend de la résolution des convertisseurs A/D. La figure 0.4 illustre l'erreur en phase du discriminant six-port en fonction du niveau du signal d'entrée. Pour une erreur limite de 1 dB/5°, les plages dynamiques sont respectivement de 70dB, 50dB et 20dB pour des convertisseurs A/D de 16, 12 et 8 bits.

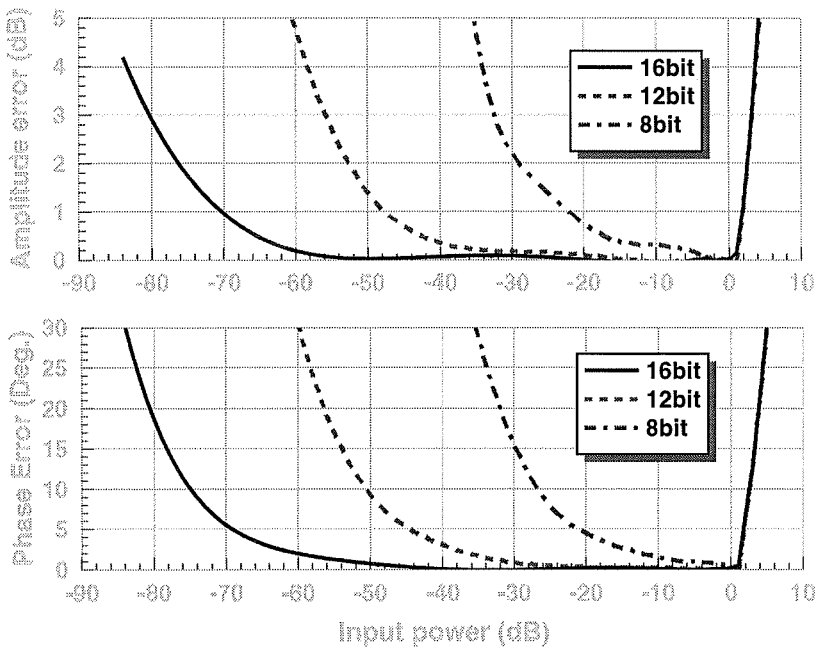

Figure 0.4 Erreurs en phase et en amplitude en fonction de la puissance d'entrée.

3.2.3) Précision du discriminant six-port en présence d'imperfection de quadrature:

La figure 0.5 illustre la précision d'un discriminant six-port présentant des imperfections de quadrature dans son circuit. La précision d'un démodulateur I-Q est aussi montrée en tant que référence. Il est clairement visible que le discriminant six-port élimine la plupart des erreurs.

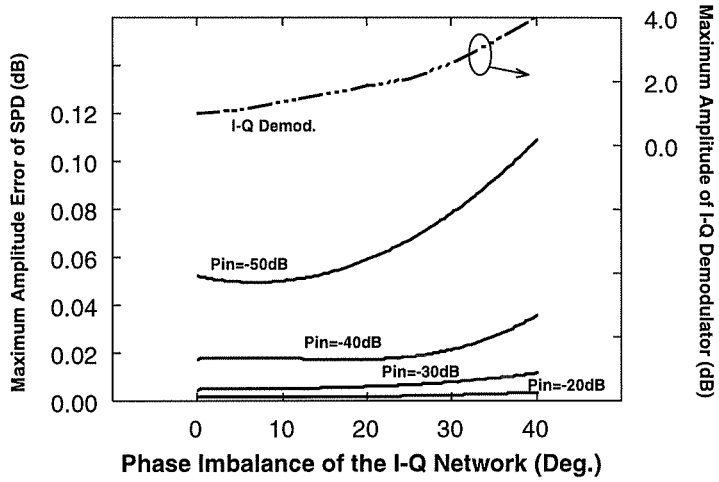

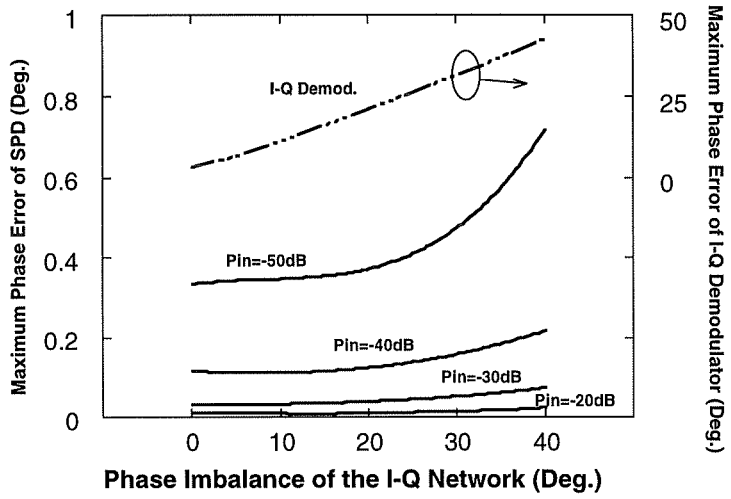

Figure 0.5 Comparaison de la précision d'un discriminant six-port et d'un démodulateur I-Q en présence d'imperfections.

3.3) Mesure du recépteur six-port

Des mesures pour la validation du concept et des simulations informatiques ont été réalisées afin de vérifier la faisabilité du recépteur proposé. La figure 0.6 montre les BER mesurés et calculés en fonction du niveau du signal d'entrée.

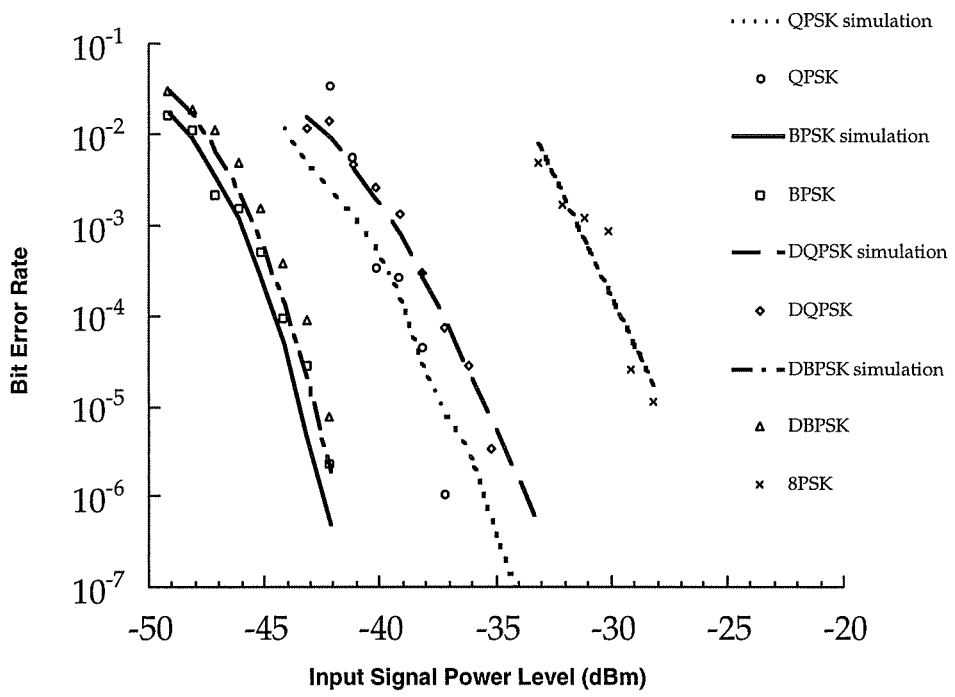

Figure 0.6 BER mesurés et calculés pour le récepteur six-port.

4. Calibration automatique du recépteur

La calibration offre au six-port la possibilité de compenser ses défauts de fabrication. Cependant, les méthodes de calibration traditionnelles demandent le branchement et le débranchement de standard micro-ondes externes, ce qui ne peut être accompli dans le cadre d'une application récepteur six-port. Une méthode de calibration bi-fréquentielle est proposée par laquelle la calibration est réalisée en injectant un signal micro-onde différent de celui de la source locale dans le port d'entrée du RDM.

Tableau 0. 1

Measured reflection coefficients using HP8510 vector network analyzer and six-port reflectometer calibrated by the use of conventional 13-std method and dual-tone method.

	26.5 GHz				33 GHz				40 GHz			
	HP8510	13-std	cw 3-level	cw 2-level	HP8510	13-std	cw 3-level	cw 2-level	HP8510	13-std	cw 3-level	cw 2-level
#1	0.973∠ -177.6°	1.043∠ -179.5°	1.010∠ 180.0°	0.968∠ -179.1°	0.997∠ -178.0°	0.980∠ 179.5°	0.978∠ 178.7°	0.970∠ 179.3°	0.985∠ 178.5°	0.990∠ 178.2°	0.996∠ 176.8°	0.998∠ 175.7°
#2	0.999∠ 91.9°	0.996∠ 88.5°	0.998∠ 88.3°	0.998∠ 88.2°	0.969∠ -103.0°	0.979∠ -107.6°	0.980∠ -107.3°	0.980∠ -107.6°	0.975∠ 36.7°	0.969∠ 36.9°	0.972∠ 36.8°	0.972∠ 36.9°
#3	0.962∠ -78.3°	0.975∠ -77.4°	0.973∠ -77.3°	0.973∠ -77.3°	0.985∠ 80.4°	0.982∠ 79.8°	0.983∠ 80.2°	0.982∠ 79.8°	0.972∠ -133.8°	0.968∠ -134.2°	0.971∠ -133.8°	0.974∠ -133.7°
#4	0.049∠ -121.5°	0.032∠ -148°	0.029∠ -156°	0.026∠ -153°	0.038∠ -77.0°	0.019∠ -46°	0.020∠ -52°	0.019∠ -51°	0.025∠ -93.2°	0.025∠ -109°	0.026∠ -95°	0.026∠ -95°
#5	0.422∠ 104.0°	0.425∠ 102.5°	0.427∠ 101.7°	0.428∠ 101.5°	0.523∠ 31.8°	0.554∠ 32.6°	0.546∠ 32.1°	0.549∠ 32.3°	0.413∠ -66.9°	0.416∠ -69.8°	0.418∠ -69.1°	0.420∠ -69.2°
#6	0.218∠ 89.3°	0.212∠ 89.5°	0.215∠ 89.5°	0.218∠ 88.6°	0.277∠ 54.1°	0.289∠ 53.3°	0.287∠ 53.1°	0.289∠ 52.8°	0.255∠ -75.6°	0.266∠ -77.3°	0.268∠ -76.9°	0.270∠ -76.1°
#7	0.066∠ -38.9°	0.091∠ -39.7°	0.093∠ -37.0°	0.092∠ -35.9°	0.061∠ -175.0°	0.048∠ 178.0°	0.049 -178.0°	0.049∠ -178.0°	0.100∠ -16.5°	0.113∠ -23.3°	0.116∠ -23.0°	0.114∠ -23.0°
#8	1.016∠ 95.7°	1.000∠ 90.7°	1.001∠ 90.7°	0.999∠ 90.3°	0.982∠ -99.8°	0.983∠ -103.9°	0.985∠ -103.6°	0.985∠ -103.5°	0.988∠ 39.2°	0.972∠ 39.7°	0.976∠ 38.8°	0.980∠ 39.4°

5. Considérations sur la conception d'un six-port

Parmi les différentes technologies disponibles, la technologie MMIC (Monolithic Microwave Integrate Circuit) et la technologie MHMIC (Miniaturized Hybrid Microwave Integrated Circuit) offrent les meilleures solutions en ce qui a trait à la taille

des circuits, à leur versatilité et à leur coût pour les systèmes futurs de communications personnelles utilisant les ondes millimétriques. On ne saurait trop insister sur le fait que les circuits du RDM doivent être de taille minimale et d'une grande sensibilité. En conséquence les règles suivantes sont donc dégagées: 1) minimiser les dimensions totales du circuit, 2) maximiser l'isolation entre le port d'entrée RF et le port LO afin de réduire les fuites du signal LO vers l'antenne, 3) minimiser les pertes d'insertion entre le port RF et et les détecteurs de puissance pour augmenter la sensibilité, 4) le choix du type de circuit (en incluant les diodes détectrices de puissance) doit prendre en compte les limites acceptables en température afin de résister aux contraintes environnementales.

6. Réalisation d'une détection PSK cohérente sans la récupération complète de la porteuse

Il y a deux types de techniques de démodulation: cohérente et incohérente (ou différentielle). En général, une détection différentielle implique un récepteur plus simple tandis que la détection cohérente est plus performante au niveau des erreurs de transmission.

Une méthode simple pour établir une référence de phase informatisée (par calcul) nécessaire pour la détection cohérente a été développée. Pour cette méthode, seul un contrôle automatique de la fréquence est nécessaire pour l'oscillateur local.

Un signal PSK reçu est décrit par l'expression suivante:

$$s(t) = A_c \cos(2\pi f_0 t + \Phi(t,a)) \tag{0.3}$$

Supposons que la fréquence LO soit très proche de la fréquence de la porteuse reçue et que la synchronisation entre l'horloge et le symbole soit réussie. Les échantillons détectés par le récepteur six-port sont décrits par:

$$s(i) = A_c \cos(2\pi \Delta f t_i + 2\pi \cdot \frac{a_i}{4} + \phi_0) \tag{0.4}$$

où $\Delta f = f_c - f_{LO}$, et pour simplifier le problème, seulement un échantillion est utilisé pour chaque symbole.

On peut observer à partir de (0.3) que la présence d'un Δf résiduel provoque la rotation de la constellation échantillonnée à une vitesse donnée par $2\pi\Delta f t$. Un registre de type FIFO (First In, First Out) de longueur N est constitué et chaque θ_i pour lequel $a_i = 0$ y est inséré. Posons la référence de phase P_0 comme la moyenne des θ_i du registre.

$$P_0 = \frac{\sum_{j=0}^{N-1} \theta_i}{N} \tag{0.5}$$

Evidemment, P_0 suivra le terme $2\pi\Delta ft$ et les φ_i deviendront relativement constants peu importe Δf. De cette façon, une fois que le contexte de synchronisation détecté, les a_i vont être convertis aux bits correspondants en conformité avec la fin de la transmission. Cette méthode s'applique ¸à toutes les modulations PSK et même aux modulations QAM.

7. Conclusions

La recherche décrite dans cette thèse est principalement rattachée à la validation du concept d'un nouveau type de récepteur numérique. Cette recherche implique différents champs de recherche active comme celui des micro-ondes, ceux des communications, des circuits numériques, du traitement numérique du signal et du génie logiciel.

Le travail de recherche décrit dans cette thèse a permis de créer des liens entre une technologie six-port sophistiquée et le vaste domaine des systèmes de télécommunications. Il a été prouvé, à l'aide de simulations informatiques et de mesures, que le nouveau récepteur numérique direct en bande millimétrique est technologiquement réaliste et économiquement réalisable. Ce travail a établi un point de départ pour une recherche détaillée et un développement commercial subséquents.

Table of Contents

ACKNOWLEDGMENT V

RÉSUMÉ VI

ABSTRACT X

摘　要 IX

RÉCEPTEUR NUMÉRIQUE DIRECT EN BANDE MILLIMÉTRIQUE (CONDENSÉ EN FRANÇAIS) XV

1. INTRODUCTION XV

2. CONCEPT DU NOUVEAU RÉCEPTEUR NUMÉRIQUE XVI

2.1) Le discriminant en amplitude/phase/fréquence six-port: XVI

2.2) Récepteur numérique direct utilisant le six-port: XVII

3. SIMULATION INFORMATIQUE DES PERFORMANCES DU RECÉPTEUR SIX-PORT XIX

3.1) Le six-port du récepteur XIX

3.2) Quelques résultats de simulation informatique XX

3.2.1) La dégradation des performances du récepteur dû aux imperfections des composants: XX

3.2.2) Plage d'opération dynamique XXI

3.2.3) Précision du discriminant six-port en présence d'imperfection de quadrature.XXII

3.3) Mesure du recépteur six-port..... *XXIV*

4. CALIBRATION AUTOMATIQUE DU RECÉPTEUR XXV

5. CONSIDÉRATIONS SUR LA CONCEPTION D'UN SIX-PORT XXV

6. RÉALISATION D'UNE DÉTECTION PSK COHÉRENTE SANS LA RÉCUPÉRATION COMPLÈTE DE LA PORTEUSE XXVI

7.CONCLUSIONS XXVIII

TABLE OF CONTENTS..... **XXIX**

LIST OF TABLES..... **XXXVI**

LIST OF FIGURES..... **XXXVII**

LIST OF ACRONYMS AND ABBREVIATIONS..... **XLII**

CHAPTER 1. INTRODUCTION..... **1**

CHAPTER 2. SIX-PORT DIRECT DIGITAL RECEIVER: CONCEPT AND SIMULATION..... **10**

ARTICLE: COMPUTER AND MEASUREMENT SIMULATION OF A NEW DIGITAL RECEIVER OPERATING DIRECTLY AT MILLIMETER-WAVE FREQUENCIES 12

ABSTRACT 12

2.1 INTRODUCTION 13

2.2 SIX-PORT DISCRIMINATOR (SPD) 17

2.3 COMPUTER SIMULATION: PERFORMANCE OF SPD VERSUS I-Q DEMODULATOR 19

2.3.1 Circuit Model of Six-Port *19*

2.3.2 Degradation of Receiver Performance Due to the Hardware Imperfections *20*

2.3.3 Operating Dynamic Range as a Function of the ADC Resolution *22*

2.3.4 Accuracy of SPD in the Presence of Quadrature Imbalances *25*

2.3.5 Effect of DC Offset on SPD Accuracy *28*

2.3.6 Effect of Adjacent Channel Interferences *30*

2.3.7 Bit Error Rate (BER) Performance *30*

2.4 MEASUREMENT SIMULATION OF THE DMR 31

2.4.1 Constellation Diagram *32*

2.4.2 Bit Error Rate Measurements *34*

2.5 CONCLUSION 36

ACKNOWLEDGMENT 36

REFERENCES 37

CHAPTER 3. ADAPTIVE CALIBRATION OF THE SIX-PORT DIRECT DIGITAL RECEIVER 43

ARTICLE: DUAL-TONE CALIBRATION OF SIX-PORT JUNCTION AND ITS APPLICATION TO THE SIX-PORT DIRECT DIGITAL MILLIMETRIC RECEIVER 45

ABSTRACT 45

3.1 INTRODUCTION 46

3.2 DUAL-TONE W-PLANE CALIBRATION OF THE SIX-PORT 49

3.2.1 W-plane calibration 49

3.2.2 Using a second carrier 50

3.2.3 Dual-tone sampling algorithm 54

3.2.4 Waveform smoothing 57

3.3 DUAL-TONE ERROR-BOX CALIBRATION OF THE SIX-PORT DMR 59

3.3.1 Error-box calibration 59

3.3.2 Necessity of error-box calibration for the six-port DMR 60

3.3.3 Dual-tone error-box calibration for DMR 61

3.4 RESULTS 64

3.5 CONCLUSION 69

ACKNOWLEDGMENT 69

REFERENCES 70

CHAPTER 4. SIX-PORT CIRCUIT DESIGN AND MODELING 72

4.1 GENERAL CONSIDERATIONS ON SIX-PORT CIRCUIT DESIGN 72

4.2 SIX-PORT CIRCUIT CONFIGURATION 74

4.3 IMPLEMENTATION OF A RECEIVER USING FIVE-PORT CIRCUITS 76

4.4 OPTIMUM DESIGN OF THE FIVE-PORT CIRCUITS 77

4.5 20 GHZ MHMIC FIVE-PORT CIRCUIT DESIGN 82

4.6 MODELING OF THE SIX-PORT 85

ARTICLE: MODELING OF THE SIX-PORT DISCRIMINATOR USED IN A MICROWAVE DIRECT DIGITAL RECEIVER 86

Abstract 86

4.6.1 Introduction 86

4.6.2 SPD Model 88

4.6.3 Verification of the Model 93

4.6.4 Conclusion 93

References 94

CHAPTER 5. RECEIVER ALGORITHMS 95

5.1 INTRODUCTION 95

5.2 DIGITAL FILTERS 97

5.3 SIX-PORT COMPUTATION 97

5.4 DECISION 100

5.5 AUTOMATIC FREQUENCY CONTROL (AFC) 101

5.6 PHASE REFERENCE RECOVERY 102

ARTICLE: A NEW DIRECT DIGITAL RECEIVER PERFORMING COHERENT PSK RECEPTION 103

Abstract 103

5.6.1 Introduction 104

5.6.2 Description of the Method 105

5.6.3 Results 108

5.6.4 Conclusion 111

References 111

CHAPTER 6. LINEARIZATION OF SCHOTTKY DIODE DETECTORS 112

6.1 INTRODUCTION 112

6.2 DIODE MODEL 113

6.2.1 Lookup Table 114

6.2.2 Hoer's model 114

6.2.3 Chen's model 115

6.3 PREVIOUSLY REPORTED LINEARIZATION METHODS 116

6.3.1 Direct calibration 116

6.3.2 Use a calibrated precision attenuator *117*

6.3.3 Repeatable two-position step attenuator *117*

6.4 THE NEW DUAL-TONE LINEARIZATION METHOD 118

ARTICLE: A SIMPLE DUAL-TONE CALIBRATION OF DIODE DETECTORS ... 119

Abstract *119*

6.4.1 Introduction *120*

6.4.2 Linearization Method *121*

6.4.3 Results *123*

6.4.4 Conclusion *126*

References *126*

CHAPTER 7. CONCLUSIONS **127**

REFERENCES **131**

APPENDIX 1. A COLLISION AVOIDANCE RADAR USING SIX-PORT PHASE/FREQUENCY DISCRIMINATOR (SPFD) **138**

APPENDIX 2. A SIX-PORT DIRECT DIGITAL MILLIMETER WAVE RECEIVER **142**

List of Tables

CONDENSÉ EN FRANÇAIS:

TABLEAU 0.1 XXV

CHAPTER 3:

TABLE 3.1. CALIBRATION COEFFICIENTS USING CONVENTIONAL 13-STD METHOD AND DUAL-TONE METHOD. 67

TABLE 3.2. MEASURED REFLECTION COEFFICIENTS USING HP8510 VECTOR NETWORK ANALYZER AND SIX-PORT REFLECTOMETER CALIBRATED BY THE USE OF CONVENTIONAL 13-STD METHOD AND DUAL-TONE METHOD. 68

List of Figures

CONDENSÉ EN FRANÇAIS:

FIGURE 0.1 DIAGRAMME BLOC DU RÉCEPTEUR DIGITAL MILLIMÉTRIQUE AVEC SON UNITÉ SIX-PORT. XVII

FIGURE 0.2. LE MODÉLE DE SIX-PORT DU RÉCEPTEUR (EXCLUANT LES FILTRES RF ET L'AMPLIFICATEUR FAIBLE BRUIT) UTILISÉ AVEC SPW. XIX

FIGURE 0.3 DÉGRADATION DU BER D'UN RÉCEPTEUR 4PSK TYPIQUE EN PRÉSENCE D'UNE ERREUR DE PHASE ET D'AMPLITUDE DANS UN CIRCUIT DÉMODULATION. XX

FIGURE 0.4 ERREURS EN PHASE ET EN AMPLITUDE EN FONCTION DE LA PUISSANCE D'ENTRÉE. XXI

FIGURE 0.5 COMPARAISON DE LA PRÉCISION D'UN DISCRIMINANT SIX-PORT ET D'UN DÉMODULATEUR I-Q EN PRÉSENCE D'IMPERFECTIONS. XXIII

FIGURE 0.6 BER MESURÉS ET CALCULÉS POUR LE RÉCEPTEUR SIX-PORT. XXIV

CHAPTER 1:

FIGURE 1.1 FUNCTIONAL BLOCK DIAGRAM OF A TYPICAL SUPER-HETERODYNE DIGITAL RECEIVER. 5

FIGURE 1.2 FUNCTIONAL BLOCK DIAGRAM OF A TYPICAL DIRECT DIGITAL RECEIVER. 6

CHAPTER 2:

FIGURE 2.1. BLOCK DIAGRAM OF THE NEW DIGITAL MILLIMETRIC RECEIVER (DMR) WITH THE SIX-PORT DISCRIMINATOR (SPD). 16

FIGURE 2.2. A SIX-PORT FUNCTIONS AS A MICROWAVE VECTOR VOLTMETER AS A_1/A_2 IS CALCULATED FROM P_i'S. 17

FIGURE 2.3. BLOCK DIAGRAM OF THE SIX-PORT MODEL USED IN THE SIMULATION OF SPD. 20

FIGURE 2.4. BER PERFORMANCE OF A QPSK RECEIVER IN THE PRESENCE OF AMPLITUDE AND PHASE IMBALANCE OF THE I-Q DEMODULATOR. 22

FIGURE 2.5. MAXIMUM AMP/PHASE ERRORS VS. INPUT POWER LEVEL OF SPD AND I-Q DEMODULATOR. 23

FIGURE 2.6. ACCURACY OF SPD AND I-Q DEMODULATOR AS FUNCTIONS OF IMBALANCES OF QUADRATURE HYBRID (16BIT ADC). 27

FIGURE 2.7. ACCURACY OF THE SPD AND THE I-Q DEMODULATOR VERSUS DC OFFSET.... 29

FIGURE 2.8. TEST SETUP FOR MEASUREMENT SIMULATION OF THE NEW DMR OPERATING AT 26.5GHZ. 32

FIGURE 2.9. SAMPLED CONSTELLATION DIAGRAM OF DIFFERENT MODULATIONS MEASURED AT 26.5GHZ BY SPD. 33

FIGURE 2.10. MEASURED AND SIMULATED BER PERFORMANCE OF THE SPD FOR VARIOUS PSK MODULATIONS. 35

CHAPTER 3:

FIGURE 3.1. A TYPICAL SIX-PORT REFLECTOMETER. 51

FIGURE 3.2. TYPICAL OUTPUT WAVEFORMS OF A SIX-PORT WITH A CW INPUT. 53

FIGURE 3.3. FLOW CHART OF THE ALGORITHM TAKING SAMPLES FOR W-PLANE CALIBRATION. 55

FIGURE 3.4. SAMPLE DISTRIBUTIONS USING 13-STANDARD METHOD AND DUAL-TONE METHOD. 56

FIGURE 3.5. WAVEFORMS BEFORE AND AFTER SMOOTHING. 58

FIGURE 3.6. W-PLANE TO Γ-PLANE BILINEAR TRANSFORMATION: THE CIRCLES ARE MAPPED INTO CIRCLES BUT NOT CONCENTRIC. 61

FIGURE 3.7. CONSTELLATION DIAGRAMS MEASURED BY A SIX-PORT DIGITAL RECEIVER CALIBRATED USING DUAL-TONE W-PLANE AND ERROR-BOX METHOD. THE ANGULAR SPREAD REPRESENTS THE PHASE/FREQUENCY JITTERS OF THE OSCILLATORS USED IN THE EXPERIMENT. 66

CHAPTER 4:

FIGURE 4.1 SIX-PORT CIRCUIT FOR VECTOR ACQUISITION. 75

FIGURE 4.2 AN ALTERNATIVE SIX-PORT CIRCUIT CONFIGURATION.....76

FIGURE 4.3 FIVE-PORT CIRCUIT CONFIGURATION.....78

FIGURE 4.4 LAYOUT OF THE OPTIMUM FIVE-PORT RECEIVER CIRCUIT. 80

FIGURE 4.5 FIVE-PORT CIRCUIT USING BRANCH LINE COUPLER AND IN-PHASE POWER DIVIDER. 81

FIGURE 4.6 MASK OF THE 20 GHZ MHMIC FIVE-PORT RECEIVER CIRCUIT. 82

FIGURE 4.7 SIMULATED S PARAMETERS OF THE FIVE-PORT MHMIC CIRCUIT. 83

FIGURE 4.8 ISOLATION BETWEEN RF AND LO PORTS. 84

FIGURE 4.9 SIMULATED Q_I POINT DISTRIBUTION OVER THE OPERATING FREQUENCY BAND.85

FIGURE 4.10. SIX-PORT JUNCTION MODEL. 90

FIGURE 4.11. COMPLETE BASIC MODEL OF THE SIX-PORT DISCRIMINATOR.....92

FIGURE 4.12. CONSTELLATION DIAGRAM AT THE SPD OUTPUT. 93

CHAPTER 5:

FIGURE 5.1 OVERVIEW OF THE FUNCTIONAL FLOW CHART OF THE SIX-PORT RECEIVER ALGORITHM. 96

FIGURE 5.2 FLOW CHART OF DSP IMPLEMENTATION OF EQUATION (3.13)..... 101

FIGURE 5.3. BLOCK DIAGRAM OF THE SIX-PORT DIRECT DIGITAL DEMODULATOR. 105

FIGURE 5.4. BLOCK DIAGRAM OF THE TEST SETUP FOR MEASUREMENT SIMULATION. 108

FIGURE 5.5. MEASURED AN COMPUTER SIMULATED BER PERFORMANCE. 110

CHAPTER 6:

FIGURE 6.1 LINEARIZATION OF THE DIODE BY A REFERENCE POWER METER. 116

FIGURE 6.2 LINEARIZATION OF DIODE DETECTOR BY A CALIBRATED PRECISE ATTENUATOR.117

FIGURE 6.3. LINEARIZATION OF DIODE DETECTOR BY REPEATABLE TWO POSITION ATTENUATOR..... 118

FIGURE 6.4 TEST SETUP OF THE DUAL-TONE CLIBRATION. 124

FIGURE 6.5 ERROR OF LINEARIZATION..... 125

FIGURE 6.6 FACTOR OF CORRECTION K_I VERSUS INPUT POWER..... 125

List of Acronyms and Abbreviations

A/D	Analog to Digital
ADC	Analog to Digital Converter
AFC	Automatic Frequency Control
AGC	Automatic Gain Control
AM	Amplitude Modulation
ASIC	Application Specific Integrated Circuit
ATG	Automatic Termination Generator
BB	Base Band
BER	Bit Error Rate
BPSK	Binary Phase Shift Keying
CNR	Carrier to Noise Ratio
CW	Continuous Wave
DMR	Digital Millimeter-wave (Microwave) Receiver
DSP	Digital Signal Processor
DUT	Device Under Test
FDMA	Frequency Division Multiple Access
FM	Frequency Modulation
FPGA	Field Programmable Gate Array

FSK	Frequency Shift Keying
GPS	Global Positioning System
HMIC	Hybrid Microwave Integrated Circuit
I-Q	Inphase-Quadrature
IC	Integrated Circuit
IEEE	Institute of Electrical and Electronics Engineers
IF	Intermediate Frequency
LAN	Local Area Network
LNA	Low Noise Amplifier
LO	Local Oscillator
MAC	Multiply ACcumulation
MDS	Microwave Design System
MHMIC	Miniaturized Microwave Integrated Circuit
MMIC	Monolithic Microwave Integrated Circuit
MTT	Microwave Theory & Techniques
NSERC	Natural Sciences and Engineering Research Council of Canada
PCS	Personal Communication System (Services)
PROM	Programmable Read Only Memory
PSK	Phase Shift Keying
QAM	Quadrature Amplitude Modulation
QPSK	Quadrature Phase Shift Keying

RDM	Récepteur Digital Millimétrique
RF	Radio Frequency
SAW	Surface Acoustic Wave
SNR	Signal to Noise Ratio
SPD	Six-Port Discriminator
SPW	Signal Processing Worksystem
UHF	Ultra High Frequency
VLSI	Very Large Scale Integrated circuit

Chapter 1

Introduction

Over the past four decades, interests in millimeter wave technology have to some extent been cyclical at best. Nevertheless, with the ever-increasing congestion of the existing allocated electromagnetic spectrum and the establishment of some specific requirements for commercial and military applications which cannot be achieved by the use of other alternatives, the millimeter wave technology manifests its superior advantages compared to its counterparts at RF and microwave frequencies [1]. In particular, the recently proposed personal communication services (PCS) and other special applications such as road-tracking radar, short-haul high-speed data links [2], as well as wireless LANs

present a principal driving force behind rapid development and growing deployment of the mm-wave communication systems.

The term millimeter wave generally refers to the portion of electromagnetic spectrum between 30 and 300 GHz, corresponding to wavelengths of 10 to 1 mm. Electrical characteristics at millimeter wave frequencies differ from those of microwaves and infrared as well. These differences make millimeter wave systems an ideal candidate for certain applications. Three principal characteristics of millimeter waves can be identified, that is, short wavelengths, large bandwidth and possible interaction with atmospheric constituents, which translate into the following advantages for the millimeter wave communication systems:

- Shorter wavelengths allow one: 1) to reduce component size, resulting in compact mobile systems; and 2) to achieve narrow beamwidths or to use small antenna apertures, for example, a 12-cm-diameter aperture antenna provides a 1.8° beamwidth at 94 GHz compared to 18° at 10 GHz.

- Wider bandwidths provide many benefits, such as: 1) high transmission data rates, therefore high information bandwidth; 2) wideband spread-spectrum capability for reduced multipath effects; 3) high immunity to common jamming and interferences.

- Environmental interaction characteristics, such as high atmospheric attenuation at certain frequencies, results in high frequency reusability that is highly desirable for PCS while signal transmission at other frequencies may becomes transparent.

Besides the above-mentioned specific reasons responsible for the growth of millimeter wave applications, there are few remaining technical problems in this field. Generation, transmission, and detection have all received considerable attention over the past few years. Adequate solid state sources and millimeter wave components have been developed and are now commercially available [3]. More specifically, the progress of the M(H)MIC technology has made it much easier to manufacture massively millimeter wave ICs for widespread applications. As for PCS development, major requirements are more or less related to the cost reduction and the search for innovative techniques that may allow for solving some particular problems and further reducing the expenditure as well as design cycles.

On the other hand, digital signal processing brings about much excitement for designers of communication systems [4,5]. Many functions that are traditionally performed using analog circuits can now be accomplished more effectively by using some relevant digital techniques. Perhaps equally exciting is the flexibility, the new features or options offered by the digital techniques that can easily be incorporated, many of which were previously expensive or not practical.

Digital signal processing operations are reproducible, so that once a circuit (e.g., a filter) is designed, each unit will work exactly in the same way. This is a considerable advantage over its analog counterparts, whose tolerances of component often cause significant unit-to-unit non-repeatability. Another major advantage of DSP is the flexibility that can be designed into the equipment if it is planned in advance. Then, by changing the content of a memory, field modifications or improvements can easily be made. For example, a user can modify the bandwidth of a filter as a service demands just by changing the content of a PROM. Another typical example is the possibility of changing the frequencies of a FSK modem or even converting a FSK modem to PSK by implementing software modifications. Conversely, systems that are integrated with digital signal processing do not usually have large dynamic range enjoyed by analog systems. This limitation has been the consequence of a relatively small number of bits available in analog-to-digital (A/D) converters operating at high speeds. Unless A/D converters are developed to approach 14- to 16-bit linearity and sampling rate above 100MHz, some analog circuitry is likely to remain in radio receivers. Nevertheless, it can be foreseen that high speed, high resolution and low-cost A/D converters and DSPs will be commercially available as the VLSI technology advances at the present rapid pace.

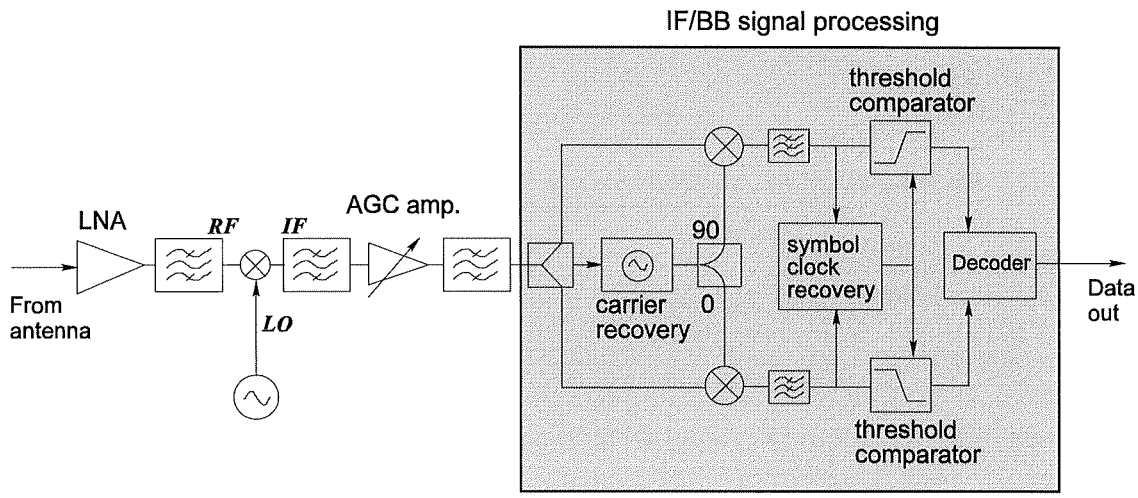

Figure 1.1 Functional block diagram of a typical super-heterodyne digital receiver.

In general, digital receivers used in millimeter wave communication systems can be divided into two categories: super-heterodyne receiver and direct conversion receiver. Figure 1.1 illustrates a simplified block diagram of a typical super-heterodyne digital receiver. The received RF signal is amplified first and then converted into a lower frequency (e.g. 70MHz IF). The desired signal is filtered to eliminate noise and interference and a succeeding high-gain AGC amplifier stabilizes the output signal level as the input RF signal level may vary due to the fading transmission channel. The carrier recovery synchronizes the local oscillator frequency with the received signal. And the clock recovery circuitry determines the optimum sampling/decision time. The super-

heterodyne receiver offers advantages such as high sensitivity, high frequency selectivity and it has been the de facto standard configuration in most communication systems.

Figure 1.2 shows the block diagram of a typical direct digital receiver. The received RF signal is directly amplified, filtered and demodulated, and therefore, the overall configuration of a direct receiver is expected to be much simpler, leading to a cost-effective solution. However, due to some limiting factors such as the inferior performance of the I-Q circuit at microwave and millimeter-wave frequencies, this type of scheme has been used only in some limited applications such as in the GPS.

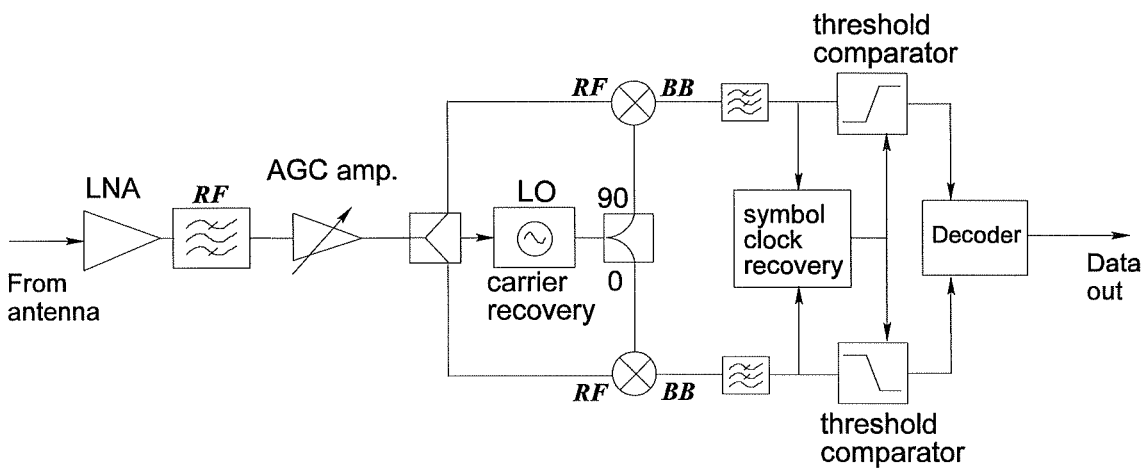

Figure 1.2 Functional block diagram of a typical direct digital receiver.

A new direct digital receiver scheme called six-port millimeter wave digital receiver is proposed and studied in this thesis. The concept of the new receiver derives from the "six-port technology", which has been under development during the past twenty years for microwave and millimeter-wave measurement applications. The proposed new scheme is able to take advantages of the state-of-art digital signal processing technology as well. The performance of this receiver depends more on DSPs, i.e. software and digital logic, rather than quality of the RF hardware. This will result in less stringent requirements for RF circuit fabrication and more flexibility for the receiver functionality.

The six-port receiver concept originated from a six-port circuit used to measure the Doppler frequency shift in an anti-collision radar [Appendix I]. A preliminary test was made to explore the feasibility of the new scheme [Appendix II]. Upon the positive conclusion drawn from the preliminary tests, a detailed computer and measurement simulation of the receiver performance was subsequently made. A special calibration method was also developed to facilitate the in-situ real-time calibration, which ensures the receiver operating under the optimum condition regardless of temperature changes and the aging of the components. Some other relevant topics, such as optimum six-port circuit design and diode detector linearization, were studied as well for better design of the proposed receivers.

This thesis is presented in the form of a collection of papers published in the IEEE MTT Transactions and international microwave and communications conferences. Each paper

addresses a specific topic related to the six-port digital receiver. The thesis is organized in the following way:

- Following a brief overall introduction, chapter 2 reveals and discusses the concept of the proposed new six-port millimeter-wave digital receiver. It also compares the new receiver with the conventional I-Q direct conversion receiver through the presentation of a series of computer simulation and measurements results. This part of the research work has been described in a full length paper published in the December 1995 issue of the IEEE Transactions on Microwave Theory and Techniques.

- Chapter 3 introduces a dual-tone method developed for the real-time receiver calibration. The new calibration method consists of two steps: W-plane calibration and "error box" calibration. Both steps make use of the output waveforms at the six-port output ports as the data source. This part of the research is described by a full length paper published in the January 1996 issue of the IEEE Transactions on Microwave Theory and Techniques.

- Chapter 4 addresses the optimum design of the six-port circuits. The discussion gives emphasis to the selection of a fix-port circuit configuration in place of the traditional six-port and the design criteria particularly suitable for the receiver application. The system modeling of the six-port is also discussed.

- Chapter 5 is about receiver algorithms. A DSP algorithm that allows coherent PSK detection without resorting to full carrier recovery is described. This work highlights the advantage of DSP in communication systems.

- Chapter 6 discusses the linearization of the diode detectors. A novel linearization method suitable for the six-port receiver is presented.

Chapter 2

Sixport Direct Digital Receiver: Concept and Simulation

This chapter is presented in the form of an article that has been published in the December 1995 issue of the "IEEE Transactions on Microwave Theory and Techniques". It is the first paper that describes in detail the concept of the proposed six-port direct millimeter-wave digital receiver as well as its computer and measurement simulation results.

To begin with, the state-of-art of the microwave digital receiver is reviewed. Followed by a brief description of the six-port theory well established for microwave reflectometer and network analyzer, a new six-port discriminator (SPD) that is capable of detecting

amplitude, phase and frequency of the incoming signal is introduced (also referring to Appendix I for more details on the SPD). The configuration of a six-port digital receiver based on the SPD is then presented.

Subsequently, a detailed computer simulation addresses some of the main concerns about the performance of the proposed new six-port receiver. A comparison with the conventional heterodyne and direct conversion receivers is also made. The conclusion is also supported by measurement results obtained from a proof-of-concept test bench operating at 26.5 GHz.

Paper published in the IEEE Transactions on Microwave Theory and Tech. VOL.43, NO.12 December 1995, pp.2766-2772.

Computer and Measurement Simulation of a New Digital Receiver Operating Directly at Millimeter-Wave Frequencies

Ji Li, Renato G. Bosisio, Fellow, IEEE and Ke Wu, Senior Member, IEEE

POLY-GRAMES Research Center
École Polytechnique, C. P. 6079, Succ. Centre Ville
Montréal, Canada H3C 3A7
FAX: (514) 340-5892

ABSTRACT

A novel digital millimetric receiver (DMR) scheme is introduced. Using a six-port phase/frequency discriminator (SPD) in conjunction with a digital signal processor (DSP), the receiver performs various PSK and QAM demodulations directly at microwave and millimeter-wave frequencies. An important feature of the new DMR is that hardware imperfections such as phase/amplitude imbalance are readily eliminated by a simple calibration procedure. The concept is proved through computer simulation and measurements at 26.5GHz. This receiver scheme is proposed for small/medium capacity digital terminals typically found in various wireless communication networks.

This work is supported by the Natural Science and Engineering Research Council of Canada (NSERC)

2.1 INTRODUCTION

Due to the increasing demand of wireless communications, there have been persistent efforts to simplify the microwave/mm-wave digital transceiver structures to bring down their size and cost. Such efforts have been intensified recently due to fast emerging demands for personal communication services (PCS). Among various choices, the direct (homodyne) transceiver architecture is an effective way to significantly reduce transceiver complexity and cost. Both direct transmitter [2.1-2.3] and receiver [2.4-2.6] for different digital modulations using different circuits ranging from hybrid microwave integrated circuit (HMIC) to monolithic microwave integrated circuit (MMIC) technologies have been reported. All these direct transceivers have one point in common: a quadrature hybrid network (I-Q network). It is well known that, as the frequency increases, the corresponding wave-length decreases proportionally, and it is therefore more difficult to obtain a quadrature hybrid with acceptable phase and amplitude accuracy. This is particularly true when the frequency goes beyond microwave into the millimeter-wave band. Although additional circuits can be introduced to compensate phase and amplitude imbalances of the I-Q hybrid [2.7,2.8], this method is obviously cumbersome, and the long-term stability of such circuits is questionable.

As a result of the latest advancement in digital integrated circuit technologies, there is noticeable interest to replace analog circuit functions with their digital implementations [2.10,2.11]. This generally brings down the cost and increases the stability as well as the flexibility of the electronic systems; particularly when DSPs are used. The processing power of the latest DSP is reported to have reached 2 bops [2.12] which makes it possible to realize some very complex algorithms at high speed. Certain types of receivers sample signals in the IF band and implement the demodulation using DSPs [2.13]. These receivers, however, still retain all the microwave parts found in the conventional heterodyne receiver. For the design of microwave transceivers, it appears to be more reasonable to simplify the microwave circuit configuration at the expense of more complicated digital circuits, such as to make a better trade-off to reduce the cost and increase the yield of MMICs.

Six-port theory was first developed in the 70's as a new means of accurate automated microwave network analysis [2.14,2.15]. The vector ratio of the incident waves at two input ports can be calculated using the output power readings at the remaining four ports. In doing this there is no need of down-converting the signal to an IF to make phase comparison. A very interesting feature of the six-port is its ability to eliminate measurement errors introduced by hardware imperfections by a suitable calibration procedure [2.22]. After more than twenty years of development the six-port technology has become highly sophisticated and some commercial products are now available on the market [2.16]. In addition, recent progress in MMIC and MHMIC six-ports

[2.17,2.18] renders such circuits better accessible for widespread commercial applications.

In this paper, we describe a novel concept of direct digital receiver, in which a six-port replaces the I-Q quadrature hybrid as the phase detector. The block diagram of the new scheme is shown in Figure 2.1. The demodulation is performed directly at microwave/mm-wave frequencies by a six-port discriminator (SPD) instead of the I-Q demodulator found in conventional digital receivers. This SPD is capable of detecting relative amplitude, phase and frequency of the received signal with respect to the local oscillator. A DSP unit executes computations necessary to perform the required demodulation in addition to carrier and clock recoveries using algorithms that are already available [2.32-2.36]. Such a receiver benefits from all the advantages of six-port technology: First of all, the fabrication requirements of the hardware can be greatly eased. An auxiliary calibration algorithm [2.19] performs the required six-port calibration from the received signal itself, monitors the real-time operation and updates the calibration coefficients as temperature and/or some other circuit parameters vary. This makes it possible to realize a direct millimeter wave digital receiver without stringent fabrication requirements; Secondly, the presence of a DSP provides a great flexibility to the receiver function: Switching between different modulations can be done by simply altering the software routines thereby avoiding hardware reconfiguration. Both differential and coherent detections are possible [2.24]. Furthermore, the demodulation and decoding functions can be combined together to further enhance the receiver system

integration; Thirdly, the proposed six-port receiver possesses unique properties such as: a) Immunity to image frequency and adjacent channel interferences, so that the specification of the channel bandpass filter can be relaxed; b) The six-port receiver allows variation in input power level. The dynamic range of the receiver is mainly a function of the A/D converter resolution. c) Wide band operation is also possible by the use of a wide-band six-port design. After all, the maximum data transmission rate is limited by the A/D converter and DSP. The data throughput is expected to increase as the speed of the DSP escalates in time.

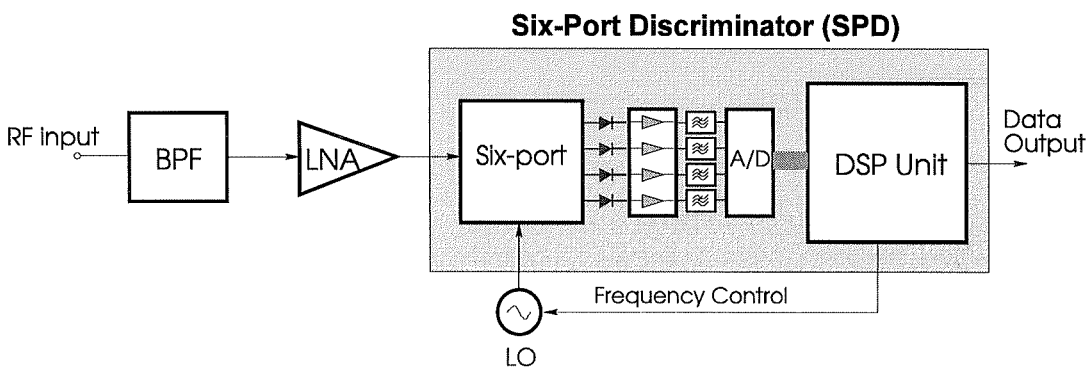

Figure 2.1. Block diagram of the new Digital Millimetric Receiver (DMR) with the six-port discriminator (SPD).

2.2 SIX-PORT DISCRIMINATOR (SPD)

Previously reported six-port applications are mostly focused on microwave measurements such as network analysis [2.20] and parameter extraction [2.21]. These measurements involve only coherent signals, i.e. the incident and reflected waves of the microwave networks are generated from the same signal source. Consider the case of a six-port used as a microwave vector voltmeter, the complex ratio of the two input signals a_1 and a_2 in figure 2.2 can be obtained as follows:

$$\vec{A} = |A|e^{j\theta} = \frac{\vec{a}_1}{\vec{a}_2} = \frac{\sum_{i=3}^{6}(a_i + jb_i)P_i}{\sum_{i=3}^{6}(c_i + jd_{i)})P_i} \qquad (2.1)$$

where constants a_i , b_i , c_i , d_i 's are calibration parameters that depict the specific six-port and can be deduced from a popular two-step calibration procedure [2.22].

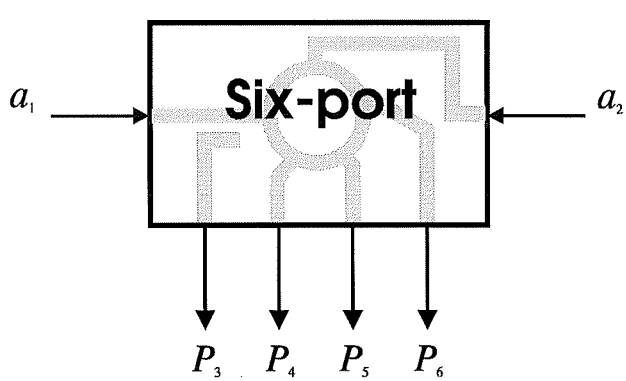

Figure 2.2. A six-port functions as a microwave vector voltmeter as a_1/a_2 is calculated from P_i's.

To extend the scope of the six-port a little further, we define the two incident waves to be at different frequencies as follows:

$$\vec{a}_1 = |a_1| \cdot e^{j(2\pi f_1 t + \phi_1)} \tag{2.2}$$

$$\vec{a}_2 = |a_2| \cdot e^{j(2\pi f_2 t + \phi_2)} \tag{2.3}$$

Suppose the frequencies f_1 and f_2 are close enough to each other such that the difference in calibration coefficients is negligible for the six-port, the measured complex ratio A will become a rotating vector in the complex plane:

$$\vec{A} = |A| \cdot e^{j\theta(t)} = |A| \cdot e^{j(2\pi(f_1 - f_2)t + \phi_1 - \phi_2)} \tag{2.4}$$

Therefore, the frequency difference $\Delta f = f_1 - f_2$ can be readily obtained from the derivative of $\theta(t)$

$$\Delta f = \frac{\theta(t_2) - \theta(t_1)}{t_2 - t_1} \tag{2.5}$$

where the time interval between two samples $\Delta t = t_2 - t_1$ is properly chosen for best accuracy. It is to be noted that the sign of Δf is a direct indication of relative position of f_1 and f_2 . In this way, the so-called six-port phase/frequency discriminator (SPD) [2.23]

is capable of dealing with all basic receiver functions which are traditionally carried out by I-Q hybrids.

2.3 COMPUTER SIMULATION: PERFORMANCE OF SPD VERSUS I-Q DEMODULATOR

The obstacles preventing conventional I-Q receiver from direct operation at higher frequencies are mainly [2.25]: (1) Phase imbalance due to circuit imperfections and reflections; (2) Amplitude imbalance due to I-Q circuit, gain imbalance of the two mixer branches, etc.; and, (3) DC offset of the I and Q channels. It is recognized that the new SPD can largely overcome such drawbacks. This will be demonstrated through a series of simulation and analysis in the following sections.

2.3.1 Circuit Model of Six-Port

A six-port circuit originally designed as a reflectometer is adopted here for simulation purposes. The block diagram of the circuit is shown in Figure 2.3. It can be seen that the six-port consists of I-Q hybrids, an in-phase power divider and interconnecting transmission lines. These components are characterized by S-parameters, so that the

hardware imperfections can be readily taken into account. A commercial microwave simulator (MDS*) was used to analyze the network. In all the simulations, a real calibration procedure was performed to obtain the corresponding calibration coefficients. Both the simulation and the analysis are performed to compare the SPD to a standard I-Q demodulator operating at the same mm-wave frequency.

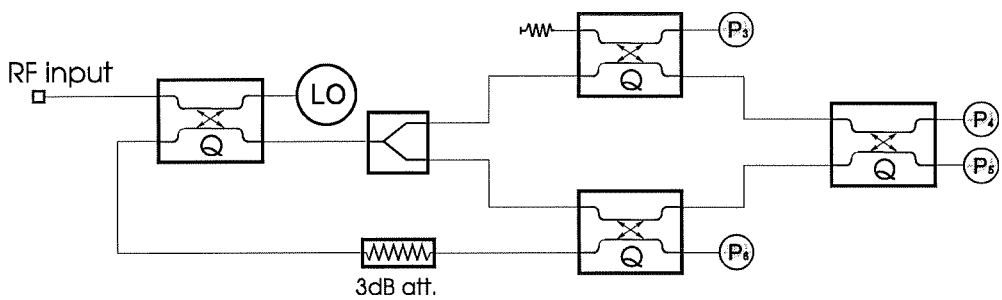

Figure 2.3. Block diagram of the six-port model used in the simulation of SPD.

2.3.2 Degradation of Receiver Performance Due to the Hardware Imperfections

Taking bit error rate (BER) as a straightforward measurement of the receiver performance, for a perfect digital receiver, the only factor affecting performance is noise.

* Trade Mark of Hewlett Packard

The degradation in performance due to various non-ideal factors such as hardware imperfections, synchronization errors and interferences can be regarded as equivalent to loss in signal to noise ratio (SNR or E_b/N_0). In order to demonstrate the advantages of using SPD over the conventional I-Q hybrid, simulations have been made for a standard heterodyne QPSK receiver. The transmitter was considered perfect and the phase/amplitude imbalances were introduced in the I-Q demodulator. Figure 2.4 shows the BER as a function of E_b/N_0 in the presence of different order of amplitude and phase imbalances. The simulated transmission data rate was 10Mb/s. The roll-off factor of the raised-cosine band-limit filter was 0.35. It is illustrated that the BER increases with the imbalance. The equivalent E_b/N_0 loss is approximately 1.5dB, 2.1dB, 2.9dB and 3.7dB for phase imbalances of 5, 10, 15 and 20 degrees, respectively, at 10^{-4} BER threshold. This E_b/N_0 loss becomes as large as 4.6dB when the phase imbalance reaches 25 degrees. It is expected that the higher level modulation schemes such as 8PSK and 16QAM are even more sensitive to such imbalances. In some circumstances, the amplitude imbalance between I-Q branches is larger than 1dB. Therefore in order to maintain a reasonable performance of the receiver, it is absolutely necessary to find an effective way to counter these adverse effects.

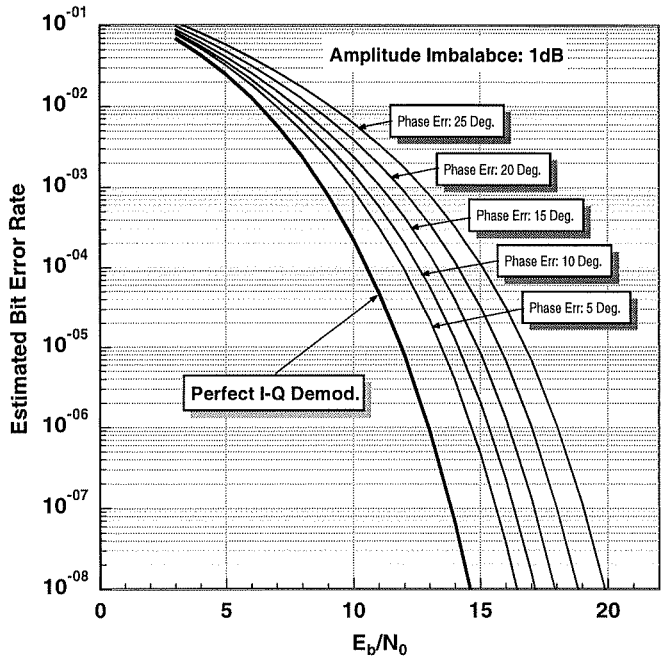

Figure 2.4. BER performance of a QPSK receiver in the presence of amplitude and phase imbalance of the I-Q demodulator.

2.3.3 Operating Dynamic Range as a Function of the ADC Resolution

In a conventional heterodyne digital receiver it is generally required that the input level of the I-Q demodulator be kept constant by using an IF automatic gain control (AGC) circuit. However, this becomes more difficult at microwave frequencies. One feature of the six-port direct digital receiver is its tolerance to input signal level variation.

Therefore the expensive microwave AGC amplifier is not required. The difference between the maximum and minimum signal levels, while maintaining a given BER margin for a specific modulation, can be defined as the operating dynamic range of the receiver. The minimum detectable signal level depends on the resolution of the A/D converters. On the other hand, an I-Q demodulator also allows variable input signal if the same A/D converters and DSP are used. Figure 2.5 illustrates the amplitude and phase errors of SPD and I-Q demodulator as functions of input signal level for 8bit, 12bit and 16bit A/D converters, respectively. It is obvious that a high resolution A/D converter not only extends the dynamic range but also abates the gain requirement of the preceding low noise amplifier. Meanwhile, the maximum acceptable input level is determined by the saturation point of the power detectors or channel DC amplifier/ADC input limits. Therefore it is concluded that a 50dB of nominal dynamic range can be readily achieved for QPSK reception using a 16bit ADC. In most applications it will be more interesting to increase the sensitivity of the SPD to facilitate the LNA design. It is also observed that SPD offers better accuracy than a digitized I-Q demodulator in all cases. For example, from Figure 2.5, at a relative input power level of -25dB, the SPD has maximum amplitude and phase error of 0.8dB and 5 degrees, respectively when a 8bit ADC is used, while these errors are 1.7dB and 8 degrees for the I-Q demodulator, respectively.

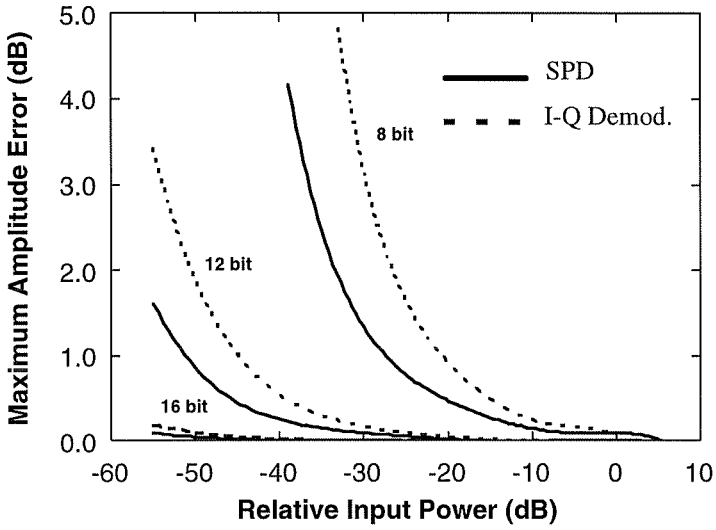

(a) Maximum amplitude error (dB)

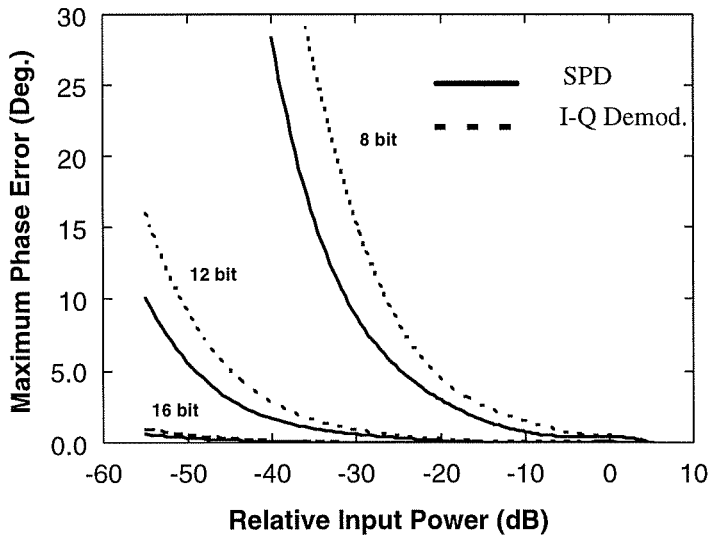

(b) Maximum phase error (Deg.)

Figure 2.5. Maximum amp/phase errors vs. input power level of SPD and I-Q demodulator.

2.3.4 Accuracy of SPD in the Presence of Quadrature Imbalances

The SPD itself can be built up by quadrature hybrids and power dividers or other suitable circuits for phase dispersal. None of these components are perfect. The six-port calibration procedure is to extract the network parameters and eliminate errors from the final measurement results. As a result of noise, the limited resolution of A/D converters and so on, there will still be residual phase and amplitude errors. A statistical simulation has been accomplished to compare the residual errors of SPD with an I-Q hybrid. Random phase and amplitude errors are assigned to each component in the SPD (Figure 2.3), and the parameters are random at maximum tolerances for all the components. Consequently, the overall performance of the SPD is the worst possible case at the corresponding error level. Figure 2.6 shows the simulation results. An 1-dB amplitude imbalance is presented in all cases. The SPD has 16 bit resolution and the I-Q demodulator uses perfect A/D conversion in the simulation. It is clearly shown that the SPD is very powerful in countering hardware imperfections: in the phase imbalance range of 0 to 40 degrees with the relative input level as low as -50dB, the maximum residual amplitude and phase errors of SPD are only 0.1dB and 0.7 degrees, respectively. Therefore it is concluded that the residual error can be considered negligible over the whole dynamic range of the SPD. In contrast, for I-Q demodulators, the errors are directly proportional to hardware errors, i.e. an amp./phase error of 1dB/25Deg. of the I-

Q hardware will result in an error of 2.0dB in amplitude and 25 degree error in phase, respectively. Although the excellent accuracy of SPD will be degraded somehow in a real receiver due to other factors that have not yet been considered in the simulation such as imperfect calibration and noise, the conclusion that the SPD presents an accuracy several orders superior than I-Q demodulator is still valid. This is confirmed by the measurement simulation.

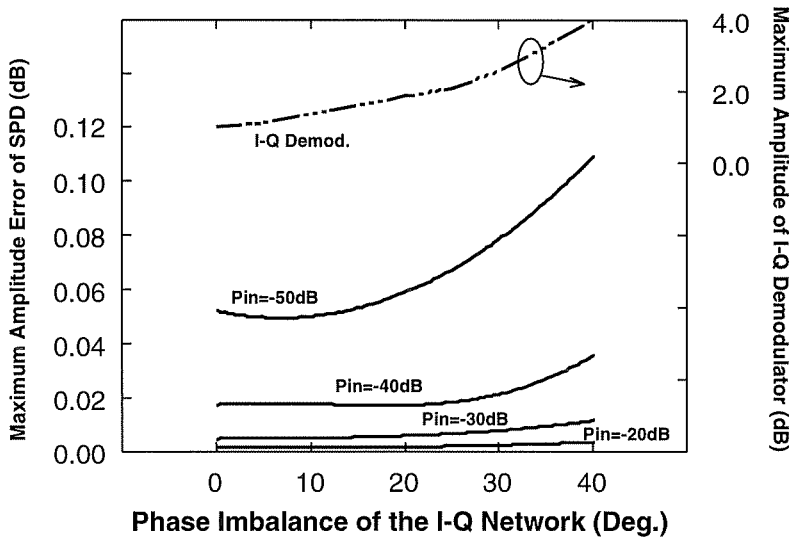

(a) Maximum amplitude error (dB)

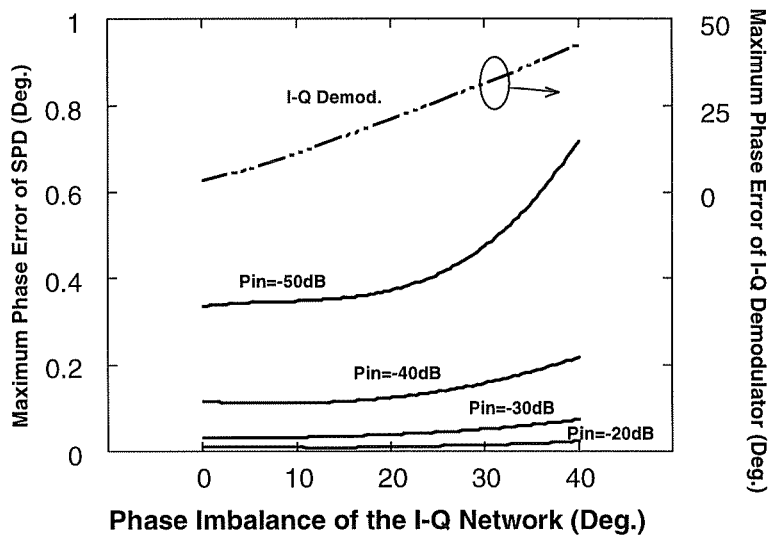

(b) Maximum phase error (Deg.)

Figure 2.6. Accuracy of SPD and I-Q demodulator as functions of imbalances of quadrature hybrid (16bit ADC).

2.3.5 Effect of DC Offset on SPD Accuracy

Fundamentally, the diodes in the SPD operate in a different fashion to their I-Q demodulator counterparts. In an I-Q demodulator the mixers behave like multipliers as the diodes act as nonlinear devices. In a SPD the diodes act as power detectors, and the emphasis is on linearity of the response. Consequently whilst at least a balanced diode pair must be used for the minimum specifications in an I-Q demodulator, a simple single Schottky diode detector is generally sufficient for a SPD.

The DC offset is primarily introduced by the diode detectors and the attached DC amplifiers, and its value is usually a function of temperature. A computer simulation reveals that, in the case of random offset, the SPD doesn't offer better accuracy than the I-Q demodulator. However, in situations where the offsets of all the channels are moving in the same direction, which is the actual case in single-chip ICs, the SPD comes up with a much greater accuracy.

Figure 2.7 displays the phase and amplitude errors as functions of the DC offset. The DC offset is defined as relative to the maximum output voltage of each channel. When the DC offset is at -40dB, the SPD maintains a minimum acceptable amplitude error of 0.6dB and a phase error of 3 degrees, while the I-Q demodulator has disastrous 5dB/26degrees amplitude/phase errors, respectively. Both amplitude and phase errors are more pronounced for the I-Q demodulator when the DC offset goes beyond -50dB.

Evidently the SPD is much less sensitive to the DC offset than its I-Q demodulator counterpart.

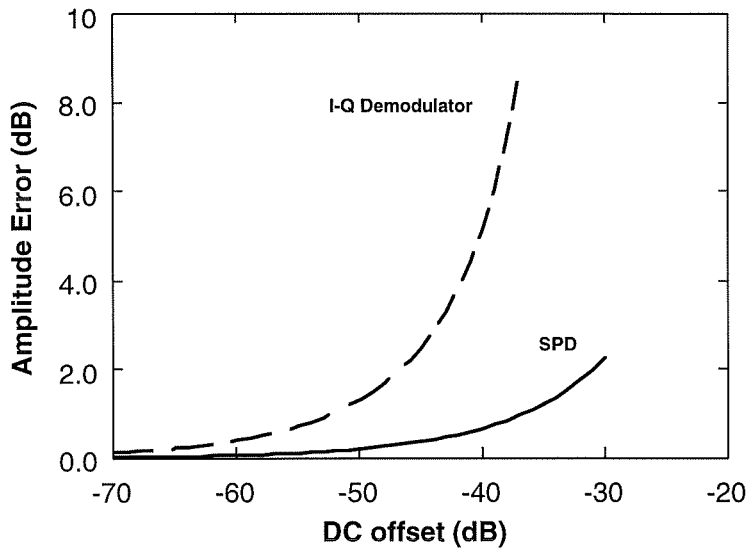

(a) Maximum amplitude error (dB)

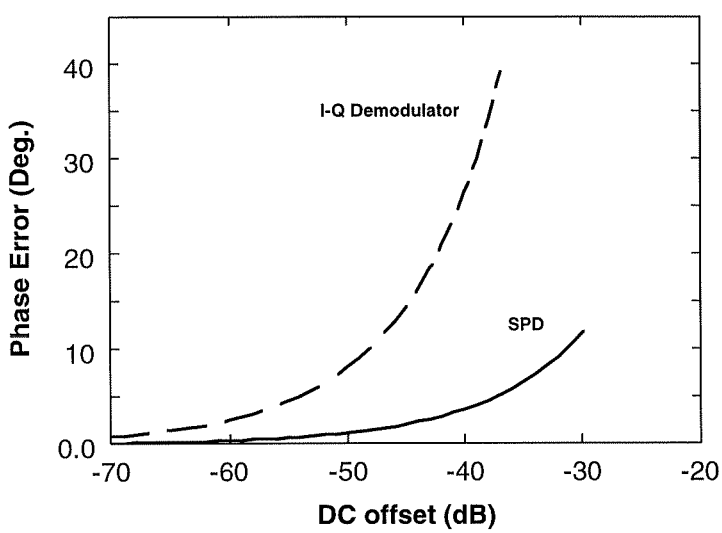

(b) Maximum phase error (Deg.)

Figure 2.7. Accuracy of the SPD and the I-Q demodulator versus DC offset.

2.3.6 Effect of Adjacent Channel Interferences

It makes common sense to use filters for most digital receivers to separate the signal from unwanted noise and interferences. While performance degradation caused by inband noise and interferences is inevitable, the SPD possesses unique immunity to out-of-band noise and interferences: For a single diode detector, let us suppose the lowpass filters have stopped all the high frequency components, thus the interference acts only on the DC output. This DC component can be seen as an equivalent DC offset of the DC amplifier. As has already been concluded in the previous section, the I-Q demodulator is more vulnerable to such interferences.

2.3.7 Bit Error Rate (BER) Performance

Bit error rate is the ultimate indication of performance of a digital receiver. A statistical computer simulation model was established to help to predict the BER performance of the DMR for various types of modulations. The simulation takes into account several error sources in the real operation, such as phase noise of the local oscillator, resolution of the A/D converter and white noise introduced in diode detectors/DC amplifiers. The results are presented in Figure 2.10 together with the measured simulation results.

2.4 MEASUREMENT SIMULATION OF THE DMR

Measurement simulations are also performed. Figure 2.8 illustrates the measurement setup. A HP8782B vector signal generator produces the desired modulated signal at an intermediate frequency (250MHz). Then a upconverter brings this IF signal up to 26.5GHz and an isolator separates the transmitter from the receiver. There is no filter inserted to suppress the LO and image signal leakage. The variation of the signal level is accomplished by control of the output level of the vector signal generator which has over 160dB of output level range. No additional bandpass filter is inserted between the transmitter and the receiver. In the SPD, a PC486 with a 16bit plug-in A/D data acquisition board executes the DSP algorithms. The SPD is constructed using discrete coaxial components for the six-port configuration of Figure 2.3. The 3dB quadrature couplers have ±1.7dB of amplitude imbalance, ±10° of phase imbalance and a minimum isolation of 14dB. The in-phase power divider has ±0.6dB of amplitude imbalance, and ±4° of phase imbalance.

The receiver LO power was about -1.5dBm for all the measurements. A second PC486 was used as a transmission analyzer for BER tests.

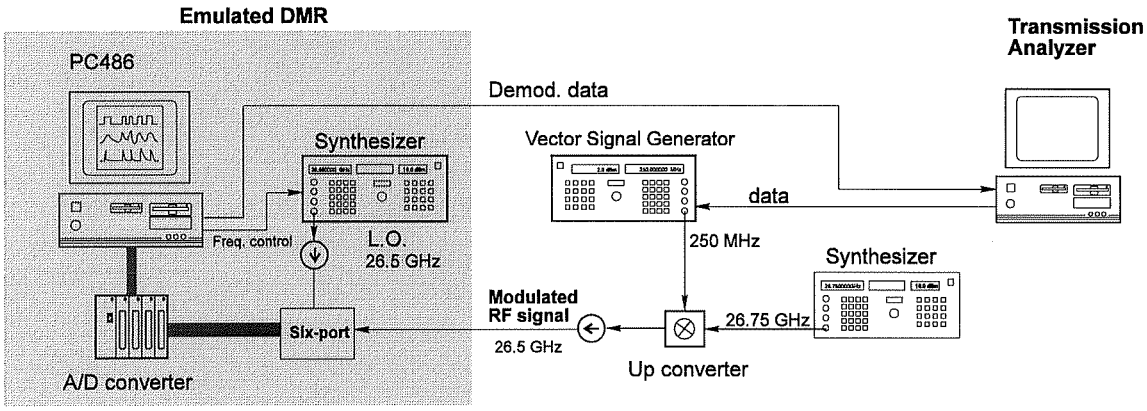

Figure 2.8. Test setup for measurement simulation of the new DMR operating at 26.5GHz.

2.4.1 Constellation Diagram

Figure 2.9 illustrates the measured constellation diagrams of BPSK, QPSK, 8PSK and 16QAM sampled by the SPD. It clearly proves the efficacy of the SPD in the correction of circuit imbalances. Neither the imbalances of the quadrature couplers nor the LO leakage impose noticeable distortion to the measured constellations. The phase spread in the constellation diagram is due to the phase noise of the oscillators, residual frequency difference and slow sample acquisition time.

It is also noticed that due to the absence of the bandpass filter at the output of transmitter, the LO component in the transmitted spectrum is more than 20dB higher than the desired signal when the output level of the IF vector signal generator is

decreased. Even in this case the observed constellation diagram does not appear to be distorted, which reflects the power of the SPD in countering out-of-band interferences.

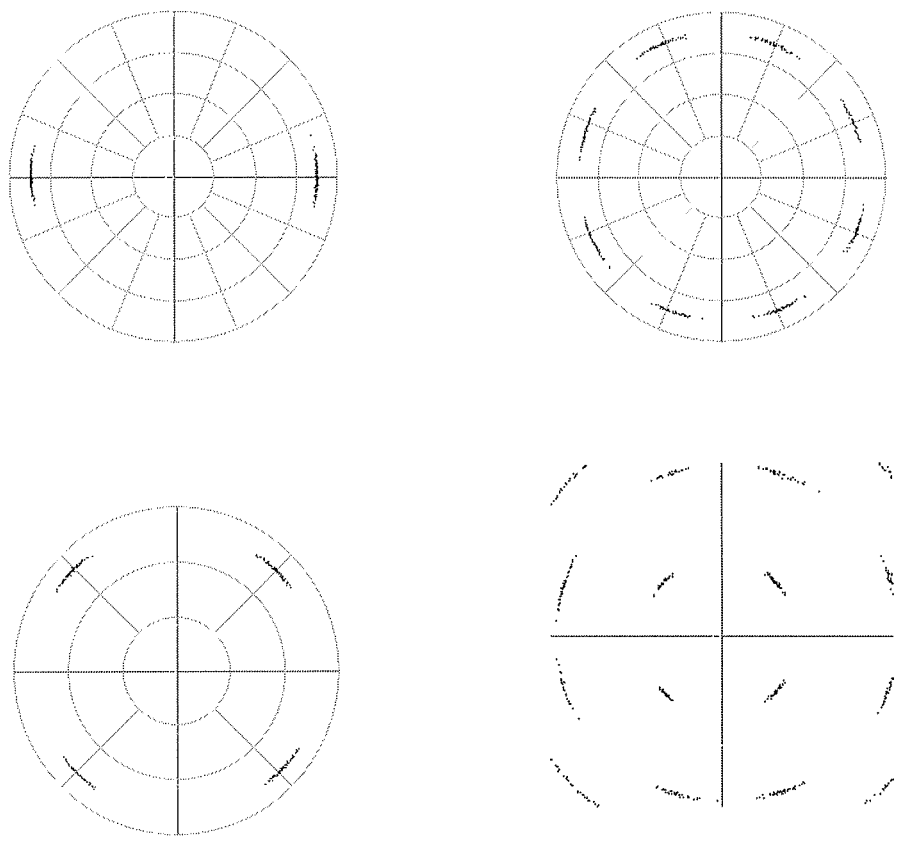

Figure 2.9. Sampled constellation diagram of different modulations measured at 26.5GHz by SPD.

2.4.2 Bit Error Rate Measurements

Demodulation algorithms have been developed for both differential and coherent PSK modulations. The phase recovery for coherent detection is achieved by a simple DSP algorithm. This feature is a better alternative to the more difficult conventional hardware phase tracking directly at microwave/mm wave frequencies.

The measured BER for coherent and differential BPSK, QPSK demodulations are compared with the computer simulation results. Figure 2.10 shows the measured and calculated BER versus the input power level. It can be seen that, as anticipated, the coherent reception is better than the differential reception and the BPSK requires minimum energy to be detected. The input power level is about -44.5dB and -39dBm for BPSK and QPSK demodulations, respectively, when the BER is 10^{-4}. It is also found that the measurement results are general in agreement with the computer simulations. The poorer agreement in the QPSK results is attributed to a unknown measurement error.

It must be mentioned that these measurements are meant to be "proof of concept" of the new receiver scheme as the transmission data rate was only in the order of several Kb/s due to equipment limitations. Thus it is primarily the ADC resolution, instead of noise, that determines the minimum detectable signal level. On the other hand, the SPD used in the measurements is far from being optimum for receiver applications. Significant improvements in sensitivity can be expected from an optimized design of the SPD.

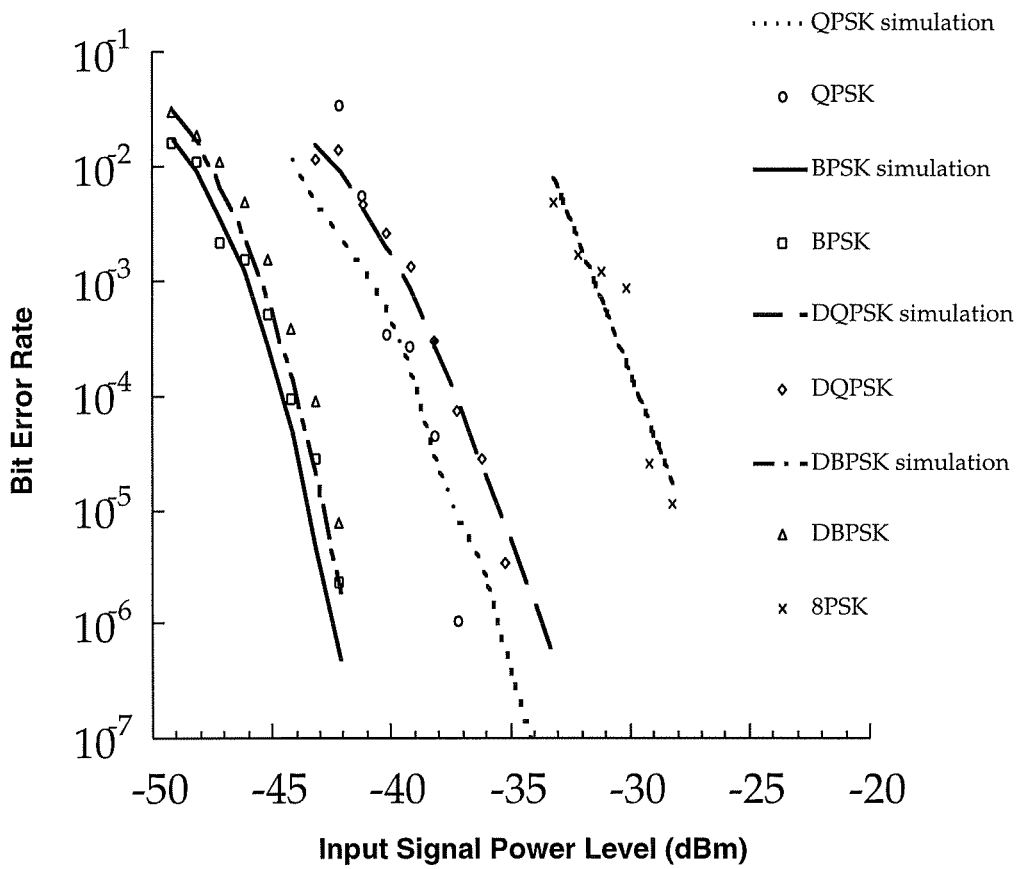

Figure 2.10. Measured and simulated BER performance of the SPD for various PSK modulations.

2.5 CONCLUSION

A novel six-port direct digital receiver is presented, and it is found to be rugged to hardware imperfections that normally prevent conventional I-Q receivers from direct operation in microwave/mm wave bands. Computer simulation and measurements at 26.5GHz validate the new receiver scheme. This work outlines a cost-effective alternative to the conventional heterodyne receiver with the following advantages: 1) High yield of circuit due to decreased fabrication requirements. 2) Low power consumption due to simplicity of the whole receiver and lower LO power demand. 3) Flexibility to switch between different modulation schemes. 4) Less stringent bandpass filter requirements. And 5) The maximum data rate heavily depends on the speed of the DSP unit and A/D converter.

It must be mentioned that although the work described in this paper focuses on mm-wave applications, the DMR can be readily adaptable to lower frequency bands such as the UHF band.

ACKNOWLEDGMENT

The authors would like to thank the Natural Sciences and Engineering Research Council of Canada (NSERC) for the research grant provided to make the above research possible.

REFERENCES

[2.1] D.S.HILBORN *et al*, "An adaptive direct conversion transmitter," IEEE Trans. Vehicular Tech., Vol.43, No.2, pp.223-233, May,1994.

[2.2] TIMOTHY O'CONNELL, PATRICJ J. MURPHY and AIDAN MURPHY, "A direct I/Q modulator at microwave frequencies using GaAs MESFETs," Microwave Journal, pp.62-76, October 1994.

[2.3] A.BÓVEDA, F.ORTIGOSO and J.I.ALONSO, "A 0.7-3 GHz GaAs QPSK/QAM direct modulator," IEEE Journal of solid-state circuits, Vol.28, No.12, pp1340-1349, Dec. 1993.

[2.4] B.D.BREWSTER and I.D.ROBERTSON, "phase compensated qpsk demodulator with a X-Band I.F. for VSAT system applications," Proc. European Microwave Conference pp.1559-1564, 1994.

[2.5] S.MOLLENKOPF and G.M.REBEIZ, "A 22 Ghz MIC active receiver/radiometer," 1994 IEEE MTT-S Digest, pp.1347-1350, May, 1994.

[2.6] T.TAKENAKA et al, "A digital signal processing demodulator with a wide frequency acquisition range," Globecom'90, pp.1418-1422, 1990.

[2.7] J.K.CAVERS and M.LIAO, "Adaptive compensation and offset losses in direct conversion transceivers," Proc. IEEE Vehicular Technology Conference, pp.578-583, 1991.

[2.8] I.TELLIEZ et al, "A compact, monolithic microwave demodulator-modulator for 64-QAM digital radio links," IEEE Trans. MTT, Vol.39, No.12, pp.1947-1954, Dec. 1991.

[2.9] B.D.BREWSTER and I.D.ROBERTSON, "A C-band microstrip varactor tuned reflection phase shifter employing UHF general purpose diodes," Microwave and Optical Technology Letters, Vol.7, No.4, pp.172-174, March.1994.

[2.10] M.P.FITZ, "A bit error probability analysis of a digital pll based demodulator of differentially encoded BPSK And QPSK modulation," IEEE Trans. Communications, Vol.42, No.1, pp.17-21, Jan. 1994.

[2.11] W.W.CHENG, "Ultra wide band analog signal processor products," RF Design, pp.42-54, Sept. 1994.

[2.12] Texas Instrument WWW server:
http://www.ti.com/sc/docs/dsps/prodinfo/datasht/c8x/

[2.13] C.OLMSTEAD and MIKE PETROWSKI, "Digital IF processing," RF Design, pp.30-40, Sept.1994.

[2.14] C.A.HOER *et al*, "Using an arbitrary six-port junction to measure complex voltage ratios," IEEE Trans. MTT-23, No.12, Dec. 1975, pp.978-984.

[2.15] ENGEN, "Determination of microwave phase and amplitude from power measurements," IEEE Trans. Instrum. Meas., vol. IM-25, No.4 pp.414-418, Dec. 1976.

[2.16] Marconi Instruments, "Test and measurement instrument systems," pp108-112, 1994.

[2.17] F.M.GHANNOUCHI, D. MAURIN, M. CUHACI and R.G. BOSISIO, "a miniaturized frequency-compensated six-port junction using MHMIC technology," Microwave and Optical Technology Letters, Vol.6 pp. 573-575, Aug. 1993.

[2.18] M.N.SOLOMON et al, "A monolithic six-port module," IEEE Microwave and guided wave letters, Vol.2 pp. 334-336, Aug. 1992.

[2.19] JI LI, R.G.BOSISIO, KE WU, "Dual-tone calibration of six-port junction and its application to direct digital receiver", Chapter 3 .

[2.20] ERIC BERGEAULT, *et al*, "accuracy analysis for six-port automated network analyzers," IEEE Trans. Instrumentation & Measurement, Vol. 39. No.3, pp.492-496, June 1990.

[2.21] F.M.GHANNOUCHI, R.L.LAROSE, and R.G.BOSISIO, "A new multi-harmonic loading method for large-signal microwave and millimeter-wave transistor characterization," IEEE Trans. Microwave Theory Tech., Vol.39, pp.986-992, June 1991.

[2.22] T.E.HODGETTS and E.J.GRIFFIN, "A unified treatment of the theory of six-port reflectometer calibration using the minimum of standards," Report No. 83003 RSRE Malvern, Aug. 1983.

[2.23] JI LI, R.G.BOSISIO and KE WU, "A collision avoidance radar using six-port phase/frequency discriminator (SPFD)," Proc. IEEE National Telesystems Conf., pp.55-58, 1994.

[2.24] JI LI, R.G.BOSISIO and KE WU, "a new direct digital receiver performing coherent PSK reception," Digest of IEEE MTT Symposium, Vol. 3, pp.1007-1010, Orlando, May, 1995

[2.25] K.VOUDOURIS *et al*, "Effects of amplitude, phase, and frequency imperfections on the performance of a direct conversion receiver (DCR) for personal communication systems," IEEE Microwave and Guided wave Letters, Vol.3, No.9, Sept. 1993, pp. 313-315.

[2.26] V.S.REINHARDT *et al*, "methods for measuring the power linearity of microwave detectors for radiometric applications," 1994 IEEE MTT-S Digest, pp.1477-1480

[2.27] S.KATO, et al, "Implementation of coded modems," IEEE Communication Magazine, pp.88-97, Dec.1991.

[2.28] XIONG, "Modem techniques in satellite communications," IEEE Communications Magazine, pp.84-98, August 1994.

[2.29] ALLAN LAMBERTI, "New directions for the microwave market," Telecommunications, pp.38-40, April, 1992.

[2.30] J.C.CHUANG, "Comparison of coherent and differential detection of BPSK And QPSK in a quasi-static fading channel," IEEE Trans. Communications, Vol.38, No.5, pp.565-567, May,1990.

[2.31] I.M.KOSTIC, "Imperfections, noise and co-channel interference," IEE Proceedings, Vol.136, Pt. I, No.5, pp.333-338, Oct.1989.

[2.32] S.W.CHEUNG, "Carrier phase synchronization for a coded PSK signal in satellite links," Globecom'90, pp.1413-1417, 1990.

[2.33] F.D.NATALI, "AFC tracking algorithms," IEEE Trans. Communications, Com-32, pp.935-947, August 1984.

[2.34] W.G.COWLEY and L.P.SABEL, "The performance of two symbol timing recovery algorithms for PSK demodulators," IEEE Trans. Communications, Vol.42, No.6, pp.2345-2355, 1994.

[2.35] E.DEL RE and R.FANTACCI, "Joint carrier and clock recovery for QPSK and MSK digital communications," IEE Proceedings, Vol.136, Pt.I, No.3, pp.208-212, June 1989.

[2.36] R.D.GAUDENZI and V.VANGHI, "Analysis of an all-digital maximum likelihood carrier phase and clock timing synchronizer for eight phase-shift

keying modulation," IEEE Trans. Communications, Vol.42, No.2/3/4, pp.773-782, 1994.

Chapter 3

Adaptive Calibration of the Sixport Direct Digital Receiver

This chapter is presented once again in the form of a paper published in the January issue of the "IEEE Transactions on Microwave Theory and Techniques". It proposes and discusses a self-calibration method for the six-port direct mm-wave digital receiver.

Calibration is a key procedure for the six-port receiver. It extracts the relevant circuit parameters through a set of measurements and yields a set of calibration coefficients. Using these coefficients, we can remove effects of the hardware imperfection of the six-port circuit and compensate the temperature variation and possible aging of the components, and so forth, so as to assure the best receiver performance.

The basic calibration theory of the six-port reflectometer is reviewed first. It has been pointed out that a conventional calibration method does not apply to six-port receiver since it is impractical to connect an external standard to an actual communication receiver that may be mobile.

An adaptive self-calibration method called dual-tone method which uses received signal as the source of calibration is then introduced. The details of such a theory and its algorithm are presented. The measurement results show that the new approach achieves the same order of accuracy as the conventional method but in a much simpler way.

Paper published in the IEEE Transactions on Microwave Theory and Tech. VOL.44, NO.1 January 1996, pp. 93-99.

Dual-Tone Calibration of Six-Port Junction and Its Application to the Six-port Direct Digital Millimetric Receiver

Ji Li, Renato G. Bosisio, Fellow, IEEE
and Ke Wu, Senior Member, IEEE

POLY-GRAMES Research Center
École Polytechnique, C. P. 6079, Succ. Centre Ville
Montréal, Canada H3C 3A7
FAX: (514) 340-5892

ABSTRACT

This paper describes a novel dual-tone calibration technique of six-port using two carriers with closely spaced frequencies. The samples for the calibration are extracted from outputs of four power detectors using a self-adaptive algorithm. The calibration procedure is fully automatic and can be implemented in a system capable of capturing the output waveforms of a six-port.

Although the proposed method is applicable to general six-port calibrations, it finds itself particularly suitable for the calibration of a new six-port direct digital mm-wave receiver. It is shown that such a calibration of the digital receiver can be fulfilled on site simply by receiving usual incoming signals. Dual-tone calibrations made at 26.5

GHz, 33 GHz and 40 GHz demonstrate the same order of accuracy as the conventional six-port calibrations. However, the new technique is much simpler and faster as it requires less effort in its implementation.

3.1 INTRODUCTION

It has been recognized that the calibration procedure proposed by Engen [3.1] and further developed by Hodgetts and Griffin [3.2] is the most robust method in the calibration of a six-port circuit. In this procedure, a six- to four-port reduction is made first to acquire five real calibration coefficients, and then a so-called 'error box' calibration is carried out to resolve the three remaining complex calibration coefficients.

When applied to the calibration of a six-port reflectometer, the six- to four-port reduction procedure can be considered as to determine parameters of a directional coupler by locating the origins of three circles in a complex plane (the so-called W-plane). The common interception point of these three circles represents the virtual reading of a reflection coefficient measured by the equivalent four-port. Fortunately, this W-plane calibration can be accomplished simply by measuring a number of arbitrary but different terminations. The exact knowledge of the reflection

coefficients of these terminations is not essential. Once the W-plane calibration is completed, an 'error box' calibration, similar to the standard procedure in a conventional vector network analyzer, is performed. The error box calibration eliminates residual errors arising from directivity, source match and frequency response of the equivalent four-port, and it fixes the position of reference plane as well.

Various methods have been used to generate the at least nine different terminations required for a W-plane calibration. The most straightforward way is to use a sliding short [3.1]. This method is very easy and reliable but difficult to automate. To automate the calibration, an "active load" method has been proposed in which a vector microwave modulator is used to feed a portion of the reference signal back into the DUT port. In this way, a variable load can be simulated [3.3]. An automatic termination generator (ATG) has also been proposed and applied to a commercial six-port reflectometer [3.4]. Such techniques require additional microwave hardware and auxiliary control circuits specifically made for such calibration purposes.

Recently, a direct mm-wave receiver (DMR) was proposed in which a six-port phase/amplitude/frequency discriminator is used [3.5,3.6]. The DMR is capable of directly demodulating various digital modulated signals such as PSK and QAM. The new receiver provides an interesting alternative in various communication systems such as point-to-point communication systems and satellite ground terminals.

However, it would be entirely impractical for a DMR to be used in a mobile digital handset to perform a calibration procedure if it were required to connect external physical standards to its input port. It is therefore necessary to develop a calibration method free from any external connection.

To accomplish this goal, a dual-tone six-port calibration method is proposed in this paper. The new dual-tone calibration is achieved by feeding a RF signal other than the reference source into the DUT port of the six-port. This signal can be either a unmodulated single carrier with a frequency adjacent to the six-port local source frequency, or a digital modulated signal with a frequency equal to or close to the local source frequency. The resulting output waveforms of the diode detectors of the six-port are actually beat-signals of the two RF signals (i.e., the six-port reference source and the second external RF signal). The voltage readings corresponding to a group of widely distributed terminations are acquired by properly sampling these waveforms. It is well known that the actual values of these terminations are not required for the W-plane calibration. Moreover, in the case where the absolute phase reference plane is not important as in a six-port DMR, the same waveform capture algorithm can also be applied to the error-box calibration without the need to use precise standards such as short, open and match loads as for a six-port reflectometer. Obviously, a real time data acqusition system capable of capturing instant voltage waveforms, such as real-time A/D converter or multi-channel digitizing oscilloscope, is essential to accomplish the proposed dual-tone calibration.

The dual-tone calibration is fully automatic in its nature: no repetitive connection of standards or tuning of sliding short is needed. The frequency difference between the two RF signals can be varied over a wide range as long as it remains below the limit of frequency response of the diode detectors and the data acquisition system. Along with a dual-tone linearization of the diode detectors [3.7,3.8], the whole internal six-port calibration can be completed in a single step. The standard error-box calibration, as used in a conventional vector network analyzer, is performed for instrumentation purposes only. The requirement of an additional RF signal generator for the dual-tone method could be somewhat difficult in some cases. On the other hand, this is definitely ideal for the six-port DMR calibration where the received signal acts as the second tone, thereby eliminates additional physical connections.

3.2 DUAL-TONE W-PLANE CALIBRATION OF THE SIX-PORT

3.2.1 W-plane calibration

The so-called W-plane calibration involves the solution of the following equation [3.2]:

$$pQ_1^2 + qA^2Q_2^2 + rB^2Q_3^2 + (r-p-q)A^2Q_1Q_2 + (q-p-r)B^2Q_2Q_3 \\ +(p-q-r)A^2B^2Q_2Q_3 + p(p-q-r)Q_1 + q(q-p-r)A^2Q_2 + r(r-p-q)B^2Q_3 + pqr = 0 \quad (3.1)$$

for p, q, r and A^2, B^2, where $Q_i = P_{i+3}/P_3$. These coefficients allow one transformation of a six-port to a perfect four-port reflectometer in a notional 'W' complex plane. The reflection coefficient is

$$W = \frac{Q_1 - A^2Q_2 + r}{2\sqrt{r}} + j\frac{r(p+q-r)+(p-q+r)Q_1 - (p-q-r)A^2Q_2 - 2rB^2Q_3}{\pm 2\sqrt{r(2pq+2qr+2pr-p^2-q^2-r^2)}} \quad (3.2)$$

Equation (3.1) may be solved by measuring at least nine (usually 13 in practice) arbitrary different terminations [3.1]. The dual-tone method is a novel technique that generates these terminations without resorting to actual physical connections.

3.2.2 Using a second carrier

Figure 3.1 shows a typical configuration of six-port reflectometer. The conventional four- to six- port reduction procedure requires at least nine connections of different loads to the DUT port. Instead of connecting a real load to the DUT port, a RF signal ('reflected wave' b) coupled from the reference source is fed into the DUT port with the same amplitude and phase as the 'incident wave' a, the equivalent reflection coefficient $\Gamma = b/a$ will be unity as if the DUT port is open-circuited. It is theoretically

possible to generate any equivalent termination by varying the amplitude/phase of the signal b. Such active load synthesis technique has been effectively used in the modeling of microwave power transistors [3.9,3.10].

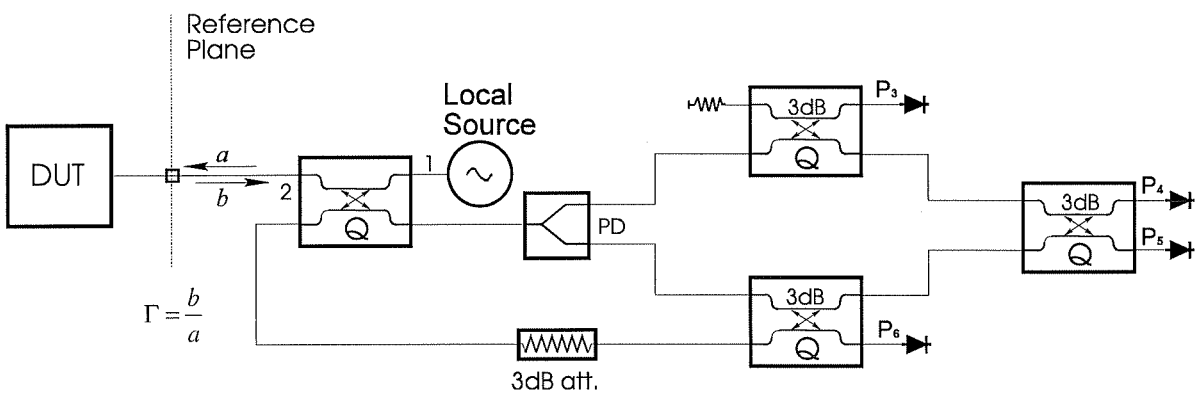

Figure 3.1. A typical six-port reflectometer.

Let us consider the case where the 'incident wave' a and the 'reflected wave' b are different in frequency, as in the following:

$$a = |a| \cdot e^{j(2\pi f_1 t + \varphi_1)} \tag{3.3}$$

$$b = |b| \cdot e^{j(2\pi f_2 t + \varphi_2)} \tag{3.4}$$

Suppose the frequency difference f_2-f_1 is very small so that the S parameters of the six-port to be calibrated can be regarded as being the same at f_1 and f_2, the equivalent reflection coefficient then becomes

$$\Gamma = \frac{b}{a} = \left|\frac{b}{a}\right| \cdot e^{j(2\pi\Delta ft + \Delta\varphi)} \tag{3.5}$$

where $\Delta f = f_2 - f_1$, and $\Delta\varphi = \varphi_2 - \varphi_1$.

Clearly, the equivalent reflection coefficient Γ becomes a time-dependent vector whose amplitude is invariant and the phase is shifting around at a constant angular speed $2\pi\Delta f$. In the case of $|a| = |b|$, it is as if a perfect sliding short moving at a constant speed is connected.

The voltage at a detector port of the six-port is a vector summation of portions of a and b waves presented at the port. Let the 'reflected wave' b be a single CW signal and the diode detectors fall in perfect square-law, the output voltage waveforms of the diode detectors are

$$V_{out,i} = \frac{1}{2}(|a_i|^2 + |b_i|^2) + |a_i| \cdot |b_i| \cos(2\pi\Delta ft + \Delta\varphi_i) \tag{3.6}$$

where a_i, b_i are incident and reflected waves at port i, respectively. Figure 3.2 plots output voltage waveforms of a typical six-port with a CW 'reflected wave' b.

It is noticed that a period of the waveform corresponds to a whole circle of Γ rotating in the complex plane. Therefore we capture waveforms of the four channels synchronously and choose the channel with maximum voltage swing as the reference channel. Selecting samples at an equal amplitude space in the whole voltage swing in this channel, these samples will present a group of equally spaced terminations on a circle in the Γ plane. By varying the amplitude of either the input CW signal or the local source, samples of Γ's well distributed over the whole Smith Chart can be obtained.

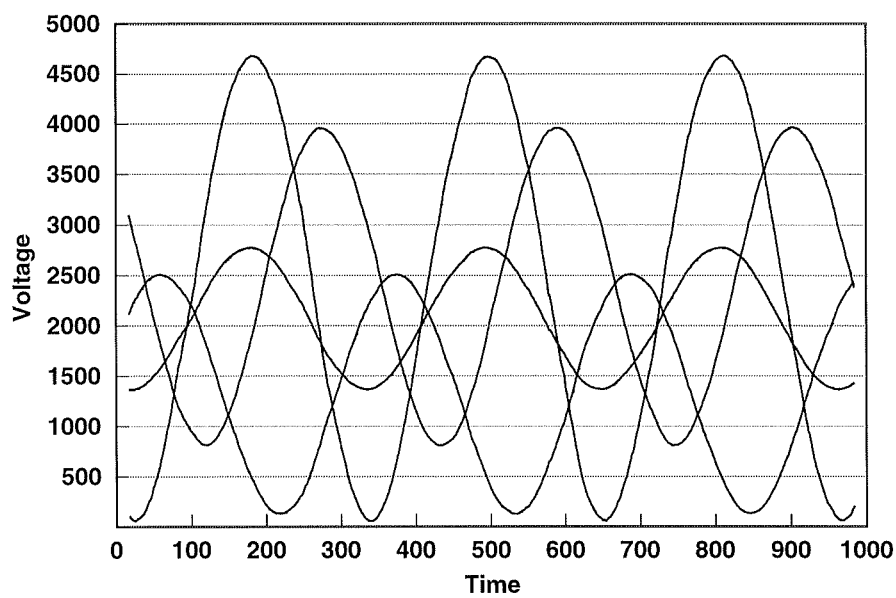

Figure 3.2. Typical output waveforms of a six-port with a CW input.

3.2.3 Dual-tone sampling algorithm

The flow chart outlining the algorithm for selecting the samples is shown in Figure 3.3 There is no particular restriction to frequency difference of the two signals. However, the maximum frequency of a capturable waveform depends on the sampling rate of the data acquisition systems and track/hold (T/H) circuit response time. It should be emphasized that the samples must be taken synchronously, i.e. the four power readings for each sample must be taken at the same instant. It is also possible to use T/H circuits to freeze the waveforms and then perform A/D conversion sequentially. The rule of thumb is that at least 20 ~ 30 samples be taken in a cycle when a CW signal is used. The power level of the 'reflected wave' b has to be strong enough to suppress noise interference. The power level step should be around 3dB but need not be precise.

The algorithm is designed to deal with a wide variety of signals such as unmodulated CW, PSK, QAM and AM signals, etc. The signals involving wide band frequency modulation may be difficult to capture when the bandwidth of data acquisition system is narrow. Figure 3.4 illustrates examples of sampling using the conventional 13-standard method and the proposed dual-tone method with different types of input signals. It can be seen that the samples are well distributed over the entire Smith chart regardless of the signal type. The slight shift of the origin of the dual-tone samples is due to the residual reflection at the DUT port.

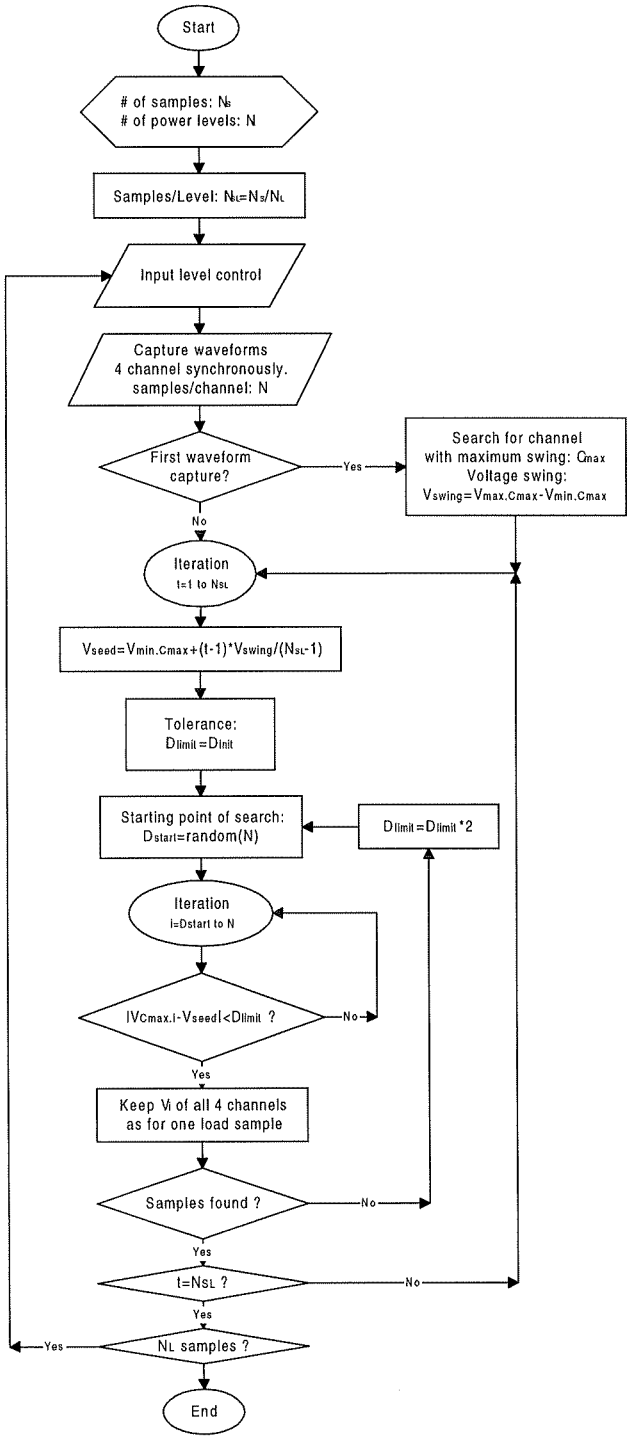

Figure 3.3. Flow chart of the algorithm taking samples for W-plane calibration.

It can be logically anticipated that for unmodulated CW signals, there should be a small frequency difference between the two carriers, whereas this is not crucial for a high-level digital modulated signal (phase states no less than four). On the other hand, a carrier-synchronized QAM (e.g. 16QAM, 64QAM) signal provides a perfect sample distribution.

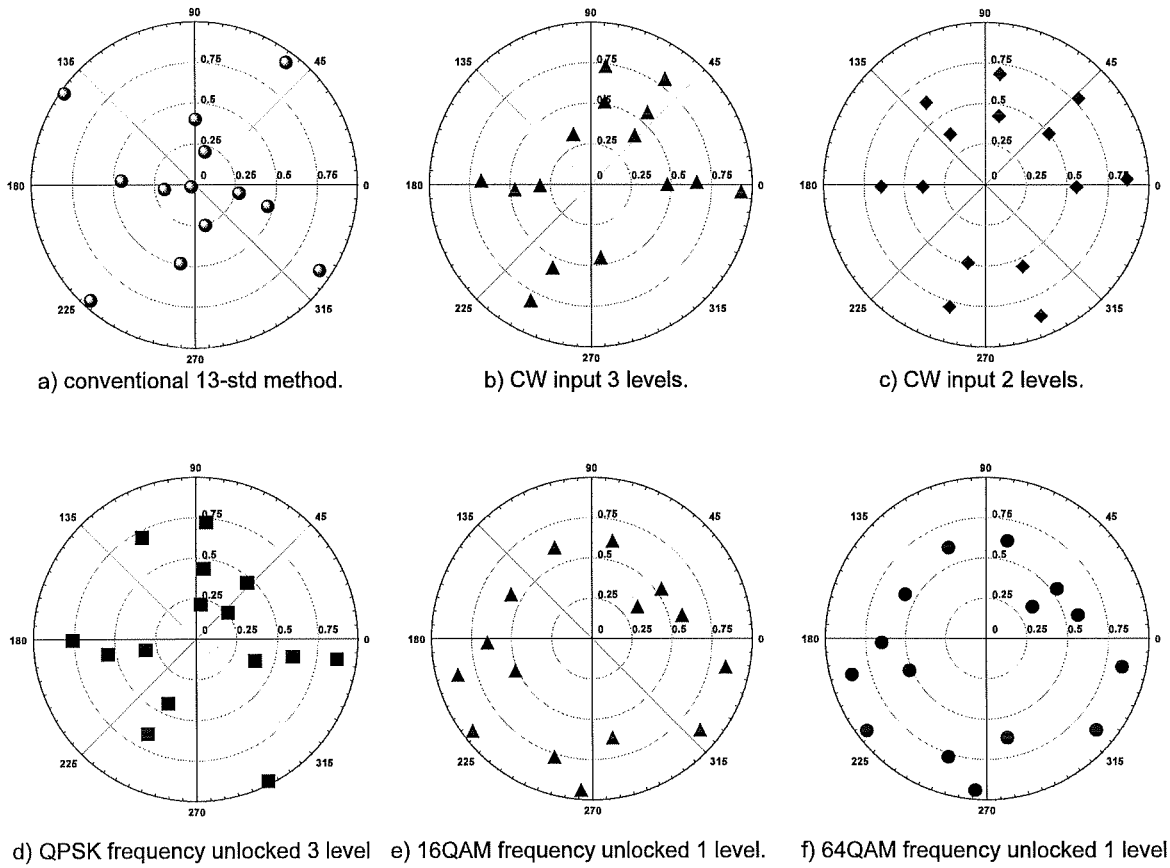

Figure 3.4. Sample distributions using 13-standard method and dual-tone method.

3.2.4 Waveform smoothing

The two carriers used in the dual-tone calibration are generally incoherent signals, i.e. not being generated from the same oscillator. Consequently, the phase noise of the two carriers will introduce random instant phase jitters in the equivalent Γ. When a CW '*b*' wave is used for the calibration, the output waveforms of detectors become noisy sinusoidal waves. It is preferable sometimes to smoothen the captured waveforms before sampling, although this usually does not affect the calibration result provided that the response time of the data acquisition circuit be fast enough to follow the jitters. A simplified Savitzky-Golay method called 'moving window average'[3.11] is found to be very effective in handling such problems. The characteristic equation of this method is

$$v_{smooth,i} = \sum_{n=-n_L}^{n_R} c_x v_{orig,i+n} \qquad (3.7)$$

where $v_{smooth,i}$ is the voltage after smoothing, v_{orig} is the original data and $c_x = 1/(n_L + n_R + 1)$, n_L and n_R are widths of the windows on the left and right sides, respectively. Figure 3.5 illustrates a real captured waveform before and after smoothing. It clearly indicates the effectiveness of the method.

The dual-tone method captures real time waveforms at the six-port power detector ports. This makes it more vulnerable to noise than a typical reflectometer calibration

using standard power meters or multi-sample/averaging A/D converters. An improved algorithm proposed by Potter and Hjipiers [3.12] could help to obtain more stable solution for equation (3.1).

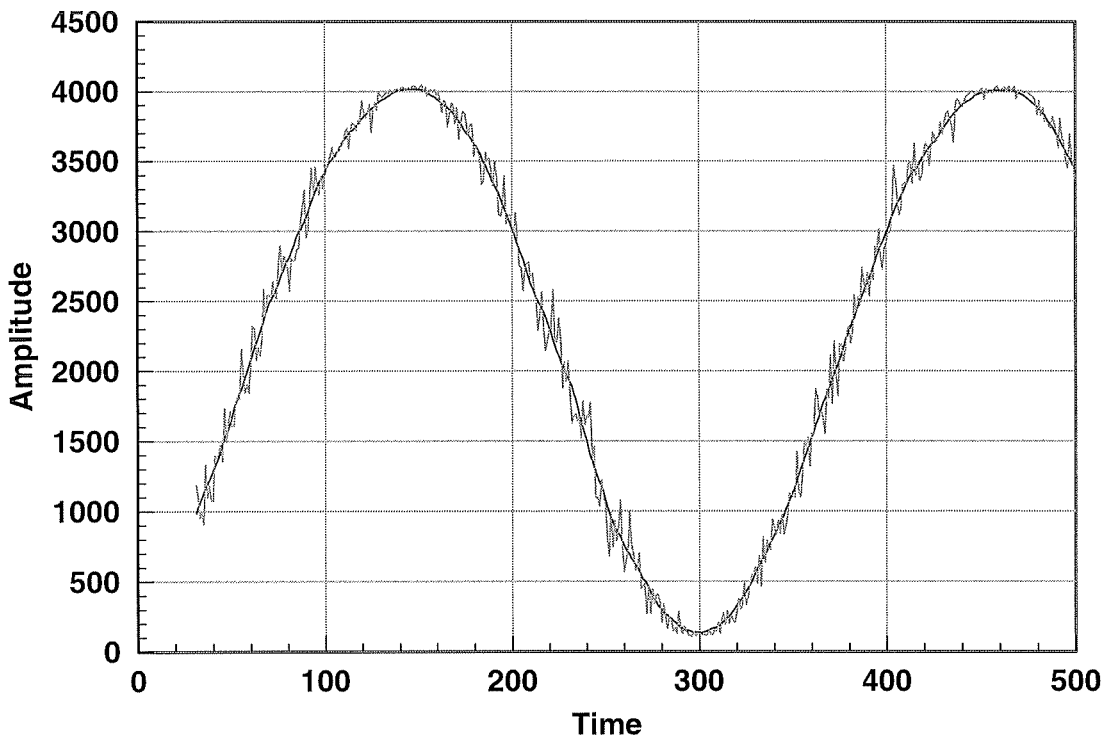

Figure 3.5. Waveforms before and after smoothing.

3.3 DUAL-TONE ERROR-BOX CALIBRATION OF THE SIX-PORT DMR

3.3.1 Error-box calibration

A two-port 'error-box' is inserted between the notional four-port and the DUT such that the virtual reflection readings from the notional perfect reflectometer obtained by W-plane calibration are transferred to the real reflection coefficients Γ. This is done through a bilinear transformation:

$$\Gamma = \frac{e - W}{cW - d} \tag{3.8}$$

where *c, d* and *e* are complex constants related to the S parameters of the 'error-box':

$$\begin{aligned} c &= -s_{22} \\ d &= s_{12}s_{21} - s_{11}s_{22} \\ e &= s_{11} \end{aligned} \tag{3.9}$$

A standard calibration using three known standards (e.g. short, open and matched loads) for a conventional vector reflectometer can be applied here. In addition, a fourth load that needs only to be roughly known has to be used to determine the sign in (3.2) [3.2].

3.3.2 Necessity of error-box calibration for the six-port DMR

It is in fact impossible to connect standards to a six-port DMR in the presence of preceding low noise amplifier and other circuits. This also inhibits the application of a typical error-box calibration to a DMR. On the other hand, the absolute phase reference plane is not important for digital demodulation, therefore a simplified error-box calibration can be adopted.

It would be nice to bypass the error-box calibration regarding the fact that the bilinear transformation (8) maps a circle in W-plane into a circle in Γ-plane. Unfortunately, it is found in most cases that the equal-reflection circles in W-plane are not concentric as shown in Figure 3.6. This results in distortion of the constellation diagram of digital modulation and it is therefore unavoidable to use transformation (3.9) for the six-port DMR.

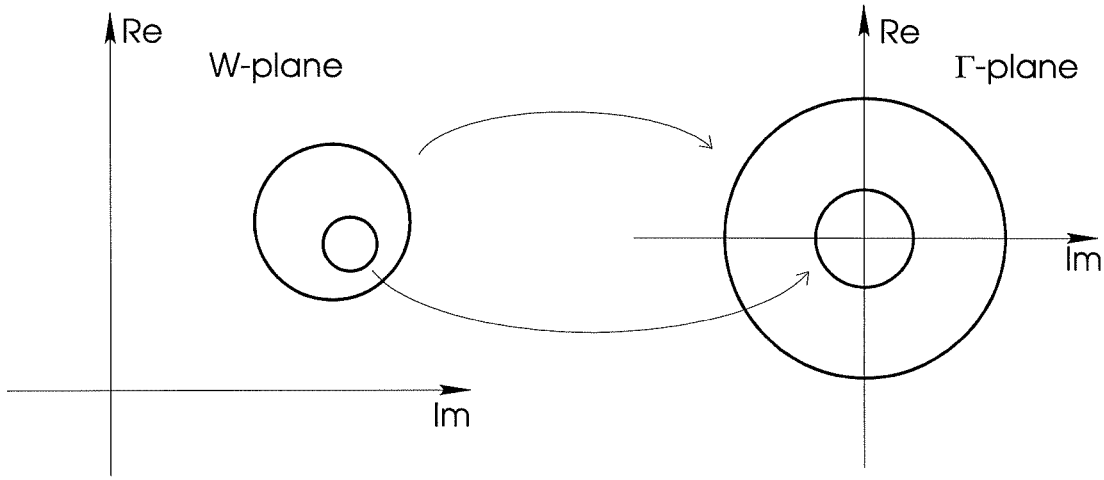

Figure 3.6. W-plane to Γ-plane bilinear transformation: the circles are mapped into circles but not concentric.

3.3.3 Dual-tone error-box calibration for DMR

In a six-port DMR, the phase reference plane is not important. This allows us to adopt a procedure that is similar to the dual-tone W-plane calibration.

Rewrite (3.6) as:

$$V_{out.i} = \frac{1}{2}(|a_i|^2 + |b_i|^2) + |a_i| \cdot |b_i| \cos(\varphi_{a_i} - \varphi_{b_i}) \qquad (3.10)$$

The $V_{out.i}$ reaches the maximum and minimum values when

$$\begin{aligned} &\text{Max.: } \varphi_{b_i} = \varphi_{a_i} - 2n\pi \\ &\text{Min.: } \varphi_{b_i} = \varphi_{a_i} - 2n\pi - \pi \qquad n = \ldots -2, -1, 0, 1, 2 \ldots \end{aligned} \tag{3.11}$$

The swing of the waveform is given by

$$\Delta V = V_{out.i.\max} - V_{out.i.\min} = 2|a_i| \cdot |b_i| \tag{3.12}$$

Let $b' = kb$, thus $b_i' = kb_i$, and the swing becomes

$$\Delta V' = V'_{out.i.\max} - V'_{out.i.\min} = 2k|a_i| \cdot |b_i| \tag{3.13}$$

Then

$$\frac{\Delta V'}{\Delta V} = k \tag{3.14}$$

From the definition of $\Gamma = b/a$, then

$$\Gamma' = \frac{b'}{a} = \frac{kb}{a} = k\Gamma \tag{3.15}$$

Obviously, the swing of waveform represents magnitude of the equivalent Γ term, and if a Γ corresponding to the maximum voltage at one port (the reference port) is taken

as the phase reference such that $\Gamma = |\Gamma| e^{j0}$, then the Γ at the minimum voltage at this port should be $\Gamma' = |\Gamma'| e^{j\pi}$.

Accordingly, we define

$$\begin{aligned} \Gamma_1 &= 1 \cdot e^{j0} && \text{at } V_{out.ref.\max} \\ \Gamma_2 &= 1 \cdot e^{j\pi} && \text{at } V_{out.ref.\min} \\ \Gamma_3 &= k \cdot e^{j0} && \text{at } V'_{out.ref.\max} \\ \Gamma_4 &= k \cdot e^{j\pi} && \text{at } V'_{out.ref.\min} \end{aligned} \tag{3.16}$$

and use these values to solve unknowns *c, d* and *e* in (3.8) such that the error-box calibration of the six-port DMR is accomplished.

The above approach cannot determine the sign in equation (3.2). Nevertheless, it is found that a wrong sign in equation (3.2) leads to a reversed phase mapping in the constellation diagram, which can be readily detected and corrected in the demodulation algorithm.

3.4 RESULTS

The proposed dual-tone calibration is performed on a six-port circuit at 26.5GHz, 33GHz and 40GHz. A PC486 is used as a controller of the measurement system. A data acquisition card with track/hold amplifiers captures waveforms in real time. CW signals with step power control are used for the dual-tone calibration. The conventional 13-standard calibration is also made using the same system.

Table 3.1 lists the W-plane calibration coefficients p, q, r, A^2 and B^2 obtained from both conventional 13-standard (13-std) method and dual-tone method at three different frequencies. It can be seen that the dual-tone method yields almost the same values of calibration coefficients as the conventional 13-std method. The insignificant difference between the two methods is basically of the same order as the fluctuation of values in two different 13-std calibrations. It is also found that a two-level power control is sufficient for a good calibration. An attempt to eliminate the power control was not successful.

Subsequently, standard error box calibrations are carried out using the W-plane calibration coefficients given in Table 3.1. Reflection coefficients of various loads are measured by the use of the calibrated reflectometer. The same loads are also measured with a HP8510 vector network analyzer for reference purpose. Table 3.2 presents the measured Γ of those loads. It can be seen that the overall maximum error is 0.6dB/5°

except for very low reflection loads #4 and #7. It is noticed that a system error appears between six-port and network analyzer measurements which might be caused by different calibration standard sets used for HP8510 and six-port. In most cases, the difference between the 13-std and the dual-tone calibrations is in the order of 0.1dB/1.0°. Note that the readings are taken from a real time continuous display of reflection coefficient, and only one sample is taken for each reading without averaging. Due to the presence of noise, the displayed reading itself has a variation of 0.1dB/1.0° for most situations. Therefore, the accuracy of the new dual-tone calibration is actually of the same order as that of a 13-std calibration.

A dual-tone error box calibration is also accomplished. Figure 3.7 shows constellation diagrams of QPSK and 16QAM modulations measured by a six-port receiver calibrated by the dual-tone method. The phase span of the vectors is caused by phase noise of the signal generators and slow acquisition time. No obvious distortion of the constellation is observed.

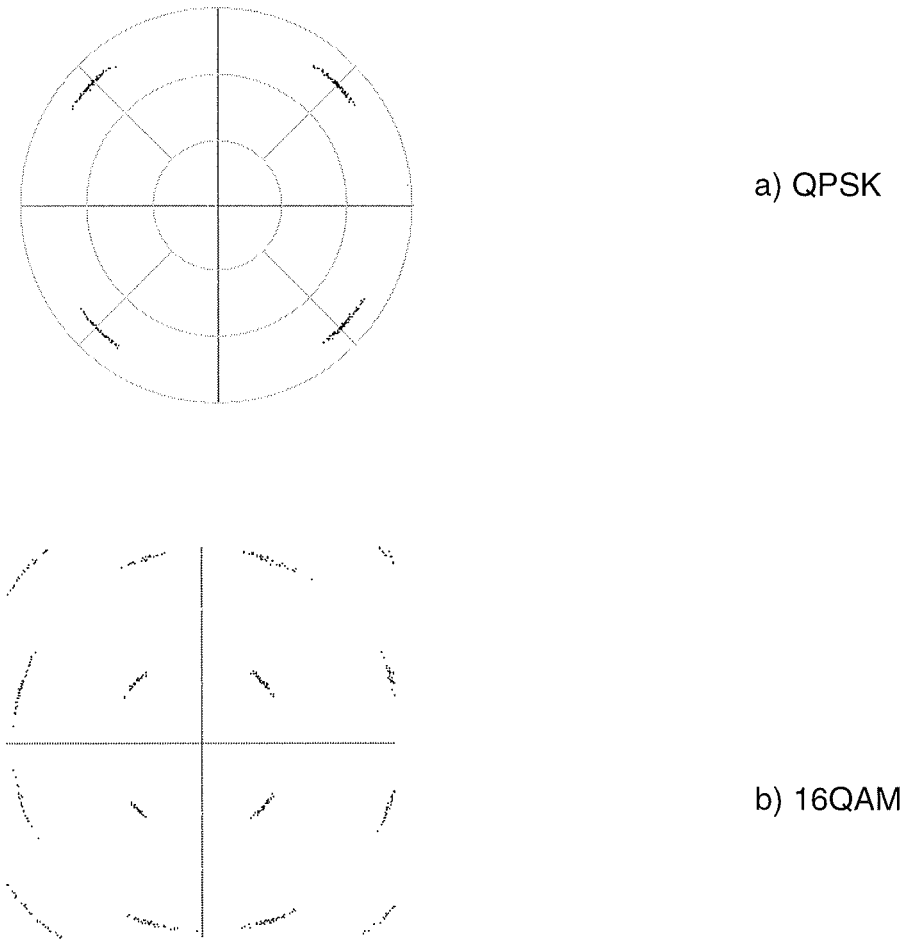

Figure 3.7. Constellation diagrams measured by a six-port digital receiver calibrated using dual-tone W-plane and error-box method. The angular spread represents the phase/frequency jitters of the oscillators used in the experiment.

Table 3.1. Calibration coefficients using conventional 13-std method and dual-tone method.

Freq.	26.5 GHz			33 GHz			40 GHz		
	13-std	**cw 3-level**	**cw 2-level**	**13-std**	**cw 3-level**	**cw 2-level**	**13-std**	**cw 3-level**	**cw 2-level**
p	2.09850	2.05330	2.00897	2.64877	2.66865	2.66332	1.54830	1.51983	1.48923
q	1.45223	1.45686	1.42006	1.71614	1.75197	1.74824	0.84404	0.81323	0.80494
r	1.40958	1.41367	1.35935	1.52518	1.50819	1.51315	1.09592	1.09138	1.07826
A^2	0.58268	0.58215	0.53294	0.29511	0.29469	0.29379	0.35069	0.35050	0.34374
B^2	1.08903	1.12284	1.07837	1.18485	1.19764	1.19214	0.71840	0.69764	0.68318

67

Table 3.2. Measured reflection coefficients using HP8510 vector network analyzer and six-port reflectometer calibrated by the use of conventional 13-std method and dual-tone method.

	26.5 GHz				33 GHz				40 GHz			
	HP8510	13-std	cw 3-level	cw 2-level	HP8510	13-std	cw 3-level	cw 2-level	HP8510	13-std	cw 3-level	cw 2-level
#1	0.973∠ -177.6°	1.043∠ -179.5°	1.010∠ 180.0°	0.968∠ -179.1°	0.997∠ -178.0°	0.980∠ 179.5°	0.978∠ 178.7°	0.970∠ 179.3°	0.985∠ 178.5°	0.990∠ 178.2°	0.996∠ 176.8°	0.998∠ 175.7°
#2	0.999∠ 91.9°	0.996∠ 88.5°	0.998∠ 88.3°	0.998∠ 88.2°	0.969∠ -103.0°	0.979∠ -107.6°	0.980∠ -107.3°	0.980∠ -107.6°	0.975∠ 36.7°	0.969∠ 36.9°	0.972∠ 36.8°	0.972∠ 36.9°
#3	0.962∠ -78.3°	0.975∠ -77.4°	0.973∠ -77.3°	0.973∠ -77.3°	0.985∠ 80.4°	0.982∠ 79.8°	0.983∠ 80.2°	0.982∠ 79.8°	0.972∠ -133.8°	0.968∠ -134.2°	0.971∠ -133.8°	0.974∠ -133.7°
#4	0.049∠ -121.5°	0.032∠ -148°	0.029∠ -156°	0.026∠ -153°	0.038∠ -77.0°	0.019∠ -46°	0.020∠ -52°	0.019∠ -51°	0.025∠ -93.2°	0.025∠ -109°	0.026∠ -95°	0.026∠ -95°
#5	0.422∠ 104.0°	0.425∠ 102.5°	0.427∠ 101.7°	0.428∠ 101.5°	0.523∠ 31.8°	0.554∠ 32.6°	0.546∠ 32.1°	0.549∠ 32.3°	0.413∠ -66.9°	0.416∠ -69.8°	0.418∠ -69.1°	0.420∠ -69.2°
#6	0.218∠ 89.3°	0.212∠ 89.5°	0.215∠ 89.5°	0.218∠ 88.6°	0.277∠ 54.1°	0.289∠ 53.3°	0.287∠ 53.1°	0.289∠ 52.8°	0.255∠ -75.6°	0.266∠ -77.3°	0.268∠ -76.9°	0.270∠ -76.1°
#7	0.066∠ -38.9°	0.091∠ -39.7°	0.093∠ -37.0°	0.092∠ -35.9°	0.061∠ -175.0°	0.048∠ 178.0°	0.049 -178.0°	0.049∠ -178.0°	0.100∠ -16.5°	0.113∠ -23.3°	0.116∠ -23.0°	0.114∠ -23.0°
#8	1.016∠ 95.7°	1.000∠ 90.7°	1.001∠ 90.7°	0.999∠ 90.3°	0.982∠ -99.8°	0.983∠ -103.9°	0.985∠ -103.6°	0.985∠ -103.5°	0.988∠ 39.2°	0.972∠ 39.7°	0.976∠ 38.8°	0.980∠ 39.4°

68

3.5 CONCLUSION

A novel dual-tone W-plane calibration for six-port is proposed and shown to be able to achieve, at a high speed, the same order of accuracy as the conventional 13-standard calibration as applied to six-port reflectometers. With the proposed dual-tone method, the calibration of a six-port direct millimetric digital receiver including diode linearization, W-plane calibration and error box calibration can be implemented as desired in an operating receiver.

ACKNOWLEDGMENT

The authors would like to thank the Natural Science and Engineering Research Council of Canada (NSERC) for its support in making the above research possible.

REFERENCES

[3.1] G.F.ENGEN, "Calibrating the six-port reflectometer by means of sliding terminations", IEEE Trans, Microwave Theory Tech., vol. MTT-26, pp. 951-957, Dec. 1978.

[3.2] E.T.HODGETTS and E.J.GRIFFIN, "A unified treatment of the theory of six-port reflectometer calibrations using the minimum of standards", Royal Signal and Radar Establishment, Malvern, Report 83003, 1983.

[3.3] E. EID, *et al*, "Self-calibration of six-port reflectometers using active loads", 1994 CPEM Digest, pp. 121-122, 1994.

[3.4] Marconi Instruments, "Design of a six-port microwave instrument", Marconi Instruments Technical Journal, issue 93/2, pp. 6-7, 1993.

[3.5] JI LI, R.G.BOSISIO and KE WU, "a six-port direct digital millimeter wave receiver", Digest IEEE MTT-S'94, pp. 1659-1662, San Diego, May, 1994.

[3.6] JI LI, R.G.BOSISIO and KE WU, "a new direct digital receiver performing coherent PSK reception", Digest IEEE MTT-S'95, pp. 1007-1010, Orlando, May, 1995.

[3.7] V.S.REINHARDT, *et al*, "Methods for measuring the power linearity of microwave detectors for radiometric applications", Digest IEEE MTT-S'94, pp. 1477-1480, May, 1994.

[3.8] JI LI, R.G.BOSISIO and KE WU, "a simple dual-tone calibration of diode detectors", Proc. IEEE IMTC'94, vol.1, pp. 276-279, May, 1994.

[3.9] Y. TAKAYAMA, "a new load-pull characterization method for microwave power transistors", Digest IEEE MTT-S'76, pp. 218-220, 1976.

[3.10] F.M.GHANNOUCHI, R.LAROSE and R.G.BOSISIO, "A new multi-harmonic loading method for large-signal microwave transistor characterization", IEEE Trans, Microwave Theory Tech., vol. MTT-39, pp. 986-992, Dec. 1991.

[3.11] W.H.PRESS, *et al*, *Numerical Recipes in FORTRAN*, Cambridge University Press, 2nd Edition, pp. 644-649, 1992.

[3.12] C.M.POTTER and G.HIJIPIERIS, "a robust six- to four- port reduction algorithm", Digest IEEE MTT-S'93, pp. 1263-1266, 1993.

Chapter 4

Six-port Circuit Design and Modeling

4.1 General consideration on six-port circuit design

As far as the design of a six-port is concerned, the utilization of a particular technology depends on its applicability and suitability for the specific working frequency range. Among different possible choices, MMIC (Monolithic microwave integrated circuit) and MHMIC (miniaturized hybrid microwave integrated circuit) are considered to provide the best solution in terms of the circuit size, the versatility and the cost for the millimeter-wave communication systems. Six-port receiver requires good stability and high sensitivity. This leads to the following design criteria:

I. Minimized overall circuit dimension.

II. Minimized insertion loss between the RF input port and power detector ports to increase sensitivity. The insertion loss to all the power detector ports should be even, as to prevent the noise of a single diode detector from deteriorating the overall performance before the threshold is reached.

III. Maximized isolation between the RF input port and LO port to reduce LO leakage to the antenna.

IV. The LO power presented at all the detector ports should be at the same order. This is to facilitate the baseband signal conditioning and A/D conversion circuit design.

V. Similar to the six-port reflectometer design, the q_i points should be equal in magnitude and 120° different from each other in phase. Suppose the RF input port and LO port are isolated, the equivalent q_i points can be expressed as $q_4 = {s_{41}}/{s_{42}}$, $q_5 = {s_{51}}/{s_{52}}$ and $q_6 = {s_{61}}/{s_{62}}$.

VI. Maximized temperature stability.

VII. Utilization of low noise, high sensitive zero-biased Schottky diodes, where possible.

4.2 Six-port circuit configuration

Figure 4.1 presents the block diagram of a six-port circuit. The six-port circuit behaves like a microwave vector voltmeter. Assume that the RF input and LO input ports are isolated and the insertion loss from RF input to all the four detectors are equal. The LO power presented at P_3~P_5 are also the same. The S parameters are listed as.

$$\begin{aligned} s_{32} &= \tfrac{1}{2}e^{-j90^\circ} & s_{31} &= \tfrac{1}{2}e^{-j90^\circ} \\ s_{42} &= \tfrac{1}{2}e^{-j0^\circ} & s_{41} &= \tfrac{1}{2}e^{-j180^\circ} \\ s_{52} &= \tfrac{1}{2}e^{-j90^\circ} & s_{51} &= \tfrac{1}{2}e^{-j0^\circ} \\ s_{62} &= \tfrac{1}{2}e^{-j0^\circ} & s_{61} &= \tfrac{1}{2}e^{-j90^\circ} \end{aligned} \tag{4.1}$$

Then the q_i points are

$$\begin{aligned} \frac{s_{32}}{s_{31}} &= e^{j0^\circ} & \frac{s_{42}}{s_{41}} &= e^{j180^\circ} \\ \frac{s_{52}}{s_{51}} &= e^{-j90^\circ} & \frac{s_{62}}{s_{61}} &= e^{j90^\circ} \end{aligned} \tag{4.2}$$

It can be seen that they are 90° different in phase, which is not the best distribution as described in criterion V.

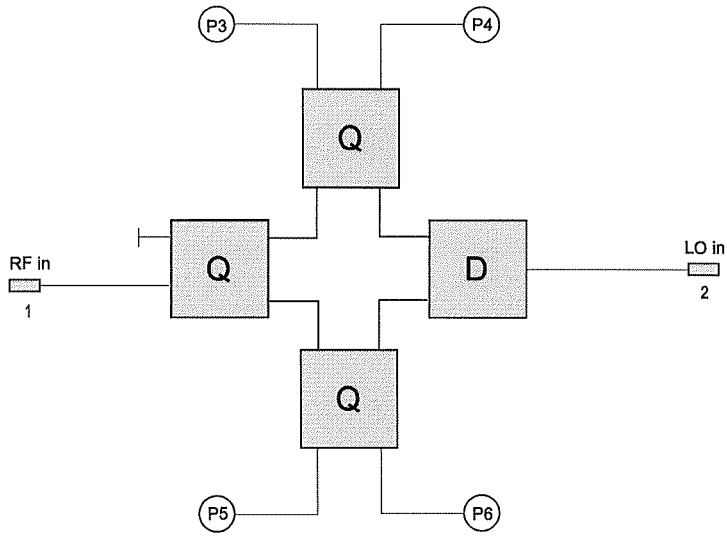

Figure 4.1 Six-port circuit for vector acquisition.

Figure 4.2 illustrates an alternative circuit configuration, whose q_i points are

$$\begin{aligned} \frac{s_{41}}{s_{42}} &= -\sqrt{2} = \sqrt{2}e^{j180^\circ} \\ \frac{s_{51}}{s_{52}} &= \frac{1-j}{\sqrt{2}} = \sqrt{2}e^{-j45^\circ} \\ \frac{s_{61}}{s_{62}} &= \frac{1+j}{\sqrt{2}} = \sqrt{2}e^{j45^\circ} \end{aligned} \tag{4.3}$$

In this circuit, the q_i points are better spread over the complex plan. However, neither RF signal nor LO power is evenly distributed among the output ports.

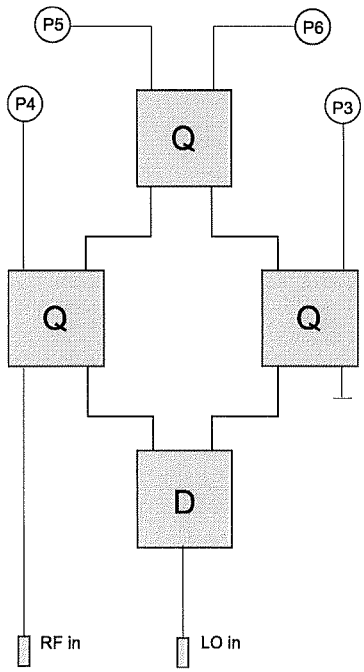

Figure 4.2 An alternative six-port circuit configuration.

4.3 Implementation of a receiver using five-port circuits

It is noticed that in Figure 4.2, only a portion of the LO power is presented at port P_3. It can be logically concluded that this port does not contribute to the detection of the RF input signal. The previous study has confirmed that the 6th port is actually redundant. This redundancy is nevertheless imperative in a reflectometer design to overcome the ambiguity caused by a $\pm$ sign in (3.2). In a six-port receiver, when the dual-tone calibration is used, this 6th port is no longer useful in determining the sign as required in the reflectometer. Such an ambiguity only causes an opposite rotation of the detected

vector which can be readily resolved by identifying a frame header or test sequence in the digital modulation signal. Moreover, reducing the number of power detector port will also boost the sensitivity and lower the LO power requirement of the receiver.

Meanwhile, the six-port theory is still valid. All the six-port formulation can still be used by assigning P_3 to a positive constant. The value of P_3 will exist as if a real power still appear at the port 3.

4.4 Optimum design of the five-port circuits

A five-port circuit configuration is proposed and illustrated in Figure 4.3. It can be seen that the circuit is inherently lossless: all the RF signal and LO power will be consumed by the power detectors, therefore high receiver sensitivity and low LO power requirement can be expected. The isolation between RF input port and LO port can be achieved by the directional coupler $Q(C_1)$. It will be shown below that by properly choosing the coupling factor C_1 , C_2 and phase shift ϕ , an optimum circuit design that satisfies all the requirements as listed in section 4.1 can be accomplished.

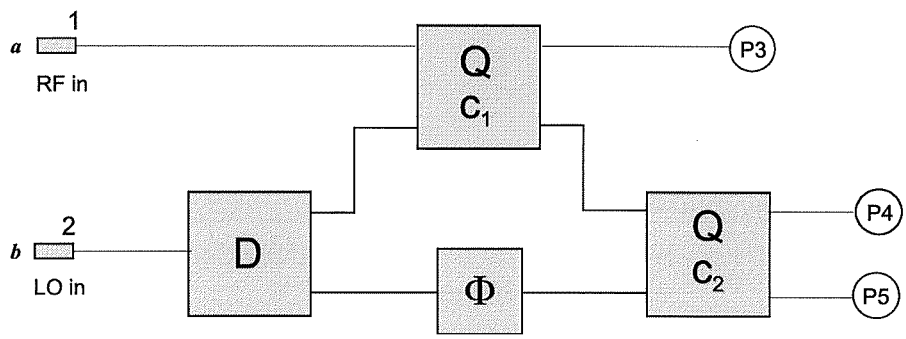

Figure 4.3 Five-port circuit configuration.

From the circuit in Figure 4.3, it can be deduced that

$$
\begin{aligned}
s_{31} &= c_2 & s_{32} &= -j\sqrt{\frac{1-c_2^2}{2}} \\
s_{41} &= -jc_3\sqrt{1-c_2^2} & s_{42} &= \frac{1}{\sqrt{2}}(c_2c_3 - j\sqrt{1-c_3^2}e^{-j\phi}) \\
s_{51} &= -\sqrt{(1-c_2^2)(1-c_3^2)} & s_{52} &= \frac{1}{\sqrt{2}}(c_3e^{-j\phi} - jc_2\sqrt{1-c_3^2})
\end{aligned}
\tag{4.4}
$$

According to the design goal II presented in 3.3.1, let

$$|s_{31}| = |s_{41}| = |s_{51}| \tag{4.5}$$

Solving equation (3.18) yields

$$c_2 = \frac{1}{\sqrt{3}} \qquad c_3 = \frac{1}{\sqrt{2}} \tag{4.6}$$

Assigning ϕ to zero, the related S parameters will be

$$
\begin{aligned}
s_{31} &= \frac{1}{\sqrt{3}} & s_{32} &= -j\frac{1}{\sqrt{3}} \\
s_{41} &= -j\frac{1}{\sqrt{3}} & s_{42} &= \frac{1}{2}(\frac{1}{\sqrt{3}} - j) \\
s_{51} &= -\frac{1}{\sqrt{3}} & s_{52} &= \frac{1}{2}(1 - j\frac{1}{\sqrt{3}})
\end{aligned}
\tag{4.7}
$$

Thus

$$
|s_{31}| = |s_{41}| = |s_{51}| = |s_{32}| = |s_{42}| = |s_{52}| = \frac{1}{\sqrt{3}} \tag{4.8}
$$

In this way, the presumed design goal II and IV are satisfied.

To verify the q_i point distribution, we obtain

$$
\begin{aligned}
q_3 &= \frac{s_{32}}{s_{31}} = -j = e^{-j90^\circ} \\
q_4 &= \frac{s_{42}}{s_{41}} = \frac{\sqrt{3}}{2} + j\frac{1}{2} = e^{j30^\circ} \\
q_5 &= \frac{s_{52}}{s_{51}} = -\frac{\sqrt{3}}{2} + j\frac{1}{2} = e^{j150^\circ}
\end{aligned}
\tag{4.9}
$$

These q_i points are equal in magnitudes and separated by 120° in phases, which satisfy also the design goal V.

It is therefore concluded that the circuit described in Figure 4.3 with (4.6) is an optimum five-port circuit for the digital receiver application. The optimum design requires a power divider, a 3dB coupler and a 4.77dB quadrature coupler. A microstrip circuit

layout is given in Figure 4.6. The diode power detectors are also integrated into the circuit layout. Wide band design is also achievable provided that the wide-band power divider and the couplers are used.

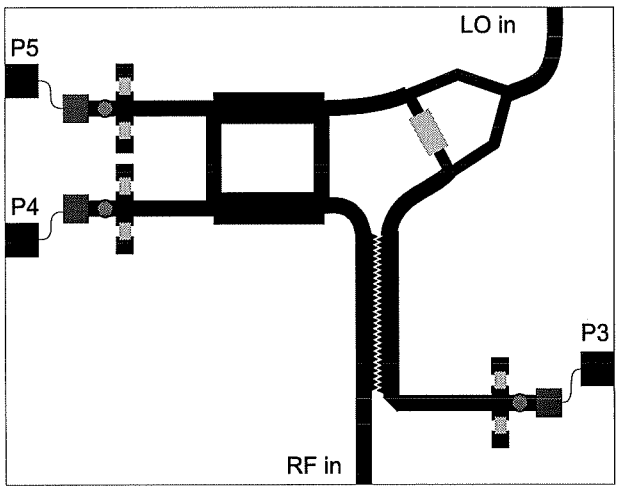

Figure 4.4 Layout of the optimum five-port receiver circuit.

Although the circuit shown in Fig. 4.4 provides the best performance, it is sometimes preferred to use a simpler 3dB coupler such as the branch line coupler to realize a narrow band circuit. The circuit layout is shown in Figure 4.7. In this case, $C_2=C_3=0.707$, and the corresponding S parameters and q_i points become

$$s_{31} = \frac{1}{\sqrt{2}} \qquad s_{32} = -j\frac{1}{2}$$
$$s_{41} = -j\frac{1}{2} \qquad s_{42} = \frac{1}{2\sqrt{2}} - j\frac{1}{2} \tag{4.10}$$
$$s_{51} = -\frac{1}{2} \qquad s_{52} = \frac{1}{2} - j\frac{1}{2\sqrt{2}}$$

$$q_3 = \frac{1}{\sqrt{2}}e^{-j90^\circ} \quad q_4 = \sqrt{\frac{3}{2}}e^{j35.26^\circ} \quad q_5 = \sqrt{\frac{3}{2}}e^{j144.74^\circ} \tag{4.11}$$

Apparently, this design somehow deviates from the theoretical optimal operating conditions. A detailed investigation is needed to reveal how much degradation this deviation will introduce to the receiver performance.

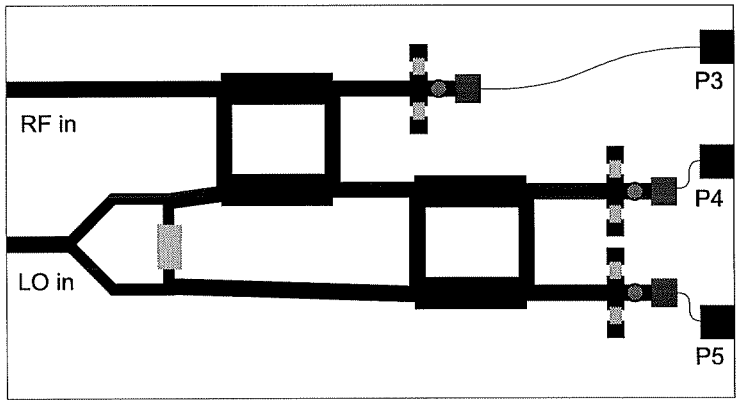

Figure 4.5 Five-port circuit using branch line coupler and in-phase power divider.

4.5 20 GHz MHMIC five-port circuit design

A 20 GHz MHMIC five-port receiver circuit is designed for millimeter-wave applications. The circuit consists of a 4.77 dB branch line coupler, a 3 dB branch line coupler, a 3 dB in-phase power splitter and three diode power detectors. Hewlett Packard's MDS (Microwave Design System) was used for the circuit simulation and layout. The circuit is designed to cover about 20% bandwidth from 18 GHz to 22 GHz.

Microstrip line transmission lines are used. Based on the standard MHMIC technology available in our laboratory, the substrate is Al_2O_3 ceramic with ε_r of 9.9 and thickness of 10 mil (0.254 mm). The square resistor is 100Ω/• .

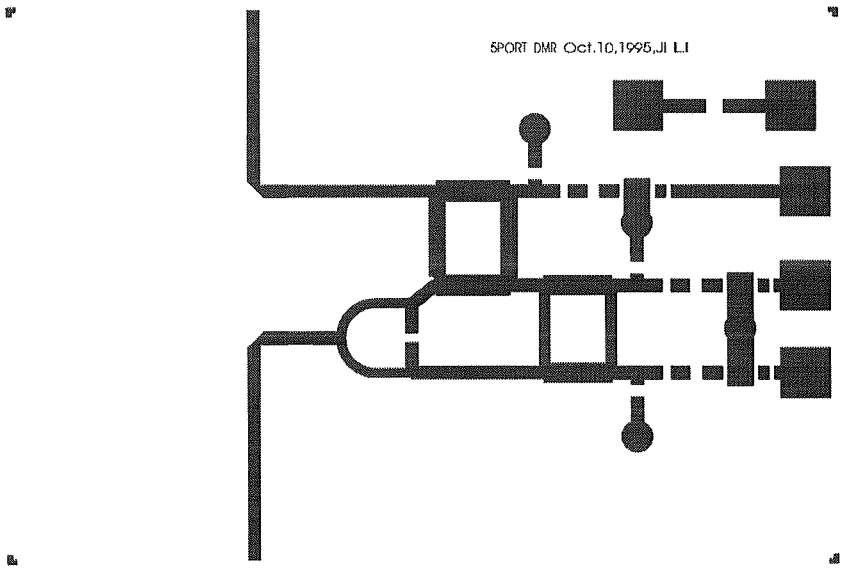

Figure 4.6 Mask of the 20 GHz MHMIC five-port receiver circuit.

Figure 4.6 is the mask layout of the proposed circuit. The size of the designed circuit is 700mil×450mil (17.78mm×11.43mm). The RF input and LO signals are connected to top and bottom ports, respectively, and the diode detectors outputs are directed to three DC pads.

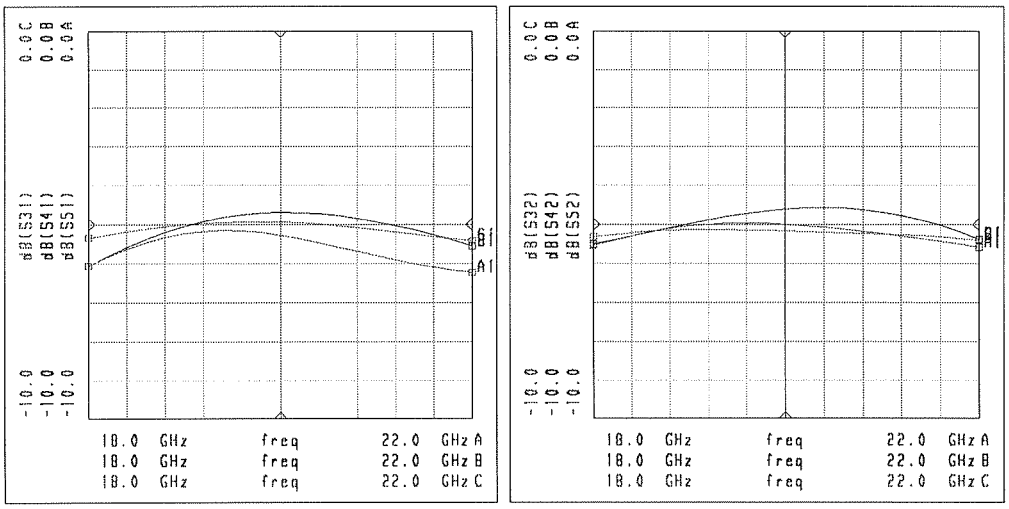

Figure 4.7 Simulated S parameters of the five-port MHMIC circuit.

Figure 4.7 illustrates the frequency response of this circuit. Under the ideal situation, the insertion loss from port 1 (RF input) and port 2 (LO input) to diode detector ports 3, 4 and 5 should be 4.77 dB. It can be seen that the real response is fluctuating above or below this point.

The isolation between RF and LO ports is an important parameter of the receiver. Figure 4.8 shows the simulated result. It can be seen that the isolation is 18 dB at the center frequency (20 GHz) and 13 dB at the edges of the band.

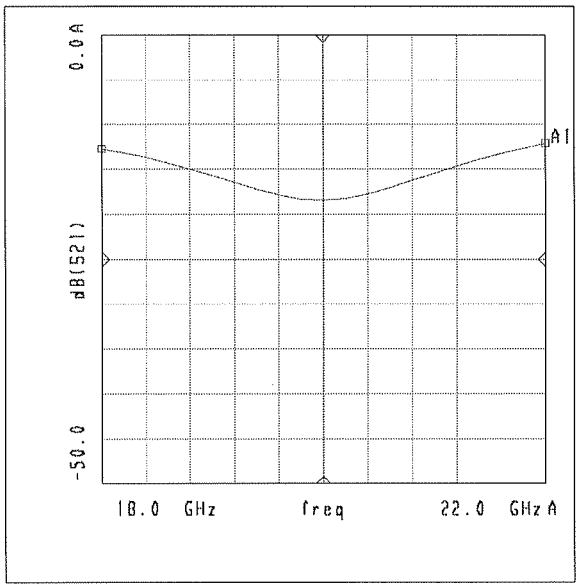

Figure 4.8 Isolation between RF and LO ports.

Figure 4.9 illustrates the Q_i points of the circuit. It is clearly shown that the Q_i points are evenly distributed on the polar plot over the whole operating frequency band. This will make it easier to calibrate and to achieve a better accuracy.

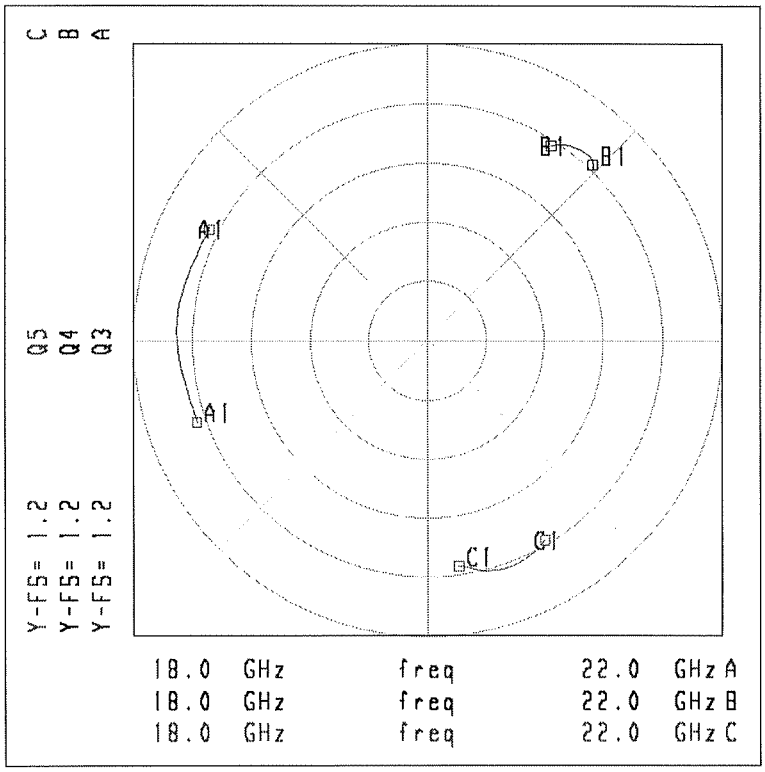

Figure 4.9 Simulated Q_i point distribution over the operating frequency band.

4.6 Modeling of the six-port

This section is presented as an article presented at the 1995 Canadian Conference on Electrical and Computer Engineering (CCECE'95, Montreal). This article describes the models of the different parts in a six-port receiver to be used with a commercial DSP system simulator SPW (Signal Processing Worksystem, Alta Group). This allows the simulation of the performance of the six-port receiver in a communication system context.

Paper presented at the 1995 Canadian Conference on Electrical and Computer Engineering; Digest pp.1164-1165.

Modeling of the Six-Port Discriminator Used in a Microwave Direct Digital Receiver

Ji Li, R. G. Bosisio and Ke Wu
Poly-GRAMES Research Center, Ecole Polytechnique de Montreal
C.P.6079, Succ. Centre Ville, Montreal, Quebec H3C 3A7
Phone: (514) 340-5891, FAX: (514) 340-5892, Email: liji@grmes.polymtl.ca

Abstract

A model of six-port discriminator (SPD) is described. This model is specially designed to perform computer simulation of a new microwave direct digital receiver, in which a six-port discriminator is a key component.

The model is based on S-parameters of the six-port circuit, which are readily obtainable from both analysis and measurement of the circuit. Simulations run on Alta group's SPW (Signal Processing Workstation) prove the validity of the model.

4.6.1 INTRODUCTION

It has recently found that a microwave six-port discriminator brings some advantages over traditional I-Q type circuit when applied to a microwave direct digital receiver [4.1,4.2]. The new six-port digital receiver consists of a six-port junction, diode power

detectors, analog to digital conversion circuit, digital signal processing unit and so forth. The demodulation of digital modulation signals such as PSK and QAM is performed directly at a microwave frequency. This new receiver scheme promises a cost-effective alternative to the super-heterodyne receivers used in various digital communication systems.

S-parameters are among the most frequently used in characterization of microwave circuits. The S-parameters describe the frequency-domain characteristics of a microwave network. Analytical and measurement methods are normally used to obtain the S-parameters of a circuit. Once the S-parameters of each components are known, the characteristics of the whole microwave system become readily accessible.

The six-port junction is generally a passive linear microwave network consisting of microwave transmission lines, power dividers, couplers and so on [4.3]. As the name suggests, it has six input/output ports. When used in the SPD, the reference signal and the unknown signal take up two input ports. The remaining four ports are considered as output ports: the amplitude/phase and frequency difference knowledge of the input signal are calculated from the 4 output power readings.

A computer simulation model of the six-port discriminator is described here. Details of the SPD, both hardware (e.g. circuit characteristics, resolution of ADCs, diode detector nonlinearity, etc.) and software (e.g. six-port computation, six-port calibration

procedure, etc.) operations can be simulated. The model is therefore ready for simulation of the performance of the six-port digital receiver in a communication system.

The model is used with Alta Group's SPW (Signal Processing Workstation) simulation software. Taking advantage of the block diagram function provided by SPW, the whole receiver is modeled using both function blocks suplied with the package and home-made blocks written in C language. Parameters obtained theoretically or by measurements can be readily substituted into the parameter fields of the blocks. Therefore components that do not have an accurate theoretical model can be easily simulated.

4.6.2 SPD MODEL

The modeling of different parts in a SPD is described as the following:

1) Six-port junction:

A six-port junction may be characterized by,

$$b = Sa \tag{4.12}$$

where a and b are normalized incident and reflected wave vectors, respectively. S is the scattering parameter matrix of the junction.

Assuming that all the 6 ports are perfectly matched, we can list only variables of interest as in (4.13)

$$\begin{bmatrix} 0 \\ 0 \\ b_3 \\ b_4 \\ b_5 \\ b_6 \end{bmatrix} = \begin{bmatrix} 0 & 0 & 0 & 0 & 0 & 0 \\ 0 & 0 & 0 & 0 & 0 & 0 \\ s_{31} & s_{32} & 0 & 0 & 0 & 0 \\ s_{41} & s_{42} & 0 & 0 & 0 & 0 \\ s_{51} & s_{52} & 0 & 0 & 0 & 0 \\ s_{61} & s_{62} & 0 & 0 & 0 & 0 \end{bmatrix} \cdot \begin{bmatrix} a_1 \\ a_2 \\ 0 \\ 0 \\ 0 \\ 0 \end{bmatrix} \tag{4.13}$$

in which a_1 and a_2 represent the incoming signal and the reference (Local Oscillator) signal, respectively. The resulting block diagram in SPW is shown in Fig. 4.10.

2) Diode power detector:

Ideally, the diode power detector is regarded as a square-law device whose response is,

$$v_{DC} = kP_{RF} \tag{4.14}$$

where k is a constant.

The nonlinear response can be modeled by using more sophisticated response function [4.4,4.5]. Noise source may also be introduced into the diode model.

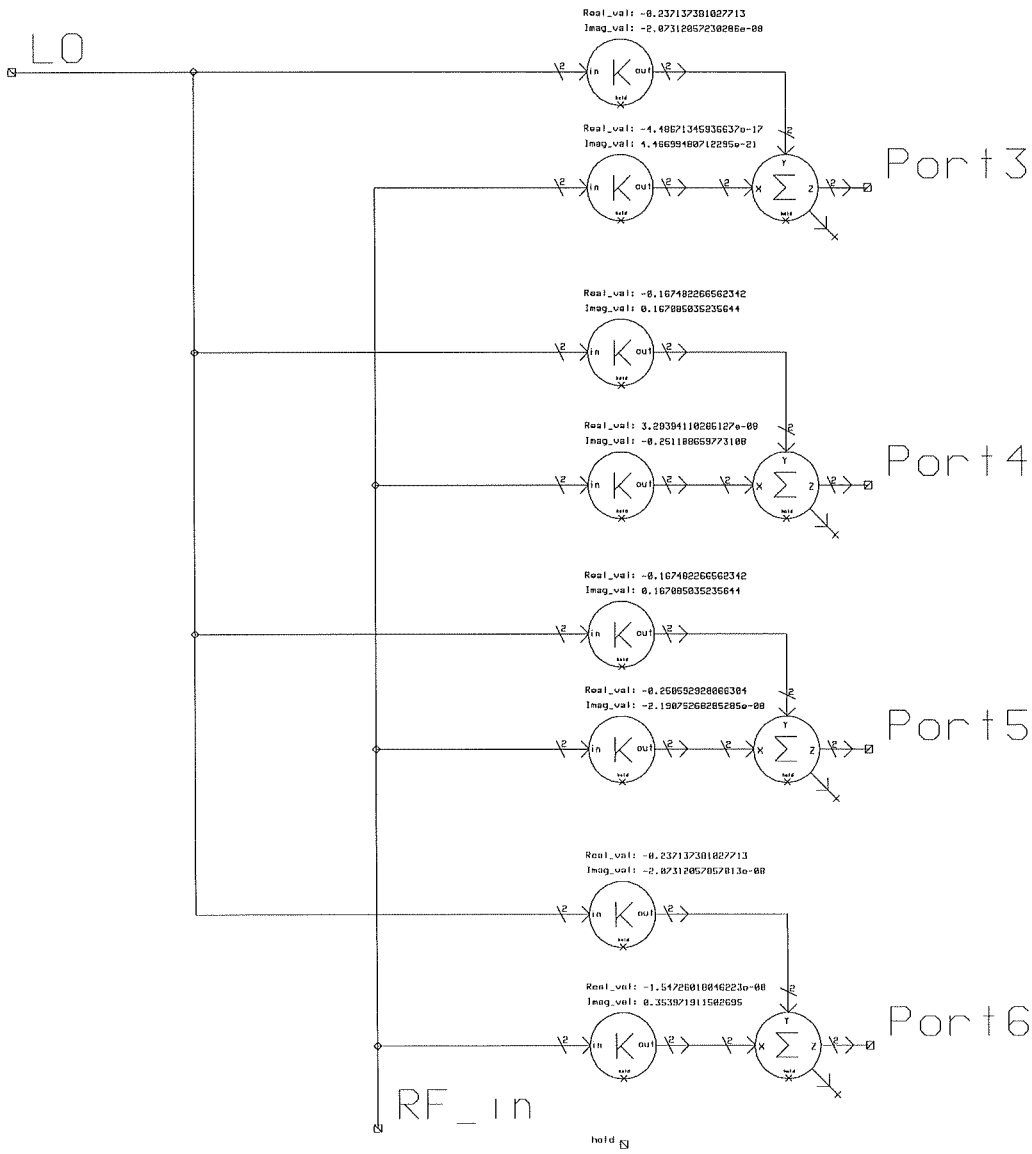

Figure 4.10. Six-port junction model.

2) Analog to digital conversion:

The purpose of the ADC block is to take into the effect of quantitization. The continuous voltages at the input ports are converted to a closest integral step voltage:

$$V_{output} = IFIX\left(\frac{2^n \cdot V_{input}}{V_{max.}}\right) \cdot \frac{V_{max.}}{2^n} \tag{4.15}$$

where n is the bit-width of the ADC.

3) Six-port computation:

This is to obtain the vector ratio, such as

$$\frac{\vec{a}_2}{\vec{a}_1} = \frac{\sum_{i=3}^{6} c_i P_i}{\sum_{i=3}^{6} d_i P_i} \tag{4.16}$$

where c_i , d_i 's are calibration coefficients of the six-port junction. Obviously, (4.16) takes full advantage of MAC (Multiply ACcumulation) operation and can be readily implemented in a DSP. This is only a function block written in C or FORTRAN in the computer simulation model.

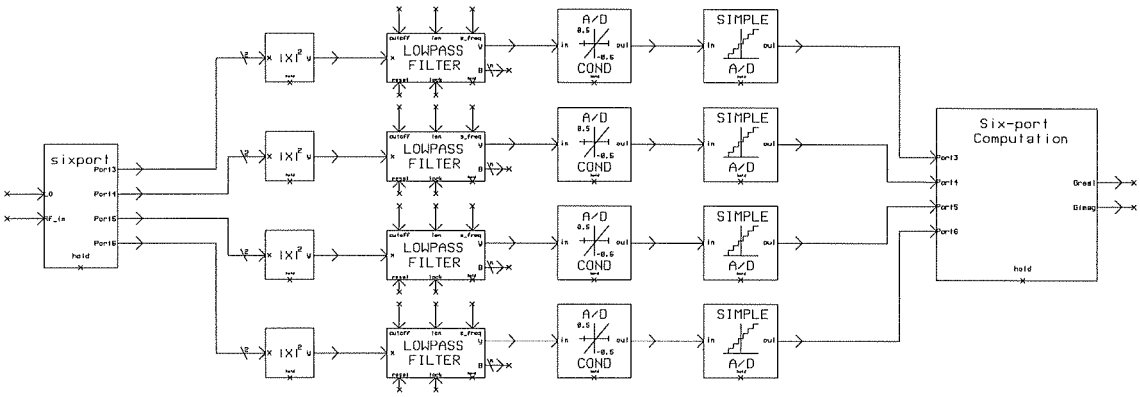

Figure 4.11. Complete basic model of the six-port discriminator.

4) Basic model of the SPD:

A complete basic model (simplified version) of the six-port discriminator is shown in Figure 4.11. The reference signal is applied to the LO port and the incoming RF signal is applied to RF input port. Standard IIR low-pass filters serve as pulse shaping filters. The output of the SPD consists of real and imaginary part of the detected vector, which correspond to in-phase and quadrature channels respectively.

4.6.3 VERIFICATION OF THE MODEL

Simulations have been performed to verify the correctness of the model. Constellation diagram is chosen as an example.

The model shown in Figure 4.11 was inserted into a perfect 64QAM digital telecommunication system. Figure 4.12 displays the constellation diagram at the output of the SPD. The SNR is 33dB. It positively identifies the validity of the model.

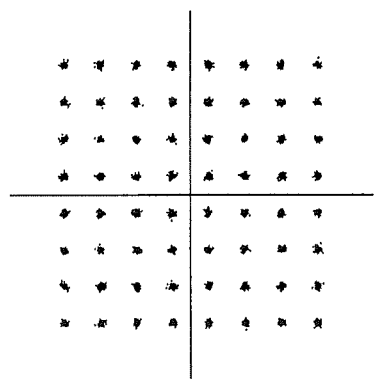

Figure 4.12. Constellation diagram at the SPD output.

4.6.4 CONCLUSION

Computer modeling of a six-port microwave direct digital receiver is introduced in this paper. The validity of the model is demonstrated by some basic simulations such as constellation diagram. This model sets a starting point of the detailed investigation of the performance of six-port digital receiver in various communication applications.

REFERENCES

[4.1] JI LI, R.G.BOSISIO and KE WU, “A six-port direct digital receiver”, Digest of IEEE MTT Symposium, Vol. 3, pp.1659-1662, San Diego, May, 1994

[4.2] JI LI, R.G.BOSISIO and KE WU, “A new direct digital receiver performing coherent PSK reception”, Digest of IEEE MTT Symposium, Vol. 3, pp.1007-1010, Orlando, May, 1995

[4.3] C.A.HOER *et al*, "Using an arbitrary six-port junction to measure complex voltage ratios", IEEE Trans. MTT-23, No.12, Dec. 1975, pp.978-984.

[4.4] C.A.HOER, *et al*, "Measuring and minimizing diode detector non-linearity", IEEE Trans. IM-25, No.4, pp.324-329, December 1976

[4.5] Z.CHEN and B.XU, "Linearization of diode detector characteristics", 1987 IEEE MTT-S Digest, pp.265-267

Chapter 5

Receiver Algorithms

5.1 Introduction

The demodulation performed by a six-port receiver is basically attributed to an appropriate implementation of the software. Therefore, DSP algorithms have to be developed to realize relevant receiver functions. Fig. 5.1 illustrates a simplified functional block diagram of a receiver algorithm. All the blocks except clock recovery have been implemented and tested in the receiver testing setup. The related calibration algorithms have already been presented in Chapter 3 while some of the remaining functional blocks will be described and discussed in detail in this section.

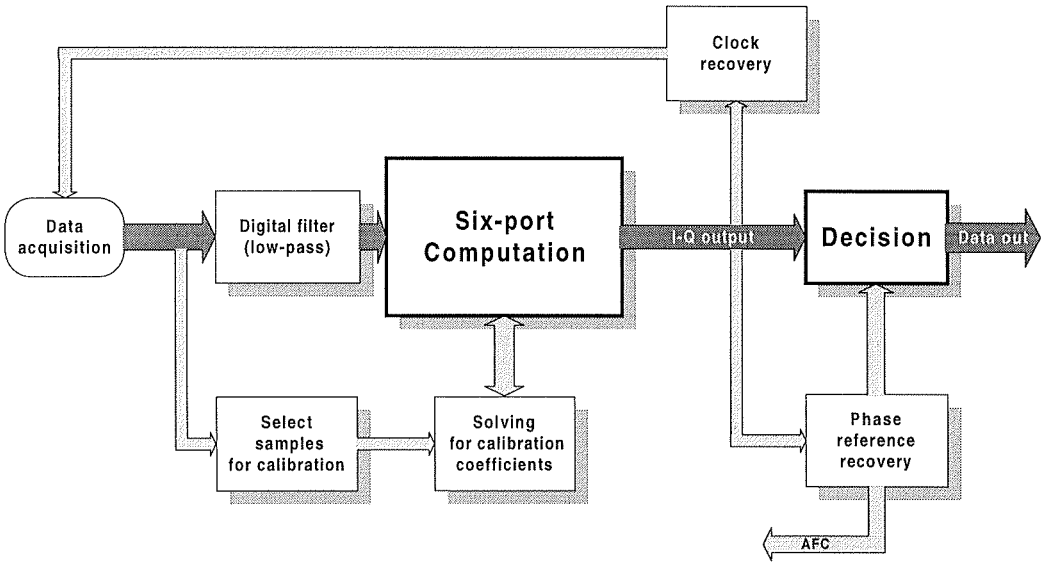

Figure 5.1 Overview of the functional flow chart of the six-port receiver algorithm.

Judging from Fig. 5.1, it can be seen that the algorithm of a demodulation consists of several parallel processes. In the proposed scheme, the line: "Data acquisition" - "Digital filter" - "Six-port computation" - "Decision" presents the main stream of the functional blocks, with the "Clock recovery" and "Phase reference recovery" serving in parallel to the main process. The calibration branch provides auxiliary function that does not require full real-time processing. It is anticipated that, in a receiver having high capacity, the functions for the main stream have to be realized in hardware such as ASIC and FPGA.

5.2 Digital filters

Digital filters eliminate any possible out-of-band interference and noise. Usually, the frequency response of these filters should comply with the system design to suppress the inter-symbol interference and to achieve the maximum spectrum efficiency.

There are four input and two output (I and Q) channels in the six-port calculation block. The digital filters can be placed either before or after this block. The filters operate in baseband, having a low-pass response. Anti-aliasing filters must precede the A/D converter to ensure a correct A/D conversion. It is also possible to use analog low-pass filters before the A/D converters as a trade-off for the cost-reduction and performance enhancement.

5.3 Six-port computation

This block acquires the received vector from A/D power readings and passes the vector to the subsequent blocks in a Real-Imaginary or Modulus/Argument format.

From Chapter 2, the vector is calculated from

$$\vec{A} = |A|e^{j\theta} = \frac{\vec{a}_1}{\vec{a}_2} = \frac{\sum_{i=3}^{6}(R_i + jI_i)P_i}{\sum_{i=3}^{6}(D_i + jE_{i)})P_i} \tag{5.1}$$

Obviously, equation (5.1) is suitable for the DSP MAC operation and hardware implementation. However, the calibration coefficients obtained from the method described in Chapter 3 are not directly applicable to (5.1), a conversion of the calibration coefficients is therefore necessary.

Using the proposed dual-tone calibration, the vector ratio is obtained by

$$\vec{A} = |A|e^{j\theta} = \frac{\vec{a}_1}{\vec{a}_2} = \frac{e - W}{cW - d} \tag{5.2}$$

where

$$W = \beta + j\frac{\alpha\beta + \gamma}{\pm\sqrt{1-\alpha^2}} = \beta + jt(\alpha\beta + \gamma) \tag{5.3}$$

with

$$\alpha = \frac{p - q - r}{2\sqrt{qr}} \tag{5.4}$$

$$\beta = \frac{r - Q_1 - A^2 Q_2}{2\sqrt{r}} = \beta_0 + \beta_1 Q_1 + \beta_2 Q_2 \tag{5.5}$$

$$\gamma = \frac{q + Q_1 - B^2 Q_3}{2\sqrt{q}} = \gamma_0 + \gamma_1 Q_1 + \gamma_2 Q_3 \tag{5.6}$$

Calibration coefficients p, q, r, A^2, B^2 and c, d, e need to be converted to R_i, I_i ,D_i and E_i.

Let

$$
\begin{aligned}
W &= u + jv \\
c &= c_1 + jc_2 \\
d &= d_1 + jd_2 \\
e &= e_1 + je_2
\end{aligned}
\tag{5.7}
$$

Then (5.2) becomes

$$
\vec{A} = |A|e^{j\theta} = \frac{\vec{a}_1}{\vec{a}_2} = \frac{(e_1 - u) + j(e_2 - v)}{(c_1 u - c_2 v - d_1) + j(c_1 v + c_2 u - d_2)} \tag{5.8}
$$

Replace (5.3) ~ (5.7) into (5.8) and compare with (5.1), the conversion equations are obtained as follows

$$
\begin{aligned}
R_3 &= e_1 - \beta_0 = e_1 - \frac{\sqrt{r}}{2} \\
R_4 &= -\beta_1 = -\frac{1}{2\sqrt{r}} \\
R_5 &= -\beta_2 = \frac{A^2}{2\sqrt{r}} \\
R_6 &= 0
\end{aligned}
\tag{5.9}
$$

$$
\begin{aligned}
I_3 &= e_2 - \alpha t\beta_0 - t\gamma_0 \\
I_4 &= -t(\gamma_1 + \alpha\beta_1) \\
I_5 &= -\alpha t\beta_2 \\
I_6 &= -t\gamma_2
\end{aligned}
\tag{5.10}
$$

$$
\begin{aligned}
D_3 &= c_1\beta_0 - c_2\alpha t\beta_0 - c_2 t\gamma_0 - d_1 \\
D_4 &= c_1\beta_1 - c_2\alpha t\beta_1 - c_2 t\gamma_1 \\
D_5 &= c_1\beta_2 - c_2\alpha t\beta_2 \\
D_6 &= -c_2 t\gamma_2
\end{aligned}
\tag{5.11}
$$

$$
\begin{aligned}
E_3 &= c_1\alpha t\beta_0 + c_1 t\gamma_0 + c_2\beta_0 - d_2 \\
E_4 &= c_1\alpha t\beta_1 + c_1 t\gamma_1 + c_2\beta_1 \\
E_5 &= c_1\alpha t\beta_2 + c_2\beta_2 \\
E_6 &= c_1 t\gamma_2
\end{aligned}
\tag{5.12}
$$

It can be shown in general that the accuracy will not be sacrificed if E_i *'s* are set to zero, since there are only 11 independent variables in the six-port calibration. Therefore (5.1) can be simplified into

$$
\vec{A} = |A|e^{j\theta} = \frac{\vec{a}_1}{\vec{a}_2} = \frac{\sum_{i=3}^{6}(R_i + jI_i)P_i}{\sum_{i=3}^{6} D_i P_i}
\tag{5.13}
$$

Equation (5.13) is better suited for the DSP operation because the denominator becomes a real number. Fig. 5.2 shows a flow chart of (5.13).

5.4 Decision

The role of the decision block makes decision as far as it is concerned with the data being received. Different modulation entails different decision algorithm. Generally speaking, it executes table-like look-up in accordance with the signal constellation and coding scheme.

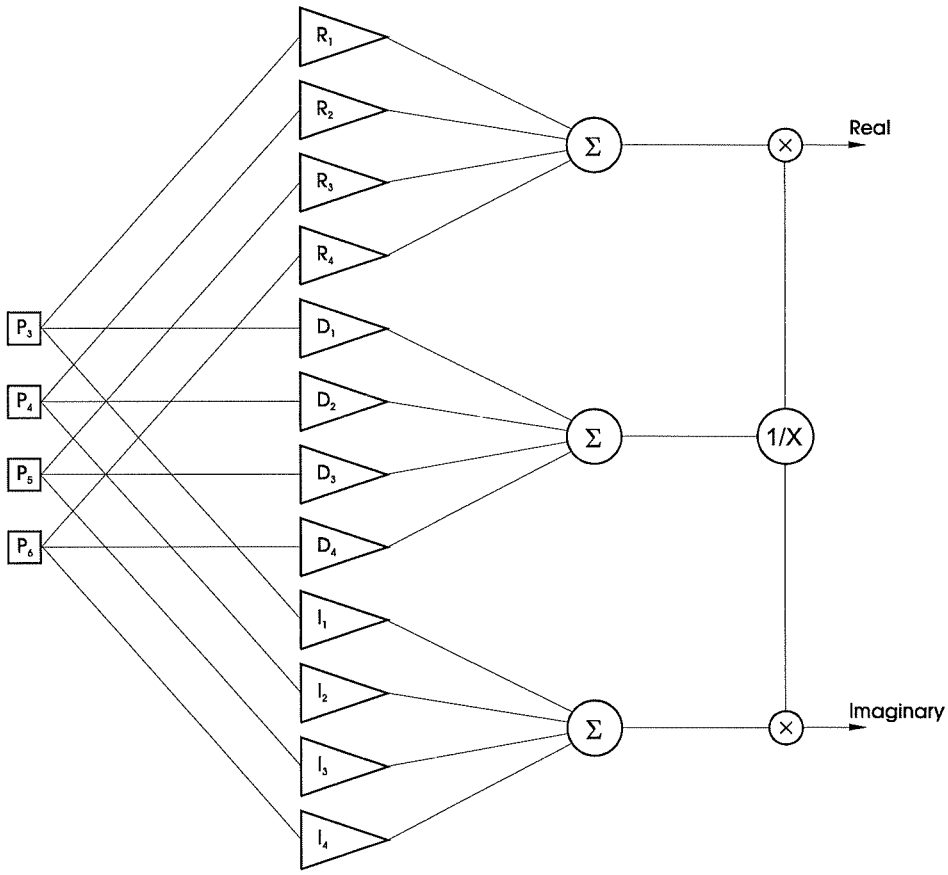

Figure 5.2 Flow chart of DSP implementation of equation (5.13).

5.5 Automatic frequency control (AFC)

The carrier recovery is required for the demodulation. A full carrier recovery is not always necessary or too difficult to accomplish in many applications, therefore AFC can

be used instead to track down the carrier frequency and minimize the residual frequency error.

A two-step AFC algorithm applies to the six-port receiver:

a) Coarse tuning: controlling the LO such that the average power at all four power ports are maximized. Due to the presence of a low-pass filter, the closer the LO frequency to incoming carrier frequency is, the higher the average power will be.

b) Fine tuning: using the algorithm described in 5.6 to further reduce the residual frequency error.

5.6 Phase reference recovery

This block serves two purposes:

1) To establish a phase reference for the coherent demodulation while the carrier recovery is not fully accomplished;

2) To evaluate the residual frequency error, and then to generate a control signal to complete the carrier recovery.

The following article presented at the 1995 MTT-S International Microwave Symposium outlines the "soft phase reference" method.

Paper presented at the 1995 IEEE MTT-Symposium; Digest pp. 1007-1010.

A NEW DIRECT DIGITAL RECEIVER PERFORMING COHERENT PSK RECEPTION

Ji Li, R.G.Bosisio and Ke Wu

POLY-GRAMES Research Center
École Polytechnique, C. P. 6079, Succ. Centre Ville
Montréal, Canada H3C 3A7
FAX: (514) 340-5892
Email: liji@grmes.polymtl.ca

Abstract

Coherent reception provides better CNR performance over its differential counterpart. However, this is generally obtained at the expense of increasing complexity of the receiver and more stringent specifications of circuits. In this paper, we describe a new coherent PSK direct receiver, in which a 'soft' phase reference is established by DSP, while the detection is performed directly at mm-wave frequencies. Both measurements and computer simulations validate the proposed new approach.

This work is supported by the Natural Science and Engineering Council of Canada (NSERC).

5.6.1 Introduction

It has been recently shown that a six-port circuit in conjunction with DSP (Digital Signal Processor) is capable of performing digital demodulation directly at frequencies ranging from microwave to mm-wave bands [5.1]. This new direct digital receiver promises reduced receiver complexity, loose fabrication requirements and fair performance in providing a cost effective alternative to the conventional heterodyne structure used in various digital terminals.

The most widely used modulation schemes in digital communication systems, such as satellite and personal communication systems, are PSK (Phase Shift Keying). There are two types of demodulation techniques: coherent and non-coherent (differential) [5.2]. In general, the differential detection brings about less complicated receiver configuration whereas the coherent detection is superior in error performance. However the complexity of a coherent receiver may be increased significantly due to the carrier recovery requirement. This task becomes particularly difficult when the carrier recovery has to be performed directly at microwave and millimeter-wave frequencies.

The presence of DSP in the six-port receiver gives us a flexibility of implementing receiver functions using simple software algorithms. In this work we introduce a simple method to establish a 'soft' phase reference needed for the coherent detection. In this way, only AFC (Automatic Frequency Control) is required for the local oscillator. Once

the LO frequency is within the 'catching up' range of the receiver, the 'soft' phase reference tracks down and compensates the phase drift introduced by residual frequency difference such that the detected signal constellation becomes fixed as though the carrier recovery is achieved.

5.6.2 Description of the Method

A block diagram of the six-port direct digital demodulator is shown in Fig. 5.3. The RF signal is fed into a six-port circuit. From the outputs of the four diode power detectors, the instant phase and frequency of the input RF signal are calculated by the DSP. The DSP controls the local oscillator to perform AFC. Once the carrier and clock recovery are achieved, the modulated data will be readily recovered.

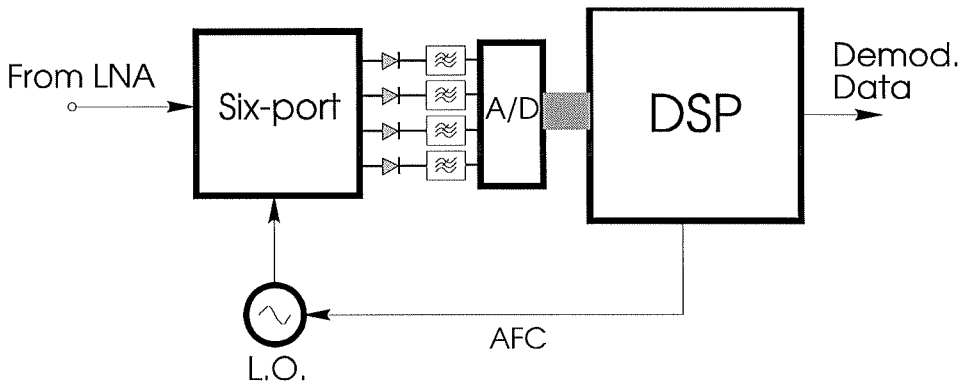

Figure 5.3. Block diagram of the six-port direct digital demodulator.

A received PSK signal is given by the following expression:

$$s(t) = A_c \cos(2\pi f_0 t + \Phi(t,a)) \tag{5.14}$$

where f_0 is the carrier frequency and the instant phase $\Phi(t,a)$ is a function of time t and the modulation data sequence a. Taking QPSK as an example and disregarding the band-limit, we have

$$\Phi(t,a) = 2\pi \cdot \frac{a_i}{4} + \phi_0 \tag{5.15}$$

where $a_i = \{0, 1, 2, 3\}$, $\phi_0 = 0$ or $\pi/4$, a_i is the ith symbol during $i\mathrm{T} < t < (i+1)\mathrm{T}$, and T is the duration of one symbol.

Suppose the LO frequency is very close to the incoming carrier frequency and the symbol clock synchronization is achieved, then samples detected by the six-port receiver are given by

$$s(i) = A_c \cos(2\pi \Delta f t_i + 2\pi \cdot \frac{a_i}{4} + \phi_0) \tag{5.16}$$

where $\Delta f = f_c - f_{LO}$, and to simplify the problem, only one sample is taken for each symbol.

It is observed from (5.16) that due to the presence of residual Δf the sampled constellation is still rotating at an angular speed of $2\pi\Delta ft$. In order to enable a coherent detection, a phase reference must be set up to counter this rotation.

For the case where f_{LO} is sufficiently close to f_c , the phase drift introduced by the term $2\pi\Delta ft$ can be considered negligible during a certain period of time NT, and in this case the instantaneous samples θ_i represent the modulation data. Taking a sample θ_0 as reference and denoting it by P_0 , for every subsequent sample θ_i , let $\varphi_i = \theta_i - P_0$ ($0 \le \varphi_i < 2\pi$), such that the 4 states of data sequence can be recovered as follows:

$$a_i = (\varphi_i + \tfrac{\pi}{4}) / (\pi/2) \tag{5.17}$$

In order to eliminate the noise, a FIFO (First-In-First-Out) register of length N is set up, and every latest θ_i that makes $a_i = 0$ is pushed into the register. Let the phase reference P_0 be the average of θ_i 's in the register:

$$P_0 = \frac{\sum_{j=0}^{N-1} \theta_i}{N} \tag{5.19}$$

In the stable state,

$$P_0 = P_0 + (\theta_{i.\text{latest}} - \theta_{i.\text{earliest}}) / N \tag{5.20}$$

Obviously, P_0 will follow the $2\pi\Delta ft$ term and the φ_i 's will become relatively fixed regardless of Δf. In this way, once the test sequence is detected, the a_i 's will be mapped into corresponding bits in conformity to the transmitting end. Although the example is given for QPSK demodulation, this method also applies to all other PSK and even QAM modulations.

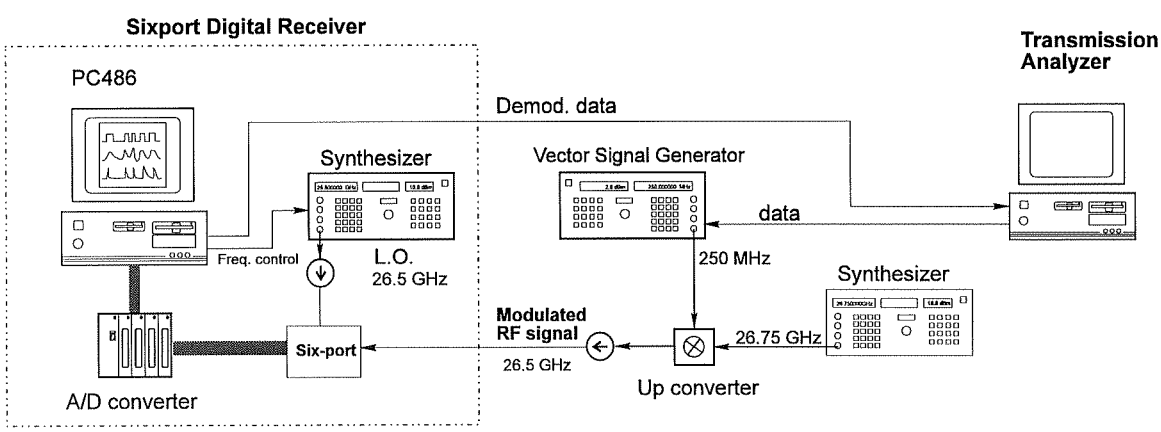

Figure 5.4. Block diagram of the test setup for measurement simulation.

5.6.3 Results

A measurement simulation was made to verify the above procedure. Figure 5.4 is the block diagram of the test setup. The transmitter is composed of a HP8782B vector signal generator, a upconvertor and a RF source. The 26.5 GHz PSK is fed into the six-port receiver. No additional amplifier is placed before the six-port junction. The receiver LO power was -1.5 dBm. A PC486 was used to simulate the DSP functions. The input power level of the receiver was controlled by the internal attenuator of the vector signal generator which provides over 160 dB of variation in output level. Five basic PSK demodulations were tested: differential and coherent BPSK, QPSK and coherent 8PSK. A small random variable frequency deviation of the receiver LO was intentionally made to simulate the residual Δf.

A statistical computer simulation was also performed to verify the measurement results. It takes into account the phase noise of the signal generators and LO, the ADC quantitized noise. The interference brought in by DC path was also considered. It is noticed that for this measurement simulation the effect of Gaussian white noise is negligible. BER (Bit Error Rate) was simulated as a function of input power level, and a perfect carrier recovery was assumed during the coherent PSK simulation.

Figure 5.5 shows the measured and simulated BER versus input powers. It is found that the coherent PSK reception presents about 1 dB (BPSK) to 2 dB (QPSK) better than their differential counterparts. The agreement between measured and calculated data suggests a good performance of the proposed coherent demodulation method. It also shows that the demodulation can be performed at a power level as low as -35 to -45 dBm. It must be mentioned that the measurement results are by far not optimized. A significant improvement in performance can be expected once the six-port junction design and system configuration are optimized.

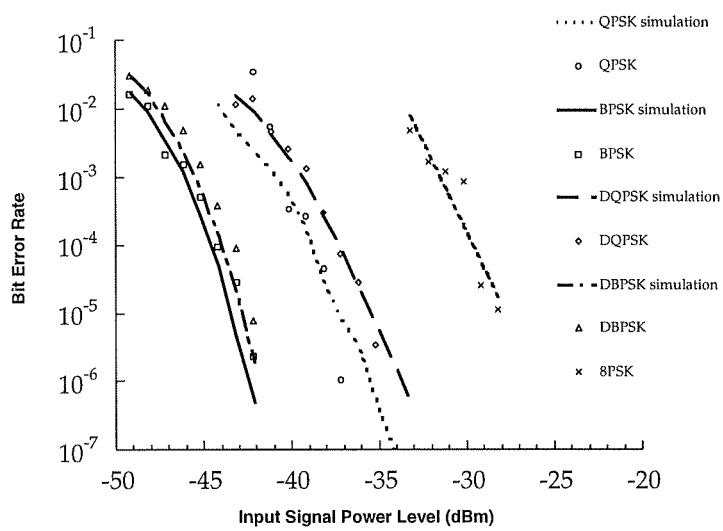

Figure 5.5. Measured an computer simulated BER performance.

5.6.4 Conclusion

A novel approach is proposed, which enables the coherent PSK demodulation directly at millimeter wave frequencies using a new receiver concept. This makes it possible for new six-port digital receiver to deal with various coherent and differential PSK modulation schemes. The receiver can be used in various wireless microwave/mm wave digital terminals to provide a cost-effective alternative to conventional heterodyne receivers.

References

[5.1] JI.LI, R.G.BOSISIO and K.WU, "A six-port direct digital receiver", Digest of IEEE MTT Symposium, Vol. 3, pp.1659-1662, San Diego, May, 1994

[5.2] F. XIONG, "Modem Z", IEEE Communication Magazine, pp 84-98, August, 1994

[5.3] GERHARD SCHULTES *et al*, "A new incoherent direct conversion receiver", IEEE Vehicular Technology Conference 1990, pp.668-674

[5.4] T.E.HODGETTES and E.J.GRIFFIN, "A unified treatment of the theory of six-port reflectometer calibration using the minimum of standards", Report No. 83003 R.S.R.E Malvern, Aug. 1983

[5.5] JI.LI, R.G.BOSISIO and K.WU, "a collision avoidance radar using six-port phase /frequency discriminator (SPFD)", Proc. of 1994 IEEE National Tele-systems Conference, pp55-58, San Diego, May, 1994

Chapter 6

Linearization of Schottky Diode Detectors

6.1 Introduction

Six-port acquires complex information, both magnitude and phase, by simple power measurements. Various RF detectors such as diodes, bolometers, or thermistors can be used to measure microwave power. Diode power is the most commonly used power detection device.

The ideal power detector should be a square-law device. Unfortunately, this is only approximately true for Schottky diode in a limited range of the input power level. It is often necessary to compensate the non-linearity of the diodes.

Although a six-port receiver usually operates at very low signal level where the diode detectors can be generally considered as linear, linearization may still be needed when very high accuracy is required to handle high modulation schemes such as 64QAM and 128QAM.

In a sixport measurement, only relative power readings are required. Therefore absolute power calibration is not necessary. Instead, the purpose of the calibration is only to correct the output voltage reading of the diode to square-law, in other words, to be proportional to the input power over its useful dynamic range. This is called linearization.

6.2 Diode Model

A diode model is used to simulate the real characteristics of the diode detector. For an ideal square-law diode

$$P = Kv \tag{6.1}$$

where P is the input power of the diode detector, $v=(V-V_0)$, V_0 is the diode output voltage when $P=0$, V is the output voltage and K is the sensitivity. The output voltage is

linearly related to the input power. For a Schottky diode the output voltage is deviated from the square-law line

$$P = f(v) \tag{6.2}$$

The linearization is to determine the parameters in the model *f(v)* through measurements. Several commonly used diode models are discussed below.

6.2.1 Lookup table

A lookup table is generated through the calibration measurements. In which each specific output voltage corresponds to an input power level. Normally only limited numbers of discrete points are stored in the table. Interpolations or extrapolations must be performed. Lookup tables are routinely used in power meters.

6.2.2 Hoer's model

C. A. Hoer proposed a useful mathematical model for diode detector in 1976 [6.1]

$$P = Kv^{\beta f(v)} \quad , \tag{6.3}$$

where K and β are constants, $v=q(V-V_0)$, q is a scale factor chosen so that v is positive and has a maximum value of about 0.5, and $f(v)$ is a polynomial in v:

$$f(v) = 1 + b_1 v + b_2 v^2 + \cdots + b_n V^n \tag{6.4}$$

For this model, the deviation from square-law is in order of

$$E(dB) = 10(\beta f(v) - 1)\log v \tag{6.5}$$

Hoer proposed the model for point contact diode and has proved that any detector whose response approaches square-law at low power levels can be completely calibrated by making ratio measurements without any known value of attenuation or power.

6.2.3 Chen's model

In 1987, Z. Chen introduced a new mathematical model [6.2] for Schottky diode detector

$$P = Kv(10^{\frac{1}{10}\sum_{i=1}^{N} a_i x^i}) \quad , \tag{6.6}$$

where $x=ln(v/q+1)$, q is a scale factor chosen so that x is positive and has a maximum value of about 0.5. The deviation from square-law is

$$E(dB) = \sum_{i=1}^{N} a_i x^i \tag{6.7}$$

The deviation E decreases with v so that the model is consistent with the square law approximation of diode detector at lower input power level. The test results demonstrate a maximum error of 0.02dB at 35GHz over a 40dB dynamic range.

6.3 Previously reported linearization methods

6.3.1 Direct calibration

The configuration is shown in Fig. 6.1. A calibrated power meter is used to measure the relative input power of the detector. The corresponding voltages are recorded. The measured data can be used to build a lookup table or fit to a mathematical model.

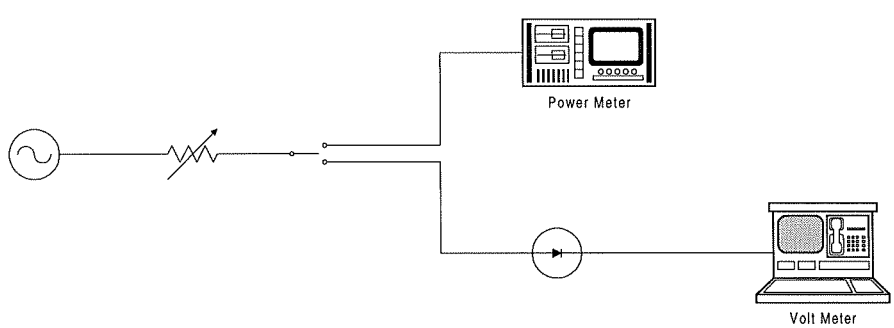

Figure 6.1 Linearization of the diode by a reference power meter.

6.3.2 Use of a calibrated precision attenuator

The test setup is shown in Fig. 6.2. The calibration procedure used is similar to that of 6.3.1. The power meter is replaced by a precision attenuator to read the relative power. More efforts have to be made to automate the procedure.

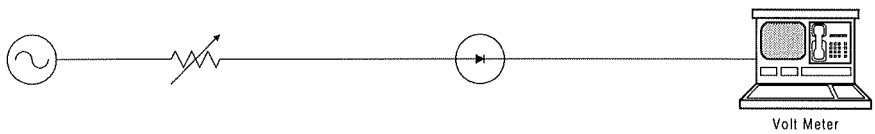

Figure 6.2 Linearization of diode detector by a calibrated precise attenuator.

6.3.3 Repeatable two-position step attenuator

This is the most commonly used method in six-port linearization. The test setup is shown in Fig. 6.3. A two-position attenuator is used. The attenuation difference between the two positions is not necessarily calibrated but good repeatibility of the two switched position is crucial. The voltages corresponding to two positions are read at different input power levels. By properly applying mathematical manipulation all the constants in the mathematical model can be obtained.

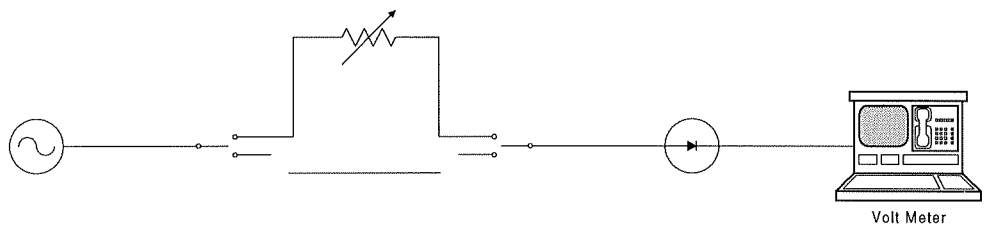

Figure 6.3. Linearization of diode detector by repeatable two position attenuator

6.4 The new dual-tone linearization method

Although the previous linearization methods are capable of providing good corrections of the P-V curve of a diode detector, the procedure involves a large number of repeated switch setting and power sweeping of the signal generator. This appears to be especially inconvenient in a six-port receiver calibration .

Following is a paper presented at the IMTC'94 on a new calibration procedure for the diode detector proposed by the author. This method is more suitable for fast diode linearization in the six-port receiver.

Paper presented at the IMTC'94, Digest pp.276-279.

A Simple Dual-Tone Calibration of Diode Detectors

Ji LI, Renato G. BOSISIO, and Ke WU

Groupe de Recherches Avancées en Microondes et en Électronique Spatiale
(POLY-GRAMES)
École Polytechnique de Montréal, C. P. 6079, Succ. Centre Ville
Montréal, Canada H3C 3A7

Abstract

A new dual-tone method to linearize diode detectors is proposed, in which two closely spaced CW carriers with equal amplitudes are fed into the diode detector to be calibrated. It is found that the output waveform of the detector is a distorted sinusoidal wave of the frequency difference between the two carriers. The deviation from the square-law response can be found from the distorted signal which is attributed to the detector through a simple iterative calculation. Measurement performed at 40GHz has shown an error within 0.2dB over a 40dB dynamic range.

6.4.1 Introduction

Diode power detectors are preferred sensors in most microwave/millimeter-wave applications due to their attractive characteristics such as low cost, high sensitivity, fast response time and large dynamic range. However, accurate calibrations have to be performed to characterize the non-square-law response at high input power levels. A practical way to fulfill the calibration is first to linearize the detector and then to calibrate the absolute power readings at a definite reference level as required. Various procedures have been proposed for the linearization [6.1-6.3]. However, most of them involve intensive efforts on measurement and/or computation.

A new dual-tone method of diode detector linearization is proposed here. The method eliminates the need for time-consuming repeat power sweep measurements of the previous methods [6.2,6.3]. No precise standards and accessories are required. Moreover, the nonlinearity of the attached DC amplifier and A/D converter can also be included in the calibration.

6.4.2 Linearization Method

To begin with, two CW signals are combined and fed into the diode detector to be calibrated. These signals can be expressed as:

$$v_1 = A_1 \cos(\omega_1 t + \varphi_1) \tag{6.8}$$

$$v_2 = A_2 \cos(\omega_2 t + \varphi_2) \tag{6.9}$$

The summation of the two signals will be

$$v = v_1 + v_2$$

$$= 2A_1 \cos \frac{(\omega_1 - \omega_2)t + \varphi_1 - \varphi_2}{2} \cos \frac{(\omega_1 + \omega_2)t + \varphi_1 + \varphi_2}{2} + (A_2 - A_1)\cos(\omega_2 t + \varphi_2) \tag{6.10}$$

To simplify the problem, let $\varphi_1=\varphi_2=0$. When $A_1 \approx A_2$, and $\omega_1 \approx \omega_2$. The power of the combined carriers is then

$$P = A^2(1 + \cos \Delta\omega t) \tag{6.11}$$

where $\Delta\omega=\omega_1-\omega_2$, $A=A_1 \approx A_2$.

For an ideal linear diode power detector, the relationship between the input power and the output voltage should be

$$P = Kv \tag{6.12}$$

However, for a real diode detector, the coefficient K no longer remains constant as the input power level varies. When the input power is in form of (6.11), due to the nonlinearity of the diode, the output voltage waveform will be a distorted sinusoidal wave. Sampling the waveform at identical time interval in a half period of $\Delta\omega$. we have

$$P_i = A^2(1+\cos\frac{i}{N}\pi) = K_i v_i \qquad i=0,1,\ldots,N \tag{6.13}$$

where N is the number of samples taken in a half of the $\Delta\omega$ period. K_i represents the distortion, i.e. the deviation from the square-law. By applying an iterative procedure

$$\frac{K_k v_k}{K_j v_j} = \frac{1+\cos\frac{k}{N}\pi}{1+\cos\frac{j}{N}\pi} \qquad j,k = 1,2,\ldots,N \tag{6.14}$$

K_i's can easily be obtained. In the case where only relative power readings are required, K_0 can be set to be unity so that K_i becomes a factor of correction at different power levels. The coefficients K_i versus output voltage can be interpolated using a polynomial obtained with the least-square method.

6.4.3 Results

Fig. 6.4 shows the block diagram of the test set-up of the dual-tone calibration. The output waveform is sampled by an A/D converter. The data are processed using a PC. The frequency difference of the two signals needs not to be known exactly as long as it is within the "catch-up" range of the data acquisition system. The sampled waveform is first smoothened by averaging and then the least-square process is used to find the polynomial.

Measurements were performed to validate the proposed method at Ka band. The frequency difference is about 500Hz and the number of samples is about 100. Fig. 6.5 shows a typical curve of K_i versus output voltage obtained. The acquired dynamic range of the waveform is around 20dB. The response below that range is considered to be linear. The calibration results is compared with a standard power meter. Fig. 6.6 plots the error of the relative power

measurement versus input power levels at 40GHz. It can be seen that the error is within 0.2dB over the 40dB dynamic range. The maximum K_i is about 3dB. Due to the noisy data acquisition system the dynamic range can not be extended to lower ends.

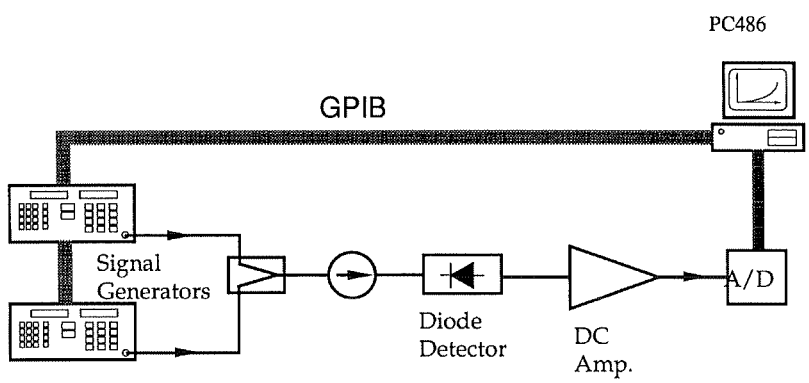

Figure 6.4 Test setup of the dual-tone clibration.

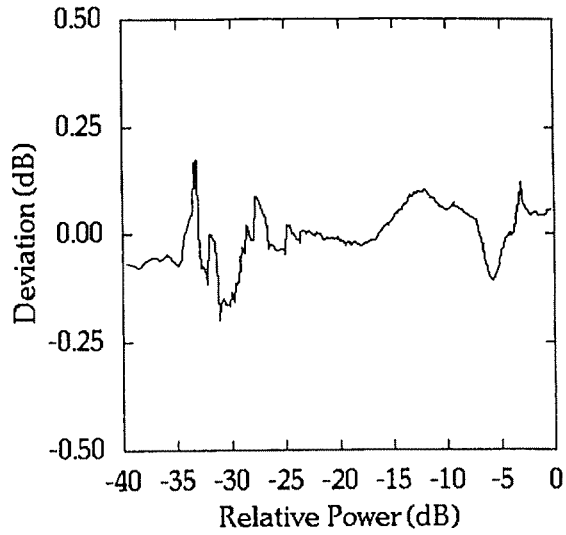

Figure 6.5 Error of linearization.

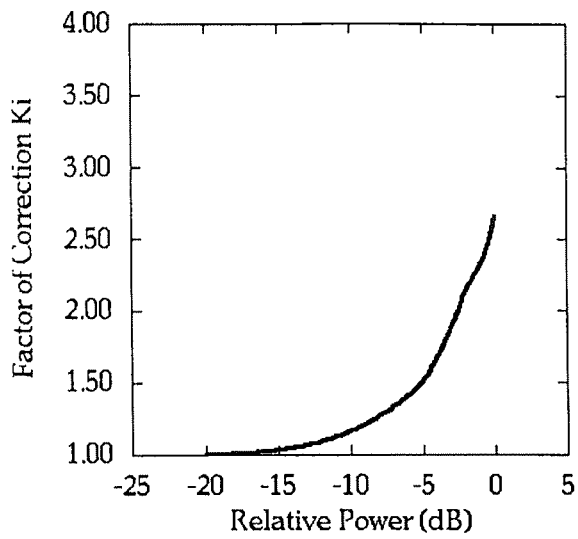

Figure 6.6 Factor of correction K_i versus input power.

6.4.4 Conclusion

A new dual-tone calibration method is presented. It eliminates the need for any precise standard or repeatable attenuators. The procedure is very quick and easy to apply to some applications such as six-port measurements. The drawback is that two signal sources are required.

References

[6.1] C.A.HOER, *et al*, "Measuring and Minimizing Diode Detector Nonlinearity", IEEE Trans. IM-25, No.4, pp.324-329, December 1976

[6.2] Z.CHEN and B.XU, "Linearization of diode detector Characteristics", 1987 IEEE MTT-S Digest, pp.265-267

[6.3] C.POTTER and A.BULLOCK, "Nonlinearity Correction of Microwave Diode Detectors Using a Repeatable Attenuation Step", Microwave Journal, Vol.36, No.5, pp.272-279, 1993

Chapter 7

Conclusions

A new millimeter-wave digital receiver based on the six-port technology has been proposed and studied. This new receiver is intended to achieve comparable performance as existing super-heterodyne receivers at a lower cost. This novel scheme is strongly motivated by the fact that the speed and performance of the state-of-the-art digital VLSI techniques be very promising and the price will be significantly reduced, while the cost of the microwave components are relatively stable. Therefore, a receiver configuration that shifts the complexity to digital signal processing part and alleviates problems associated with the RF components will be better-off in terms of cost and functionality in the long run.

The proposed six-port receiver scheme falls into the direct conversion (homodyne) receiver category. Historically, this type of receiver played insignificant role due to some of its inherent drawbacks. The six-port receiver makes it possible to improve the direct receiver performance which can be stated in the following:

- In the early years, the amplification of a RF signal was very expensive so that it had to be carried out at a lower frequency, i.e. IF, As the technology advanced, low-cost high gain microwave transistors (below 20 GHz) have become available such that the cost of these transistors is no longer a major factor in the overall design of a receiver. This makes it easier than ever to adopt a direct receiver configuration.

- Wide band microwave amplifier design techniques have matured to maintain uniform gain and noise figure over a wide frequency band. The sensitivity non-uniformity of the early homodyne receiver has been overcome.

- I-Q network has been the only way to detect phase in all the conventional receivers. As discussed in Chapter 1, the fabrication tolerances inhibits an acceptable performance of such circuits at microwave/mm wave frequencies. Six-port calibration eliminates most of the errors related to imperfect circuit fabrication to allow the six-port receiver operating at a millimeter-wave frequency without any compromise with regards to phase accuracy.

- The recent development of VLSI and ASIC technology makes the high speed digital signal processing practical and cost effective. This is a main impetus behind the emergence of the six-port receiver.

Six-port receiver has some drawbacks:

- The six-port receiver operates at zero IF, where the $1/f$ noise coming from Schottky diodes may deteriorate the sensitivity of the receiver. Therefore, the dynamic range is limited (max. 60 dB) and higher LNA gain is required.

- In certain applications such as the FDMA mobile cellular phone system, narrow band multiple carriers varies largely at signal level. The dynamic range of the signals can be as high as 100 dB. It is very difficult to place a channel selection filter before the six-port circuit due to the extremely narrow relative bandwidth requirement. In this case, a strong interference could effectively saturate the power detectors. A super-heterodyne multi-conversion receiver with high dynamic range down-converters and high quality IF filters (e.g. SAW filters) is a better choice in such a situation.

- Six-port receiver requires calibration, although this procedure can be carried out with minimum additional hardware and in a non-interruptible fashion.

- The local oscillator has to be fine-tunable to perform the carrier recovery at microwave carrier frequency. This is more difficult to achieve than at IF.
- It requires high speed ADCs that matches the transmission symbol rate.

The research work described in this thesis has bridged a gap between a relatively sophisticated six-port technology usually used in microwave instrumentation and a much wider telecommunication field. It is proven through a number of computer and measurement simulations that the proposed six-port millimeter wave direct digital receiver is a technologically sound and economically feasible new scheme. The work has set up a starting point for subsequent in-depth research and commercial development.

Important progress has been made recently on the digital implementation of digital PSK/QAM demodulators using ASIC technology. The powerful PSK/QAM demodulator ICs and FEC ICs with data rate up to 80Mb/s are becoming widely commercially available at very low price. This chips already have all the necessary carrier recovery and clock recovery circuitry integrated. The author has observed the possibility of interfacing these chips with a six-port receiver. In which a small FPGA/ASIC performs six-port computation only, and all the subsequent signal processing functionality is executed by the commercial demodulator chips.

References

[1] BHARTIA, P, BAHL, I.J. (1983). *Millimeter Wave Engineering and Applications,* John Wiley & Sons.

[2] LAMBERTI, A. (1992). New directions for the microwave market, Telecommunications, 38-40.

[3] MOLLENKOPF, S. and REBEIZ, G.M. (1994). A 22 GHz MIC active receiver/radiometer, 1994 IEEE MTT-S Digest,1347-1350.

[4] FRERKING, M.E. (1994). *Digital Signal Processing in Communication Systems,* Van Nostrand Reinhold.

[5] FEHER, K. (1990). *Advanced Digital Communications: Systems and Signal Processing Techniques,* Prentice-Hall.

[6] OLIVER A.D. (1994). *Microwave and Optical Transmission,* John Wiley & Sons.

[7] HILBORN, D.S., *et al*, (1994). An adaptive direct conversion transmitter, IEEE Trans. Vehicular Tech., Vol.43, No.2, 223-233.

[8] LI, S., (1982). Automatic analysis of multi-port microwave networks, Thèse doctorat, DGEGI, Ecole Polytecnhiqnue de Montréal.

[9] O'CONNELL, T., MURPHY, P. J. and MURPHY A. (1994). A direct I/Q modulator at microwave frequencies using GaAs MESFETs, Microwave Journal, October, 62-76.

[10] BÓVEDA, A., ORTIGOSO, F. and ALONSO, J.I. (1993). A 0.7-3 GHz GaAs QPSK/QAM direct modulator, IEEE Journal of solid-state circuits, Vol.28, No.12, 1340-1349.

[11] BREWSTER, B.D. and ROBERTSON, I.D. (1994). Phase compensated QPSK demodulator with a X-Band I.F. for VSAT system applications, Proc. European Microwave Conference, 1559-1564.

[12] TAKENAKA, T. *et al*, (1990). A digital signal processing demodulator with a wide frequency acquisition range, Globecom'90, 1418-1422.

[13] CAVERS, J.K. and LIAO, M., (1991). Adaptive compensation and offset losses in direct conversion transceivers, Proc. IEEE Vehicular Technology Conference, 578-583.

[14] TELLIEZ, I. *et al*, (1991). A compact, monolithic microwave demodulator-modulator for 64-QAM digital radio links, IEEE Trans. MTT, Vol.39, No.12, 1947-1954.

[15] BREWSTER, B.D. and ROBERTSON, I.D. (1994). A C-band microstrip varactor tuned reflection phase shifter employing UHF general purpose diodes, Microwave and Optical Technology Letters, Vol.7, No.4, 172-174.

[16] FITZ, M.P. (1994). A bit error probability analysis of a digital PLL based demodulator of differentially encoded BPSK And QPSK modulation, IEEE Trans. Communications, Vol.42, No.1, 17-21.

[17] CHENG, W.W. (1994). Ultra wide band analog signal processor products, RF Design, 42-54.

[18] Texas Instrument WWW server: http://www.ti.com/sc/docs/dsps/prodinfo/datasht/c8x/

[19] OLMSTEAD, C. and PETROWSKI, M. (1994). Digital IF processing, RF Design, 30-40.

[20] HOER, C.A. *et al*, (1975) Using an arbitrary six-port junction to measure complex voltage ratios, IEEE Trans. MTT-23, No.12, 978-984.

[21] Engen, G.F. (1976). Determination of microwave phase and amplitude from power measurements, IEEE Trans. Instrum. Meas., vol. IM-25, No.4, 414-418.

[22] Marconi Instruments, (1994). Test and measurement instrument systems, 108-112.

[23] GHANNOUCHI, F.M., MAURIN, D., CUHACI, M. and BOSISIO, R.G. (1993). A miniaturized frequency-compensated six-port junction using MHMIC technology, Microwave and Optical Technology Letters, Vol.6, 573-575.

[24] SOLOMON, M.N. *et al*, (1992). A monolithic six-port module, IEEE Microwave and guided wave letters, Vol.2, 334-336.

[25] 李世鹤，王智. (1989). 微波六端口技术，人民邮电出版社. ISBN7-115-03933-X/TN•218.

[26] 高葆新，洪兴楠，等编著. (1988). 微波电路计算机辅助设计（下），清华大学出版社. ISBN7-302-00014-X/TP•1.

[27] BERGEAULT, E., *et al*, (1990). Accuracy analysis for six-port automated network analyzers, IEEE Trans. Instrumentation & Measurement, Vol. 39. No.3, 492-496.

[28] GHANNOUCHI, F.M., LAROSE, R.L., and BOSISIO, R.G. (1991). A new nultiharmonic loading method for large-signal microwave and millimeter-wave transistor characterization, IEEE Trans. Microwave Theory Tech., Vol.39, 986-992.

[29] HODGETTS, T.E. and GRIFFIN. E.J. (1983). A unified treatment of the theory of six-port reflectometer calibration using the minimum of standards, Report No. 83003 RSRE Malvern.

[30] VOUDOURIS. K. *et al*, (1993) effects of amplitude, phase, and frequency imperfections on the performance of a direct conversion receiver (DCR) for personal communication systems, IEEE Microwave and Guided wave Letters, Vol.3, No.9, 313-315.

[31] REINHARDT. V.S. *et al*, (1994). Methods for measuring the power linearity of microwave detectors for radiometric applications, IEEE MTT-S Digest,1477-1480.

[32] KATO, S., *et al*, (1991). Implementation of coded modems, IEEE Communication Magazine, 88-97.

[33] XIONG, F., (1994). Modem techniques in satellite communications, IEEE Communications Magazine, 84-98.

[34] CHUANG, J.C. (1990). Comparison of coherent and differential detection of BPSK and QPSK in a quasistatic fading channel, IEEE Trans. Communications, Vol.38, No.5, 565-567.

[35] KOSTIC. I.M. (1989). Imperfections, noise and cochannel interference, IEE Proceedings, Vol.136, Pt. I, No.5, 333-338, Oct..

[36] CHEUNG, S.W. (1990). Carrier phase synchronization for a coded PSK signal in satellite links, Globecom'90, 1413-1417.

[37] NATALI. F.D. (1984). AFC tracking algorithms, IEEE Trans. Communications, Com-32, 935-947.

[38] COWLEY, W.G. and SABEL, L.P. (1994). The performance of two symbol timing recovery algorithms for PSK demodulators, IEEE Trans. Communications, Vol.42, No.6, 2345-2355.

[39] RE, E.D. and FANTACCI, R. (1989). Joint carrier and clock recovery for QPSK and MSK digital communications, IEE Proceedings, Vol.136, Pt.I, No.3, 208-212.

[40] GAUDENZI, R.D. and VANGHI, V. (1994). Analysis of an all-digital maximum likelihood carrier phase and clock timing synchronizer for eight phase-shift keying modulation, IEEE Trans. Communications, Vol.42, No.2/3/4, 773-782.

[41] ENGEN, G.F., (1978). Calibrating the six-port reflectometer by means of sliding terminations, IEEE Trans, Microwave Theory Tech., vol. MTT-26, 951-957.

[42] EID, E. *et al*, (1994). Self-calibration of six-port reflectometers using active loads, CPEM'94 Digest, 121-122.

[43] Marconi Instruments, (1993). Design of a six-port microwave instrument, Marconi Instruments Technical Journal, issue 93/2, 6-7.

[44] REINHARDT, V.S., *et al*, (1994). Methods for measuring the power linearity of microwave detectors for radiometric applications, Digest IEEE MTT-S'94, 1477-1480.

[45] TAKAYAMA, Y., (1976). A new load-pull characterization method for microwave power transistors, Digest IEEE MTT-S'76, 218-220.

[46] GHANNOUCHI, F.M., LAROSE, R. and BOSISIO, R.G. (1991). A new multi-harmonic loading method for large-signal microwave transistor characterization, IEEE Trans, Microwave Theory Tech., vol. MTT-39, 986-992.

[47] PRESS, W.H., *et al*, (1992). *Numerical Recipes in FORTRAN*, Cambridge University Press, 2nd Edition, 644-649.

[48] POTTER, C.M. and HIJIPIERIS, G. (1993). A robust six- to four- port reduction algorithm, Digest IEEE MTT-S'93, 1263-1266.

Appendix I.

A COLLISION AVOIDANCE RADAR USING SIX-PORT PHASE/FREQUENCY DISCRIMINATOR (SPFD)

Ji LI, Renato G. BOSISIO, and Ke WU

Groupe de Recherches Avancées en Microondes et en Électronique Spatiale
(POLY-GRAMES)
École Polytechnique de Montrèal, C. P. 6079, Succ. Centre Ville
Montréal, Canada H3C 3A7

ABSTRACT

A novel technique is proposed for collision avoidance radar used in automobiles, in which a new six-port microwave/millimeter wave digital phase/frequency discriminator (SPFD) is used to measure Doppler frequency shifts. Both relative speed and moving direction of the target are readily obtained. Ranging is implemented by the measurement of phase difference at two adjacent frequencies. Preliminary experimental simulation proves the validity of the proposed alternative approach.

INTRODUCTION

The ever-increasing demand for reliability and safety of modern automobiles has been promoting applications of various advanced technologies, especially microelectronic technologies. Much attention has been given to technologies related to intelligent electronic vehicles [1]. In the next generation cruise control systems, Doppler sensing and ranging are essential for both lateral and longitudinal controls [2]. On the other hand, low cost and high reliability is crucial for the global competitiveness of its widespread applications.

The six-port junction [3] has been well known for its unique ability to accurately measure the scattering parameters of microwave/millimeter-wave networks, where phase information is extracted by a set of amplitude measurements. The phase/frequency detection is directly made at microwavv/millimeter wave frequencies. Therefore expensive heterodyne receivers and phase detectors can be effectively avoided. In particular, the state-of-the-art M(H)MIC technology [4,5] renders it possible to miniaturize the six-port junctions. This is attractive for applications that require low-cost and compact size.

Conventional Doppler sensors are realized by reading 'beat frequency' of the transmitted and reflected signals. A commonly used ranging method is to frequency modulate the transmitted signal. This kind of sensor known as FM/CW radar has been well accepted in terms of its simplicity. However, several drawbacks prevent such scheme from further improvement in performance. First, the Doppler frequency is counted by the numbers of zero-crossing or through digital spectrum estimation technique such as FFT. Useful reading can be accomplished only after multiple periods of the beat cycles. This sampling time interval is rather long when a high accuracy of the lower relative velocity is required. In addition, there is no indication of the direction of relative movement which is very important in collision avoidance radars. Furthermore, in order to improve the resolution of the range measurement, the bandwidth of the FM signal has to be increased significantly which may cause additional technical problems as well as cost escalation.

In this paper, we propose a new scheme of collision avoidance sensor, in which a SPFD is used. As will be shown later the Doppler frequency is read by measuring the rate of phase variation $d\phi/dt$ of the received vector. In principle, a much shorter acquisition time is required because the Doppler frequency is obtained even within a cycle of the beat

TH 3A

CH3389-4/94/0000-1553$01.00 © 1994 IEEE

frequency. The direction of the relative movement is acquired as well. This provides rapid and accurate information in collision avoidance applications. By measuring the phase difference between two properly spaced frequencies, short distance ranging is readily achieved.

OPERATING PRINCIPLE OF THE SPFD

The six-port junction is a passive microwave network with six ports as shown in Fig.1. The vector relation of two microwave signals (a_1 and a_2) applied at two ports can be obtained by measuring power levels at the remaining four ports. Let the signals a_1 and a_2 be as follows:

$$a_1 = |a_1| \cdot e^{j(\omega_1 t + \phi_1)} \quad (1)$$

$$a_2 = |a_2| \cdot e^{j(\omega_2 t + \phi_2)} \quad (2)$$

where ω_1, ϕ_1, ω_2, and ϕ_2 represent frequencies and phases of the two signals. Then it can be shown that

$$A = |A| e^{j\theta} = \frac{a_1}{a_2} = \frac{\sum_{i=3}^{6} (c_i + js_i) P_i}{\sum_{i=3}^{6} \beta_i P_i} \quad (3)$$

where P_i is power reading at corresponding port. And c_i, s_i and b_i are calibration coefficients of the six-port junction. These coefficients can be obtained through an appropriate calibration procedure.

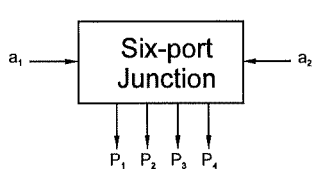

Figure 1. Six-port junction

In the case $\omega_1=\omega_2$, the six-port acts as a vector voltmeter or reflectometer. The unknown reflection coefficient Γ at a reference plane is calculated from power readings P_i. This feature has been widely employed to measure scattering parameters of microwave circuits and networks.

When the case $\omega_1 \neq \omega_2$ is considered, the six-port turns out to be a frequency discriminator. The complex power ratio A becomes a vector rotating at an angular rate of Dw in a complex plane. The frequency difference Δf can be determined by measuring the rotating velocity of A. The sign of $\Delta\omega$ is indicated by clockwise or counter-clockwise rotation of the vector.

$$\Delta f = \frac{\Delta\theta}{2\pi \cdot \Delta t} \quad (4)$$

where $\Delta f = \Delta\omega / 2\pi = f_{trans} - f_{rec}$. The value of Δf may be positive or negative which in turn indicates a higher or lower frequency of the reflected signal. Note that the maximum unambiguous value of $\Delta\theta$ is π. For a given sampling rate this condition also determines the maximum detectable frequency difference.

The SPFD is insensitive to additive white noise as well as amplitude variation of the received signal, so that no automatic gain control circuit is required. In the real Doppler measurements, the spectrum expansion of the reflected signal can be seen as a multi-vector composition. The SPFD only traces the compound vector.

DESCRIPTION OF THE RADAR

A block diagram of the proposed radar is shown in Fig.2. It is similar to a conventional homodyne FM/CW radar: a small portion of the transmitted signal is directed to the receiving end as the reference. A SPFD replaces the mixer. The output of the six-port is processed by a signal processor. Compared with the popular scheme where digital processing technology such as FFT is employed, the computational effort of the new scheme is greatly reduced. The oscillator output is switched between two frequencies whose difference is known. The short distance of the target is readily calculated from the phase difference between the two reflected signals.

In CW type radars, one of the most serious problems is to achieve sufficient isolation between transmission and reception. To prevent the receiver from saturation, separate transmitting and receiving antennas are often used. This results in unwanted larger volume

and higher cost. Some other solutions such as Reflected Power Canceller (RPC) [6] are proposed and implemented, however the cost and complexity are still high. In contrast, by using new SPFD it is very easy to integrate a RPC into the sensor at the expense of only a vector modulator (phase shifter and attenuator). The single antenna scheme is shown in Fig.3. In the six-port PFD, the leakage of the transmitted signal yields a deviation of the detected vector from the origin. A feedback algorithm can be adopted to control the loop to realign the vector to the origin, such that the leakage power is canceled out.

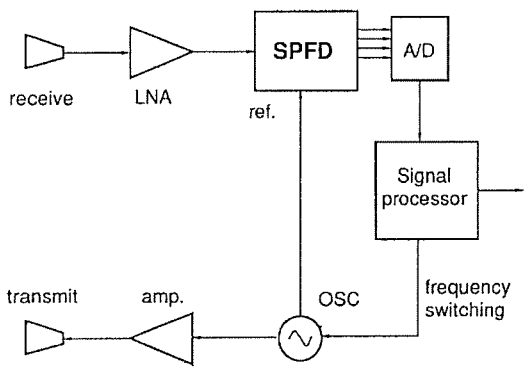

Figure 2. Dual antenna configuration of collision avoidance radar

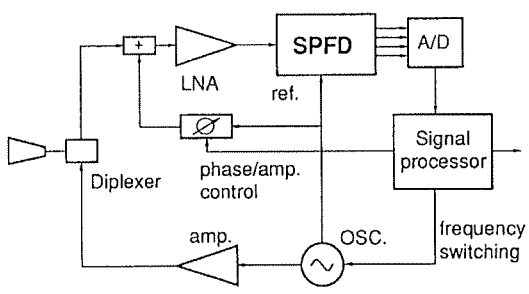

Figure 3. Single antenna collision avoidance radar with adaptive RPC

EXPERIMENTAL SIMULATION

Experiments were performed in order to demonstrate the feasibility of the SPFD. Two millimeter wave signal generators provide the two signals to be compared (f_1 and f_2). A simultaneous sampling of the output at the four ports is performed by a data acquisition system. The sampling rate was set to be 1MHz, namely Dt=1ms. The frequency difference Df was measured from 1KHz to 20KHz. The bandwidth of the DC amplifier determines the upper limit of detectable Df. The measurements were done at two different frequency points (27GHz and 35GHz).

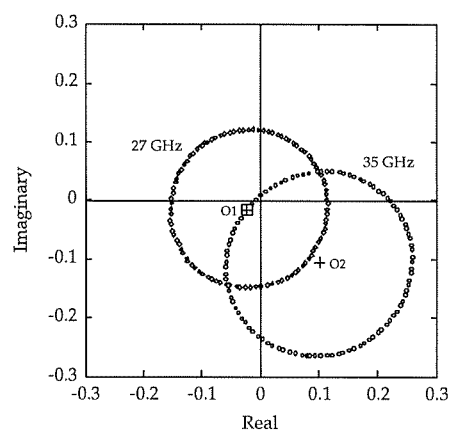

Figure 4. Samples of the measured vector ratio A

Fig.4 shows the traces of the measured A value which rotate in the complex plane. The origin of the circles are moved due to reflections of signal $f1$ at port 2. The origins (O_1 and O_2) are obtained by measuring A while signal $f2$ is turned off. The averaging of the sampled vectors leads to the same results. This is one way to achieve RPC function as proposed above. Fig.5 plots a statistical normal deviation in percentage of the measured Δf value. It is concluded that there is no correlation between the error and the magnitude of Δf, which suggests that the measurable Δf range could be further expanded as the bandwidth of the DC amplifiers and sampling rate increase.

Fig.6 illustrates the relationship between the normal deviation (%) and absolute power ratio $|A|$. It is seen that for a power ratio as high as 40 dB the resulting error remains to be as low as 5% (at 35 GHz). It has to be point out that all the measurements are made in a small fraction of the beat signal period. Much better accuracy is expected if the acquisition time becomes longer. On the other hand, because $|A|$ can be greater or smaller than unity so that the overall dynamic range can be even larger. When a limiter is incorporated at the output of the receiving amplifier the detectable dynamic range could be further expanded.

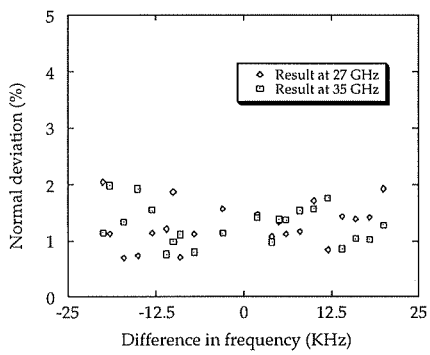

Figure 5. Normal deviation of the measured Δf

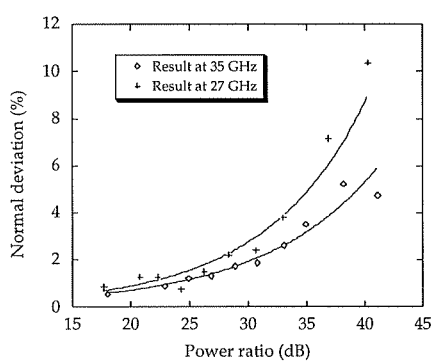

Figure 6. Normal deviation of Δf versus power ration A

CONCLUSION

A new simple scheme of collision avoidance radar is proposed. Preliminary experiments has demonstrated the potential of the six-port Doppler sensor. The advantages of the new sensor over the conventional ones are summarized as follows: a) a faster sampling rate is achieved; b) information on the direction of relative movement is easily obtained; c) the single antenna configuration is readily realized by employing adaptive leakage cancellation; and d) low cost and small volume are expected.

REFERENCES

[1] Ulf Palmquist, "Intelligent Cruise Control and Roadside Information",IEEE Micro Magazine, vol. 13, No.1, pp. 20-28, Feb. 1993.

[2] E.F. Belohoubek, "Radar Control for Automotive Collision Mitigation and Headway Spacing," IEEE Trans. Vehicular Tech., vol. VT-31, pp.89-99, May 1982.

[3] G.F. Engen, "Determination of Microwave Phase and Amplitude from Power Measurements", IEEE Trans. Instrum. Meas., vol. IM-25, No.4 pp.414-418, Dec. 1976.

[4] F.M.Ghannouchi, D. Maurin, M. Cuhaci and R.G. Bosisio, "A Miniaturized Frequency-compensated Six-port Junction Using MHMIC Technology," Microwave and Optical Technology Letters, Vol.6 pp. 573-575, Aug. 1993.

[5] M.N.Solomon et al, "A monolithic six-port module" IEEE Microwave and guided wave letters, Vol.2 pp. 334-336, Aug. 1992.

[6] P.D.L. Beasley et al, "Solving the problems of a single antenna frequency modulated CW radar," National Telesystems Conference, Atlanta 1993 pp.391-395.

Appendix II.

TH4A-1

A Six-port Direct Digital Millimeter Wave Receiver

Ji Li, R.G.Bosisio and Ke Wu

Groupe de Recherches Avancées en Microondes et en Électronique Spatiale
(POLY-GRAMES)
École Polytechnique, C. P. 6079, Succ. Centre Ville
Montréal, Canada H3C 3A7

ABSTRACT

A novel approach is proposed for direct demodulation of various digitally modulated signals at microwave/millimeter wave frequencies using a six-port phase/frequency discriminator (SPFD). The proposed six-port direct digital receiver is capable of handling PSK and QAM as well as their varieties. Preliminary measurements on demodulation of DBPSK signals at 26.5GHz, 33GHz and 40GHz have revealed great potential of this new receiver.

INTRODUCTION

Direct homodyne reception has been attracting constant attention due to its inherent advantages over its heterodyne counterpart. The recent development of personal communication systems (PCS) has ignited a new round of efforts to achieve low cost, robust and miniaturized versatile microwave/mm-wave digital terminals. Considerable effort has been made on digital direct conversion receivers (DCR) [1]-[3] in which conventional I-Q structure is adopted. However, the difficulties involved in implementing perfectly matched orthogonal I-Q circuits prevents such technology from applications at higher frequency bands.

Six-port technique has been known for its ability to accurately measure the scattering parameters, both amplitude and phase, of microwave networks. Instead of using heterodyne receiver a six-port junction accomplishes direct measurements at microwave and mm wave frequencies by extracting power levels at four of the six ports. The imperfections of the hardware can be readily eliminated by an appropriate calibration procedure. Very accurate measurements can be made over large dynamic range and wide frequency range. Six-port junction consists of passive microwave components such as directional couplers and power dividers as well as diode detectors. The circuit ca be easily integrated as MHMIC or MMIC. Recently we have proposed a new approach, in which a six-port junction is used for accurate frequency comparison. The frequency differences are found by direct measurements of the derivatives of the phase variations. This features a new digital microwave/mm wave six-port phase/frequency discriminator (SPFD)[4].

TH 4A

CH3389-4/94/0000-1659$01.00 © 1994 IEEE

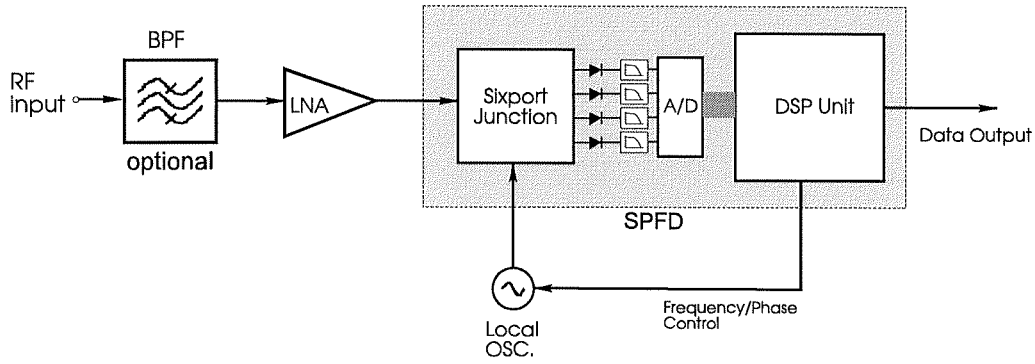

Figure 1. Block diagram of the sixport direct digital receiver.

In this paper we present a new six-port digital receiver (SDR). It performs direct phase/amplitude demodulation at microwave/mm wave frequencies. The receiver is simple and potentially low cost. Furthermore, the SDR can easily cover a wide frequency band by using a broadband design of the six-port junction. This SDR is proposed for low/medium speed receivers with data transmission rate lower than 15Mb/s.

DESCRIPTION OF THE SDR

The functional block diagram of the SDR is shown in Fig.1. The traditional I-Q block in a receiver is replaced by a six-port phase/frequency discriminator (SPFD), which contains a six-port junction and a digital signal processing (DSP) unit. The incoming digitally modulated (e.g. PSK, QAM) RF signal is compared with the output of a digital controlled local oscillator. Carrier recovery is first performed. The DSP unit detects the frequency difference of the signals and then controls the local oscillator to track the incoming signal. Once the carrier is recovered the instantaneous phase of the received signal is detected and decoded so as to recover the original modulated data. Symbol synchronization can also be achieved simultaneously. Incoherent reception can be used where the LO frequency need not to be exactly the same as the carrier frequency. The maximum tolerable frequency deviation depends on the data transmission rate and the modulation scheme. The maximum data transmission rate is determined mainly by the sampling rate of the A/D converters and processing speed of the DSP unit.

Regarding the practical feasibility of the direct digital phase demodulation, the new SDR features some advantages over the conventional I-Q direct reception schemes. First, by performing a simple calibration procedure [5], the hardware imperfections such as phase error of the bridges, imbalance of the power detectors can be readily eliminated. This significantly eases the requirement of the hardware implementation and enables the SDR to operate over a wide band up to millimeter wave frequencies. Second, in the SDR, the magnitude and phase are acquired independently. Therefore the phase modulation of the incoming signal can still be correctly detected even though the amplitude of the incoming signal changes over a large dynamic range. Third, the DSP unit gives much flexibility to the SDR.

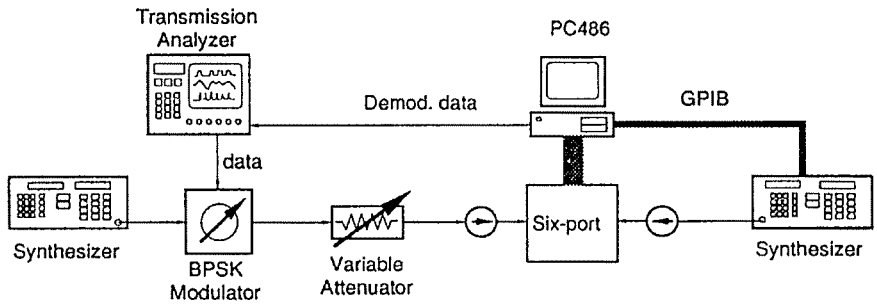

Figure 2. Test Set-up of the bit error rate measurement

Switching between different modulations can be readily accomplished by slight alternations of the algorithm. Advanced error correction coding techniques can also be integrated into the same unit. Aside from PSK modulations, amplitude/phase modulation such as QAM is readily detectable by employing an algorithm which takes into account the fading effect in the transmission path.

MEASUREMENT RESULTS

Measurements are performed to demonstrate the potential of the new SDR. The test setup is shown in Fig.2. A simple differential binary phase shift keying modulator generates a DBPSK signal. The LO frequency is controlled to track the carrier frequency. The output of the modulator was directly fed into the SPFD with no amplification additional. A PC486 equipped with a A/D converter is used as the DSP unit.

A constellation map measured at 33 GHz corresponding to different incoming signal levels is shown in Fig.3. It clearly indicates both magnitude and phase of the received signal. The imbalance of the BPSK modulator can also be clearly observed. The span of the phase might be introduced by phase noise of the two microwave synthesizers (The local oscillator and DBPSK signal generator). It is noticed that a coherent reception is also possible with a proper phase lock of the local oscillator.

Bit error performance was measured at 26.5GHz, 33GHz and 40GHz using the same receiver. Fig.4 plots the BER versus incoming signal level. The levels between the saturation point of diode detectors and a specified BER point is considered as the operating dynamic range. The saturation point of the detectors used is about 10dBm. Counting the approximate 10dB insertion loss between the input port and the detectors the maximum power level at the input port of the six-port can be 20dBm so that the overall dynamic range is around 60~70dB without any additional level control. Note that the operating dynamic range is mainly determined by the resolution of the A/D converter. In this measurement a 16-bit A/D converter is used. The difference in BER performance at the three frequencies is believed to be caused mainly by the frequency response of the diode detectors.

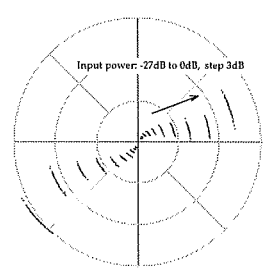

Figure 3. Measured constellation of the BPSK signal at different power levels (Freq.=33GHz)

CONCLUSIONS

A novel scheme for direct microwave/mm wave digital phase demodulation is presented. Some drawbacks of the conventional I-Q direct conversion digital receiver are overcome by using a six-port phase/frequency discriminator incorporated with a digital signal processing unit. This technology is potentially low cost and it is promising in various small/medium capacity digital communication systems such as point-to-point data links, micro-cell mobile terminals and wireless LAN's etc.

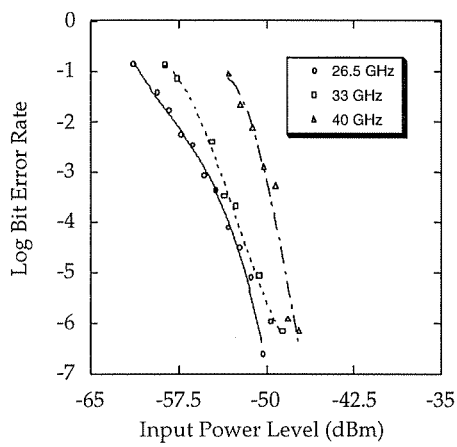

Figure 4. Measured BER performance of the six-port direct digital receiver

REFERENCES

[1] Gerhard Schultes *et al*, "A New Incoherent Direct Conversion Receiver", IEEE Vehicular Technology Conference 1990, pp.668-674

[2] K.Anvari *et al*, "Performance of a direct conversion receiver with p/4-DQPSK modulated signal", IEEE Vehicular Technology Conference 1991, pp.822-827

[3] K.Voudouris *et al*, "Effects of Amplitude, Phase, and Frequency Imperfections on the Performance of a Direct Conversion Receiver (DCR) for Personal Communication Systems", IEEE Microwave and Guided wave Letters, Vol.3, No.9, Sept. 1993, pp. 313-315

[4] J. Li, R.G.Bosisio and K. Wu, "A Collision Avoidance Radar Using Six-port Phase/Frequency Discriminator (SPFD)", to be presented at NTC'94, San Diego, May,1994

[5] C.A.Hoer *et al*, "Using an Arbitrary Six-Port Junction to Measure Complex Voltage Ratios", IEEE Trans. MTT-23, No.12, Dec. 1975, pp.978-984

ÉCOLE POLYTECHNIQUE DE MONTRÉAL
3 9334 00171192 6

CA
UP
19
L6